SEDIMENTARY FACIES ANALYSIS, PETROGRAPHY AND DIAGENESIS OF THE EARLY MIOCENE NUTAYSH MEMBER OF THE BURQAN FORMATION IN MIDYAN BASIN, NW SAUDI ARABIA.

BY

Muhammad Naveed Tahir Butt

A Thesis Presented to the
DEANSHIP OF GRADUATE STUDIES

KING FAHD UNIVERSITY OF PETROLEUM & MINERALS

DHAHRAN, SAUDI ARABIA

In Partial Fulfillment of the
Requirements for the Degree of

MASTER OF SCIENCE

In

GEOLOGY

DECEMBER 2017

KING FAHD UNIVERSITY OF PETROLEUM & MINERALS

DHAHRAN- 31261, SAUDI ARABIA

DEANSHIP OF GRADUATE STUDIES

This thesis, written by **MUHAMMAD NAVEED TAHIR BUTT** under the direction his thesis advisor and approved by his thesis committee, has been presented and accepted by the Dean of Graduate Studies, in partial fulfillment of the requirements for the degree of **MASTER OF SCIENCE IN GEOLOGY.**

Dr. Khalid Al-Ramadan
(Advisor)

Dr. John Reijmer
(Member)

Dr. Abdulaziz Al-Shaibani
Department Chairman

Dr. Waleed Abdulghani
(Member)

Dr. Salam A. Zummo
Dean of Graduate Studies

28/12/12

Date

Dedication

To my beloved parents and my dear brother Muhammad Suleman…

ACKNOWLEDGMENTS

In the name of Allah (SWA) Almighty, the most gracious and the most merciful. All the praises and gratitude to Allah (SWA), Who have provided me with the great opportunity to pursue my master in geology in KFUPM and made me capable to accomplish the goal successfully.

My profound gratitude and my heartfelt esteem goes to my advisor, Dr. Khalid Al-Ramadan, for his counselling, sharing scientific knowledge, improving my research and presentation skills and persistent encouragements towards my academic imperfections. He has tolerated me with a great deal of patience over the past few years.

I am grateful to my thesis committee members, Prof. Dr. John Reijmer and Dr. Waleed Abdulghani, for sharing their invaluable time for my write-up corrections, scientific discussions and support during the course the research. My honest gratitude goes to Dr. Stephen Franks from *RockFluid Systems, Inc.* for the detailed discussions related to the improvement of conceptual depositional model of the Burqan Formation. I also want to pay my sincere regards to Mr. Salem Al-Shammary (Aramco) for opening the floor of discussion while measuring stratigraphic sections in the field. His encouraging behavior has greatly improved my confidence during fieldwork. Likewise, I want to say thanks to Mr. Mohammad Al-Sadah (Aramco) to accompany us during detailed fieldwork and sharing some factual information about the Burqan Formation in the subsurface.

Moreover, I would also like to thank Dr. John Humphrey (Assistant Chairman-CPG) and Dr. Muhittin Senalp (Consultant) for sharing their knowledge and mind-expanding discussion related to my research during the fieldwork in Midyan region. I am also grateful to Dr. Abduljamiu Olalekan Amao for carrying out several geochemical analysis for my research and spending enormous time for data interpretation and improving data presentation in thesis.

I am especially grateful to the Chairman of Geoscience Department, Dr. Abdulaziz Al-Shaibani, for the opportunity he provided me to serve the department as Teaching Assistant throughout the course of my masters. I feel deeply grateful to all my teachers, staff members of geosciences department especially Mr. Mushabab, Mr. Elias, Mr. Hamid, Mr. Aziz, Mr. Sameer (E-learning), Mr. Abdullah Abdulgadir (E-learning), my fellow graduate and undergraduate students including Omar Radwan, Septri, Dipta, Andy, Ali Al-Abyadh, Omar Al-Ajaji, Abdurrahman Al-Hussaini, Hassan Al-Saihati and many more who made my stay pleasant at KFUPM. I am grateful to my friends from Pakistani community especially, Syed Haroon Ali, Waleed, Hammad Malik, Asif, Usman Saeed, Hafiz Muhammad Afzal, Usama Irshad, Nadeem Baig, Hafiz Mudaser and many more who were supportive all the time and their presence made KFUPM student housing like my second home.

I feel very proud while thanking my family: my parents and my brother Muhammad Suleman, for their understandings and continuous support during the course of research. I genuinely feel that the goal to accomplish my masters would be impossible without the endless prayers and encouragement from my family.

The thesis work was fully funded by the project number ES2358 as part of trilateral collaboration between KFUPM-Saudi Aramco-Stanford University under the supervision of Dr. Khalid Al-Ramadan.

TABLE OF CONTENTS

ACKNOWLEDGMENTS ..... **v**

TABLE OF CONTENTS ..... **viii**

LIST OF FIGURES ..... **xi**

LIST OF TABLES ..... **xxiii**

ABSTRACT ..... **xxiv**

ملخص الرسالة ..... **xxv**

CHAPTER 1 INTRODUCTION **1**

1.1 Thesis Format 2

1.2 Background and problem statement 3

1.3 Research Objectives 7

1.4 Research Approach 7

CHAPTER 2 LITERATURE REVIEW **10**

2.1 Geologic Background 10

2.2 Tectonic Evolution of the Midyan Basin 12

2.3 Tectonic Elements of the Midyan Peninsula 15

2.4 Stratigraphy of the Saudi Arabian Red Sea 15

2.4.1 Proterozoic Basement 15

2.4.2 Pre-Rift Successions 16

2.4.3 Syn-Rift Successions 18

2.4.4 Post-Rift Successions 21

CHAPTER 3 RESULTS 22

3.1 Facies Analysis 22

3.1.1 Stratigraphic Section 3 23

3.1.2 Stratigraphic Section 3 31

3.1.3 Stratigraphic Section 4 37

3.1.4 Stratigraphic Section 4 43

3.1.5 Stratigraphic Section 5 56

3.1.6 Stratigraphic Section 5 72

3.1.7 Stratigraphic Section 6 81

3.1.8 Stratigraphic Section 6 90

3.1.9 Stratigraphic Section 7 100

3.1.10 Stratigraphic Section 7 103

3.2 Petrology 106

3.2.1 Provenance 107

3.2.2 Petrography 108

3.2.3 Texture 109

3.2.4 Composition 110

3.3 Diagenesis 140

3.3.1 Mechanical Compaction 140
3.3.2 Carbonate Cementation 140
3.3.3 Pyrite, Iron Oxide and Quartz Cementation 141
3.3.4 Clay Minerals 142
3.3.5 Porosity 151
CHAPTER 4 DISCUSSION 159
4.1 Facies Analysis 159
4.2 Petrography and Provenance 163
4.3 Diagenesis and Diagenetic Evolution 164
4.3.1 Physical Compaction and Porosity Preservation 165
4.3.2 Corroded Quartz Periphery 166
4.3.3 Carbonate cements 166
4.3.4 Accessory Cements 166
4.4 Reservoir Quality of Burqan Formation 168
4.5 Conceptual Submarine Fan Model of the Burqan Formation 171
CHAPTER 5 CONCLUSION 173
REFERENCES 175
Vitae 189

LIST OF FIGURES

Figure 1.1: Tectonic map of the Arabian Plate (After Sharland *et al.*, 2001). The red box marks the location of the Midyan Peninsula (Study Area) in the NW Saudi Arabia. Magnified false-colored Landsat image of the study area (Modified after Tubbs *et al.*, 2014). Digits show the location of studied outcrops. 4

Figure 1.2: Geological map of the Al Bad' quadrangle (Midyan region), sheet 28A, NW Saudi Arabia. (Clark,1986)..... 5

Figure 1.3: Location of representative outcrops of the Burqan Formation in the Midyan region, NW Saudi Arabia (Courtesy to Google Earth Pro ®)..... 6

Figure 1.4: Field photograph showing sedimentary structures observed in Nutaysh Member of the Burqan Formation located on the west side of the Burqan valley.The outcrop shows the typical divisions of the Bouma Sequence. 9

Figure 2.1: Generalized stratigraphic column of different lithostratigraphic units of Saudi Arabian Red Sea region and neighboring Gulf of Suez (Hughes and Johnson, 2005). The Burqan Formation of Saudi Arabia is correlative to the Lower Rudeis Formation of Gulf of Suez, Egypt..... 11

Figure 2.2: Field photograph showing the lower sand-dominated Nutaysh member (right) and the upper, shale-dominated, Subayti member as found in section 4 in the central part of the Midyan Basin. Person as scale. 13

Figure 2.3: The paleogeographic reconstruction maps show the separation of the Arabian Platform from African Plate during the Late Rupelian (32-29 Ma; Early Oligocene). Red lines show the plate boundaries whereas bold black lines mark the major fault zones (Meulenkamp and Sissingh, 2003). 14

Figure 2.4: Field photograph showing the Proterozoic basement in the Midyan Basin. The igneous basement is intruded by dark colored dolerite and basaltic dikes. 17

Figure 2.5: Outcrop of cross-bedded sandstone of the Adaffa Formation in the Midyan region. 18

Figure 3.1: Field photograph showing the erosional, unconformable contact between the sediments of the Musayr Formation and the Burqan Formation at the base of Section-3. 25

Figure 3.2: Field photo showing two fining and thinning upward sequences (blue traingles) in the first 115 meters of stratigraphic section-3..... 26

Figure 3.3: Field photograph showing a lenticular shaped conglomerate base lag unit of a submarine fan channel. 27

Figure 3.4: Field photo showing the upper part of the Section-3. Massive, friable, medium to coarse-grained and bioturbated sandstone unit of the Burqan Formation. Hammer for scale. 28

Figure 3.5: Field photograph showing the lower sandstone unit containing abundant reworked shells of sand dollar (Echinoderms-yellow arrows) and oysters (red box) and overlying oyster bearing, cream colored thick limestone unit. Hammer for scale, 30 cm. 29

Figure 3.6: Detailed stratigraphic and sedimentological section-3 of the Burqan Formation in Midyan basin, NW Saudi Arabia. 30

Figure 3.7: Horizontal burrows on top of medium grained sandstone unit in section-4. 39

Figure 3.8: a) Field photo showing in-situ large transported coral head limestone boulder within the sandstone unit. (b) Field photograph showing several eroded and

scattered coral head limestone pieces presumably derived from large coral head boulder. 41

Figure 3.9: Detailed stratigraphic and sedimentological section-4 of the Burqan Formation in Midyan basin, NW Saudi Arabia. 42

Figure 3.10: Field photograph showing basal coarsening upward sequence in measure section 5 along the coastal road south of Maqna. Jacob staff (1.5 m) is used as a scale in the middle of the photograph. 57

Figure 3.11: Field photo showing the normal grading in the sandstone unit of first coarsening upward sequence of measured section 5. Pencil Scale = 14cm. 58

Figure 3.12: The field photo showing the burrowed and bioturbated lower surface of sandstone unit within the first coarsening upward sequence of section-5 in the Midyan region. Pencil Scale = 14cm..... 59

Figure 3.13: Field photo of second coarsening upward sequence of section-5 in the Midyan region. The thickness of sandstone units is increasing as we move to the top of the sequence. Jacob Staff (1.5 m) is taken as a scale. 60

Figure 3.14: Field photo of a normally graded bed within second coarsening upward sequence in section-5. Pencil Scale = 14cm. 61

Figure 3.15: Field photo showing the massive sandstone unit in the lower part of the first fining upward sequence of section-5. Jacob Staff (1.5 m) is used as a scale..... 63

Figure 3.16: Field picture showing inverse grading in massive sandstone unit of first fining upward sequence of section-5. Jacob Staff (1.5 m) is used as a scale. 64

Figure 3.17: Field photo showing the interbedded sand-shale interval of classical turbidites above the fining upward sequence in section-5. 65

Figure 3.18: Field photo of fining and thinning upward sequence within section-5 in Midyan region (Person for scale). 66

Figure 3.19: A closer view of a sandstone unit showing grain size variations (Multiple grading) within a sandstone unit. The smaller grains are present at the base and top of the unit while coarse grains are concentrated in the middle of the sandstone unit. Hammer 30 cm for scale. 68

Figure 3.20: Field photo of the uppermost sequence of the section-5. The lenticular sandstone units have mud intraclasts (red arrows) near its base. 70

Figure 3.21: Detailed stratigraphic and sedimentological section-5 of the Burqan Formation in Midyan basin, NW Saudi Arabia. 71

Figure 3.22: a) Field photograph showing the first coarsening upward, progradational sequence of measure section-6. Person as Scale. (b) Field photo showing vertical burrows in the upper part of the sequence. Hammer (30 cm) as scale. 83

Figure 3.23: Field photographs showing common sedimentary structures observed in section-6. a) Groove casts. (b) Flute marks. (c) Normal grading T_a, T_b. 84

Figure 3.24: Field photograph showing divisions of classical Bouma Sequence within measured section 6. T_d division may have been eroded before the deposition of T_e. 86

Figure 3.25: Field photo is showing lenticular, channel filled pebbly sandstone deposited in the deepest part of the channel. 87

Figure 3.26: Field photo showing inverse grading from base of the unit to the middle and then grain size decreases towards the top of this thick sandstone unit in section-6. 88

Figure 3.27: Detailed stratigraphic and sedimentological section-6 of the Burqan Formation in Midyan basin, NW Saudi Arabia. 89
Figure 3.28: Detailed stratigraphic and sedimentological section-7 of the Burqan Formation in Midyan basin, NW Saudi Arabia. 102
Figure 3.29: a) PPL-view (4X): Photomicrographs showing very poorly sorted and angular to sub-rounded framework grains. (b) XPL-view (4X): Majority of quartz grains are monocrystalline in nature. Undulose extinction in a large quartz grain lying in lower left corner is visible. Sericitization on the surface of large albite grain can be observed 111
Figure 3.30: a & b) Magnification-20X: Optical micrographs showing the presence of rutile in siltstone sample. c & d) Magnification-10X: Heavy mineral zircon with very high relief and characteristic variegated color is present in a sandstone sample... 112
Figure 3.31: Compositional (QFL) plot showing different source terrains of Burqan Formation in the Midyan region. 113
Figure 3.32: According to folk's classification of sandstones, the ternary plot of QFL showing that the sandstone samples are compositionally arkosic, sub-arkosic and lithic arkosic in nature (Modified after Folk, 1980). 114
Figure 3.33: (a) Facies-wise ternary plot of Section-3, (b) Facies-wise ternary plot of Section-4, (c) Facies-wise ternary plot of Section-5, (d) Facies-wise ternary plot of Section-6, (e) Facies-wise ternary plot of Section-7. Facies-wise ternary plots of all stratigraphic sections are based on Folk's Classification. 117
Figure 3.34: a) PPL-view (4X): Optical micrograph showing different framework grains, cement and porosity types. Q_m= monocrystalline quartz, O= Orthoclase, Red

Arrows are showing hematite cement engulfing the calcite cement while black arrows are pointing towards calcite cement clogging the pores. (b) XPL-view (4X): Abundant monocrystalline quartz grains are present. The coarse grained orthoclase shows Carlsbad twinning and Perthitic texture. 125

Figure 3.35: a) PPL-view (4X): Photomicrograph showing mono- and polycrystalline quartz and plutonic rock fragments. Red Arrow shows hematite cement while black arrows show secondary porosity (partial grain dissolution). (b) XPL-view (4X): Photomicrograph showing non-undulatory monocrystalline quartz crystal (Q_m) embedded next to polycrystalline quartz grain (Q_p) consists of several crystals. Plagioclase (P_g=Albite) shows characteristic polysynthetic twinning. A large plutonic rock fragment is also present. Red arrow indicates hematite cement. 126

Figure 3.36: a) PPL-view (4X): Optical micrograph showing bioclast composed of calcium carbonate (BC). Red arrows indicate syn-depositional calcite cement while yellow arrows indicate patches of early diagenetic pyrite cement engulfed by calcite cement. Secondary porosity is visible which is created due to the dissolution of framework grains and cement. (b) XPL-view (4X): xnicol view of micrograph-a. (c) PPL-view (4X): Optical micrograph showing large piece of dolomitized red algae. Secondary porosity is shown by blue color. (d) XPL-view (4X): xnicol view of micrograph-c. 127

Figure 3.37: a) PPL-view (10X): Red arrows in optical micrograph are indicating towards high primary intergranular porosity. This is due to lack of sufficient cement. (b) XPL-view (10X): Photomicrograph showing Orthoclase grain (O) with perthitic texture, Plagioclase (Albite-Pg with multiple twinning) with tiny serecite mica

flakes on the surface, Microcline (M) shows characteristics cross-hatch twinning. Black arrows indicate towards patches of calcite cement. 128

Figure 3.38: a) PPL-view (4X): Photomicrograph showing highly fractured quartz grain with argillaceous matrix between the grains. The primary cement between the grains is calcite. Sparse early diagenetic pyrite cement is also present. High secondary porosity (blue colored spaces) is visible due to the partial dissolution of framework grains and cement. (b) XPL-view (4X). Cross nicols view of optical micrograph-a. 129

Figure 3.39: a) PPL-view (4X): Optical photomicrograph showing mud intraclast (red arrow) squeezed between quartz grains. (b) XPL-view (4X): Black arrows indicates towards undulatory quartz grains while yellow arrows are showing early diagenetic pyrite cement present as patches. Calcite cement is the major cement occluding all the primary pore spaces. 130

Figure 3.40: a) PPL-view (4X): Optical micrograph is showing a pebble of plutonic rock fragment. The size of the grain is larger than 4 mm and the grain boundaries are going out of the field of view. (b) XPL-view (4X): Crossed nicols view of optical micrograph-a. 131

Figure 3.41: a) PPL-view (4X): Photomicrograph showing low compaction, high intergranular porosity in friable sandstone sample of Burqan Formation due to the absence of any cement. Only early diagenetic pyrite cement is present as small patches. (b) XPL-view (4X): Optical micrograph showing the relative abundance of monocrystalline quartz Q_m over polycrystalline quartz Q_p. Few detrital biotite mica grains are also present. 132

Figure 3.42: a) PPL-view (4X): Optical micrograph showing the secondary porosity created by partial dissolution of quartz grain and calcite cement. Similarly, fracture porosity is also visible near the left corner of the picture. Large patch of late diagenetic stage thick patch of hematite cement is present (b) XPL-view (4X): Optical micrograph showing abundant altered feldspar grains of different shapes and sizes. 133

Figure 3.43: Photomicrographs showing the comparison between lowest matrix content in calcite cemented sandstone sample (a & b) and highest matrix in siltstone sample (c & d). Magnification-4X. 134

Figure 3.44: Photomicrographs showing the inherited quartz overgrowths. The thickness of overgrowth is variable and not euhedral around the grain showing its inherited nature. The black arrows indicate the dust line while red arrows show syntaxial inherited quartz overgrowths. Yellow colored arrows are indicating the presence of high relief Zircon (heavy mineral) grain in (c) and (d). a &b has 20X magnification. c & d has 10X magnification. 135

Figure 3.45: a) PPL-view (10X): Optical micrograph showing very high primary porosity and little bending in detrital biotite grains indicating towards low to moderate compaction. (b) XPL-view (10X): Optical micrograph showing perthitic texture associated with microcline grain. The surface of the plagioclase feldspar is showing flakes of sericite mica in response to hydrothermal alteration. No major cement is present except minor patches of early diagenetic pyrite cement. 136

Figure 3.46: (a) PPL-view (10X): Photomicrograph showing the remnant outline of completely dissolved grain, later replaced by hematite cement in the center of

the micrograph. (b) XPL-view (10X): A metamorphic rock fragment. Coarse-crystalline and euhedral rhombic crystals of dolomite cement is filling the intergranular pores and reducing the primary porosty. (c) PPL-view (4X): Photo micrograph showing different phases of cementation. Calcite cement (Phase-1) filled the pores and hematite cement came later (Phase-2) and filling the space created due to the dissolution of calcite cement. Secondary dissolution porosity is visible. (d) PPL-view (4X): Photomicrograph showing a polycrystalline quartz of metamorphic origin. Perthitic texture on nearby large orthoclase crystal is also visible. 137

Figure 3.47: a) PPL-view (4X): Photomicrograph showing fracture porosity and hematite cement as coating within the chert (Ch) fragment. (b) XPL-view (4X): Photomicrograph contains perthitic texture within orthoclase (O), monocrystalline quartz (Q_m), calcite cement (C) and microcrystalline quartz/Chert (Ch) fragment. (c) PPL-view (4X): A quartz rich sandstone sample with very high primary and secondary porosity. (d) XPL-view (4X): Photomicrograph showing monocrystalline quartz (Q_m), sericitized plagioclase feldspar (P_g) and chert fragment (C_h)..... 138

Figure 3.48: (a) PPL-view (4X): The primary porosity has been lost due to syndepositional euhedral to subhedral dolomite cement. A Carbonate rock fragment (CRF) is also present. Red arrows show the replacement of partially dissolved grains with hematite cement. (b) XPL-view (4X): Yellow arrows show that Coarse-mosaic dolomite cement is killing the primary porosity. 139

Figure 3.49: a) PPL-view (4X): Optical micrograph showing very low primary porosity (Blue color). Red arrows indicate towards biotite grains showing no effect of mechanical compaction as bending is absent. b) XPL-view (4X): Pre-compactional Fe-dolomite is filling primary pores and reducing the overall porosity. 143

Figure 3.50: a) PPL-view (4X): Optical micrograph showing abundant pre-compaction calcite cement filling the primary pores among framework grains. The secondary porosity has been created due to the grain and cement dissolution (blue color). Pyrite cement is engulfed by the calcite cement shows it's predate precipitation than post-date calcite cementation. (b) XPL-view (4X): cross nicols view of the same photomicrograph. 150

Figure 3.51: PPL-view (10X): Optical micrographs showing low to moderate compaction indicated by slight bending in biotite micas due to relatively low overburden pressure. Splitting of biotite grain is shown in photomicrograph (b) due to the invasion of feldspar grain. Very high primary porosity is visible between framework grains. Grain dissolution and fracture porosities are also present. Sporadic early stage pyrite cement is also visible. 152

Figure 3.52: a) PPL-view (20X): Optical micrograph is showing two booklet-like patches of kaolinite clay near the upper left part of large quartz grain. b) XPL-view (20X): Kaolinite clay patch of 50-200 micron in size. Euhedral dolomite cement is present as pore filling cement c) SEM micrograph showing the presence of honeycomb-like smectite clay as grain coating. d) SEM micrograph showing high primary porosity, secondary porosity and large crystal of altered grain near

the upper right and left corner with smectite clay as an alteration product on the corroded grain surface..... 153

Figure 3.53: (a) PPL-view (20X): High primary porosity is visible. Red arrow indicates hematite cement. (b) XPL-view (20X): Yellow arrow shows partially altered and dissolved feldspar grain. Small white arrows are indicating towards probably smectite clay coating around quartz grains to inhibit quartz overgrowth. (c) SEM micrograph showing secondary porosity in feldspar grain and semctite clay as alteration product on its surface. 154

Figure 3.54: Photomicrographs showing abraded morphology of quartz overgrowth with uneven thickness around the dust line. Magnification-10X..... 155

Figure 3.55: a) PPL-view (4X): Quartz rich sandstone cemented with finely crystalline precompactional authigenic calcite (Cc) present as pore-filling cement and filling almost all the pores. Yellow arrows indicate the cast of unknown framework grain dissolved and later replaced by calcite cement. Red arrows are indicating the secondary porosity. b) XPL-view (4X) of the same thin section. c) PPL-view (4X): Micritic calcite cement is present as fracture filling. Twinning planes are also visible. Hematite cement (phase-2) postdate the calcite cement. d) XPL-view (4X): Lamellar twinning is visible in fracture-filling calcite cement. 156

Figure 3.56: (a & b) XPL-view (10X): White arrows in optical micrographs are indicating towards rims of authigenic carbonate cement precipitated within pits of corroded boundaries of quartz grains. Finely crystalline authigenic calcite cement (Cc) occur as pore-filling occluding almost all pore spaces. A Bioclast (Bc) and

secondary porosity is visible in optical micrograph-b. The framework grains show “Floating Texture” due to the presence of precompactional calcite cement. 157

Figure 3.57: a) PPL-view (4X): Optical micrograph showing secondary porosity (red arrows) created due to partial dissolution of framework grains. Primary porosity is reduced due to cloudy dolomite cement (dc). b) XPL-view (4X): Photomicrograph showing coarse crystalline rhombs of dolomite cement (dc) present between the framework grains. Perthitic texture is present on the surface of orthoclase grain (O). 158

Figure 4.1: Paragenetic sequence summary chart showing the relative occurrence of diagenetic events in the Burqan Formation. 170

Figure 4.2: The submarine fan model of the Burqan Formation in the Midyan region, NW Saudi Arabia..... 171

LIST OF TABLES

Table 1: Summary of lithofacies description identified in stratigraphic section-3 of the Burqan Formation in Midyan Basin. 31

Table 2: Summary of lithofacies description identified in stratigraphic section-4 of the Burqan Formation in Midyan Basin. 43

Table 3: Summary of lithofacies description identified in stratigraphic section-5 of the Burqan Formation in Midyan Basin. 72

Table 4: Summary of lithofacies description identified in stratigraphic section-6 of the Burqan Formation in Midyan Basin. 90

Table 5: Summary of lithofacies description identified in stratigraphic section-7 of the Burqan Formation in Midyan Basin. 103

Table 6: Summarized modal analysis (framework grain, diagenetic minerals, porosity types, bioclasts, matrix content, heavy minerals and Pickering Facies) of 70 representative sandstone and siltstone samples from Burqan Formation..... 121

Table 7: The table showing average composition of major framework grains in all samples of the Burqan Formation. 124

Table 8: Summarized XRD analysis results of representative sandstone samples from Burqan Formation. 144

Table 9: Summarized quantitative results obtained from electron microprobe analysis (EMP) for various type of carbonate cements in sandstone samples of Burqan Formation.... 149

ABSTRACT

The Nutaysh member of the Burqan Formation makes up the syn-rift infill of the Midyan Basin located in the northwest of Saudi Arabia during early Miocene. The detailed lithofacies analysis was performed on five well-exposed outcrops of these siliciclastic deposits in the proximity of northern, central and southwestern margin of the Midyan basin. It allowed the identification of four facies associations and thirteen sub lithofacies by using descriptive lithofacies identification scheme of Pickering *et al.*, 1986. The submarine fan system with variable paleocurrent direction can be interpreted based on the distribution of facies association and architectural framework observed in the stratigraphic sections. The compositional analysis of seventy representative thin sections of sandstone and siltstone was carried out by mean of modal analysis and petrographic characterization. The composition of majority of the studied samples from the Nutaysh member falls in the category of subarkose, arkose and lithic arkose whereas few samples are sublitharenite and feldspathic litharenite compositionally. The petrographic characterization and modal analysis suggests the presence of igneous basement, metamorphic and sedimentary rocks in the provenance region. The eo- and telodiagenetic stages were interpreted from petrographic features, scanning electron microscopic micrographs and X-ray diffraction techniques. The samples shows low to moderate degree of compaction. Pre-compaction calcite, Fe-dolomite and dolomite cements constitutes 5-20 percent of the whole rock volume in cemented samples. The diagenetic clays are less than 1 percent by volume. The average visual porosity ranges from 8-22 percent.

ملخص الرسالة

الاسم الكامل: محمد نافيد طاهر بوت.

عنوان الرسالة: دراسة السحنات الرسوبية، الوصف الصخري وعمليات النشأة المتأخرة لعضو نوتيش بمتكون برقان ذو عمر الميوسين في حوض مدين، شمال غرب المملكة العربية السعودية

التخصص: الجيولوجيا.

تاريخ الدرجة العلمية: ديسمبر 2017

يتكون عضو نوتيش بمتكون برقان من رسوبيات متزامنة مع حدوث الصدع أثناء عمر الميوسين التي تملأ حوض مدين بشمال غرب المملكة العربية السعودية. تم وصف السحنات الصخرية لخمس مكاشف لهذه الرسوبيات الفتاتية بالقرب من شمال، وسط، وجنوب غرب حوض مدين. وتم التعرف على أربع مجموعة سحنات و ثلاثة عشر سحنة صخرية طبقا لمخطط بيكرنج عام 1986. وبناءً على مجموعة السحنات والإطار المعماري الملاحظ في الرسوبيات، تم تفسيرها على أنها تمثل مراوح البحرية متعددة الاتجاهات. وبناء على تحليل مكونات سبعين شريحة دقيقة لعينات الصخور الرملية والغرين، بواسطة التوصيف الصخري وعد النقاط، تم تصنيف أغلب العينات المدروسة كدون أركوز، أركوز، وأركوز حجري مع وجود قلة من أصناف دون أرينايت صخري و أرينايت صخري فلسباري. وهذا يشير إلى وجود صخور نارية، متحولة ورسوبية في صخور المصدر. وتم إيجاد عمليات نشأة متأخرة (أولية ونهائية) بناءً على تحاليل المجهر الإلكتروني وجهاز حيود الأشعة السينية.

1 INTRODUCTION

Large number of sedimentary basins around the world contain siliciclastic turbidites deposited in a submarine fan environment that are part of economically significant petroleum reservoirs (Shanmugam and Moiola, 1988; Weimer and Link, 1991; Li *et al.*, 2014). The geometry and reservoir properties of these hydrocarbon-bearing reservoirs are strongly affected by their depositional settings. The turbidite reservoir units occur in tectonic settings ranging from lacustrine, oceanic rift basins, post-rift related intracratonic settings to forearc, foreland and transform settings related basins (Weimer and Link, 1991; McCaffrey and Kneller, 2001; Li *et al.*, 2014). The last few decades, deep-sea turbidite reservoir facies such as the Burqan Formation deposited along the passive margin of the Red Sea have become the primary focus for future hydrocarbon exploration in Saudi Arabia. Regardless of discoveries of huge oil fields along passive margins around the world, still significant number of oil-fields need to be discovered (Pettingill, 1998; Anderson *et al.*, 2000; Mansurbeg *et al.*, 2008).

To develop effective exploration schemes, it is very important to understand the factors which govern the quality of the reservoir sands and their potential as commercial hydrocarbon accumulations (Weimer and Link, 1991). Rift-related sedimentary basins, such as Midyan Basin located in the NW Saudi Arabia, host significant mineral and hydrocarbon deposits as well as geothermal energy resources. Large petroleum provinces are related to the rift systems such as Red Sea-Gulf of Suez Basin rift system, Dnieper Donets grabens, North Sea rift basin, Mississippi and Niger deltas (Ziegler, 1992). Rift

basin types range from amalgamated continental/marine, shallow to deep marine basins. The architecture of syn-rift sediments is extremely variable in each type of passive margin basin due to continuous variations in sediment supply, accommodation space and relative sea level during progressive rifting. Subsidence and rotation of the basin floor have major impact while eustatic sea level variations have a minor impact on creating the accommodation space (Ravnås and Steel, 1998).

This research project concentrates on the detailed description of different lithofacies, their depositional processes and the effect of diagenetic changes on the reservoir quality of the sediments of the Burqan Formation. Detailed sedimentological logs were constructed to describe different lithofacies and their related depositional processes whereas petrographic studies were carried out to understand the diagenetic changes of the Nutaysh member of the Burqan Formation. These tasks have been achieved with geochemical and sedimentological approach. The well-exposed outcrops of the Burqan Formation are located in the Midyan Peninsula, NW Saudi Arabia. The Burqan Formation comprises sand and conglomerate dominated lower Nutaysh member and calcareous mudstone dominated upper Subayti member. It has lower unconformable contact with Musayr Formation of the Tayran group while it is unconformably overlain by Kial Formation of Maqna group.

The white digits on false-color Landsat image shows the outcrop locations of the Burqan Formation (Figure 1.1).

1.1 Thesis Format

This thesis consists of five main chapters. The 1st chapter is an introductory part which covers general introduction of petroleum systems, rift basin types and architecture of

sediments related to rift systems around the globe, background and problem statements which provide motivation to carry out this research, primary objective of the research as well as research plan. Chapter (2) consists of thorough review of the published literature related to tectonic evolution of the Red Sea and the Midyan basin, lithostratigraphy including basement and sedimentary successions. This chapter will give a brief review of research conducted by different researchers on different formations and disciplines of geology such as micropaleontology, geochemistry and etc in the Midyan Basin. The 3rd chapter deals with the outcomes of the research including detailed description of different lithofacies and their depositional processes and results related to the diagenesis of the Burqan Formation. The second last chapter (Chapter-4) is related to the discussion and integration of the field and lab results. Chapter (5) is conclusive which includes the research findings along with the answers to the posed queries brought in this section.

1.2 Background and problem statement

The Midyan Basin provides an excellent opportunity to access complete Neogene sedimentary succession including the sediments of the early Miocene Burqan Formation. Movement along syn-depositional basin margin faults, salt tectonics and strike slip movement associated with the Red Sea rifting (Tubbs *et al.*, 2014) influence the exposure quality of the sediments. Up to now no detailed research has been done on defining the lithofacies and their depositional processes, as well as the detailed sedimentological and diagenetic evolution of the Burqan Formation. Only a few studies of limited datasets related to sedimentology and reservoir quality prediction were published by Al-Ramadan *et al.* (2013) and Al-Laboun *et al.* (2014). The main objective to select the Burqan

Formation to detail the sedimentology and diagenetic history of the Burqan Formation. These sediment were selected while these sediments are time equivalent to those of the Rudeis Formation which in the Sinai Peninsula in the Gulf of Suez is acting as a major reservoir in several oil fields (Alsharhan, 2003). Hence, to understand the reservoir potential and architecture of the Burqan Formation can be of help to predict the distribution of the reservoir quality in subsurface in Saudi Arabian Red Sea region.

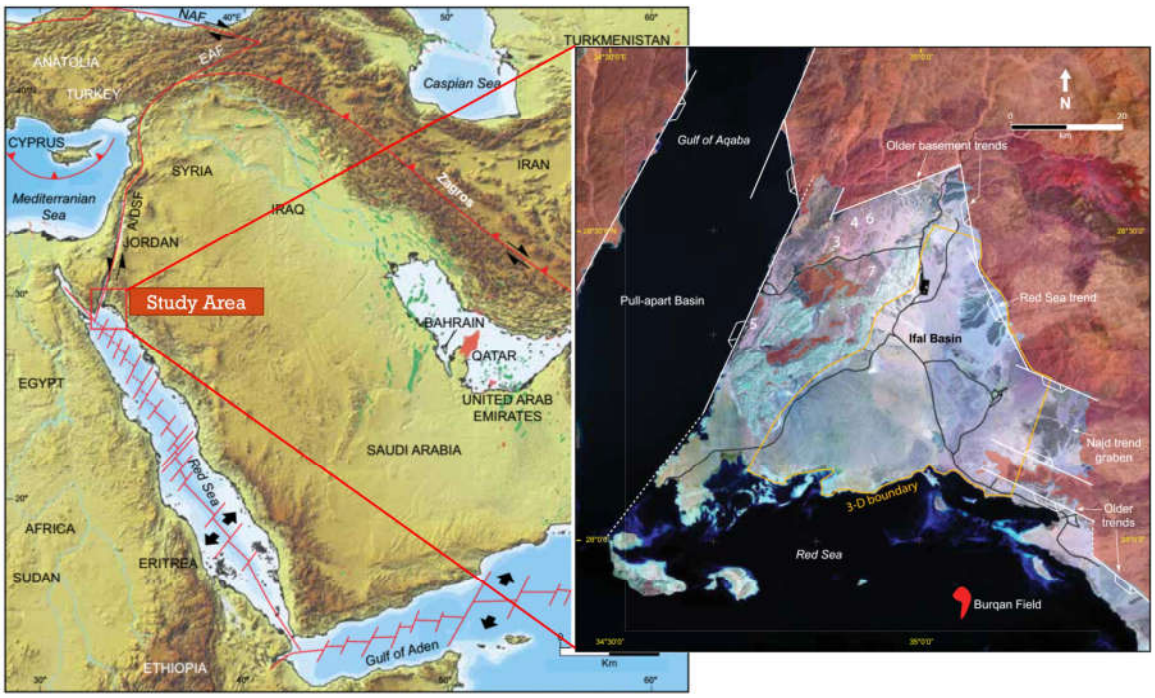

Figure 1.1: Tectonic map of the Arabian Plate (After Sharland *et al.*, 2001). The red box marks the location of the Midyan Peninsula (Study Area) in the NW Saudi Arabia. Magnified false-colored Landsat image of the study area (Modified after Tubbs *et al.*, 2014). Digits show the location of studied outcrops.

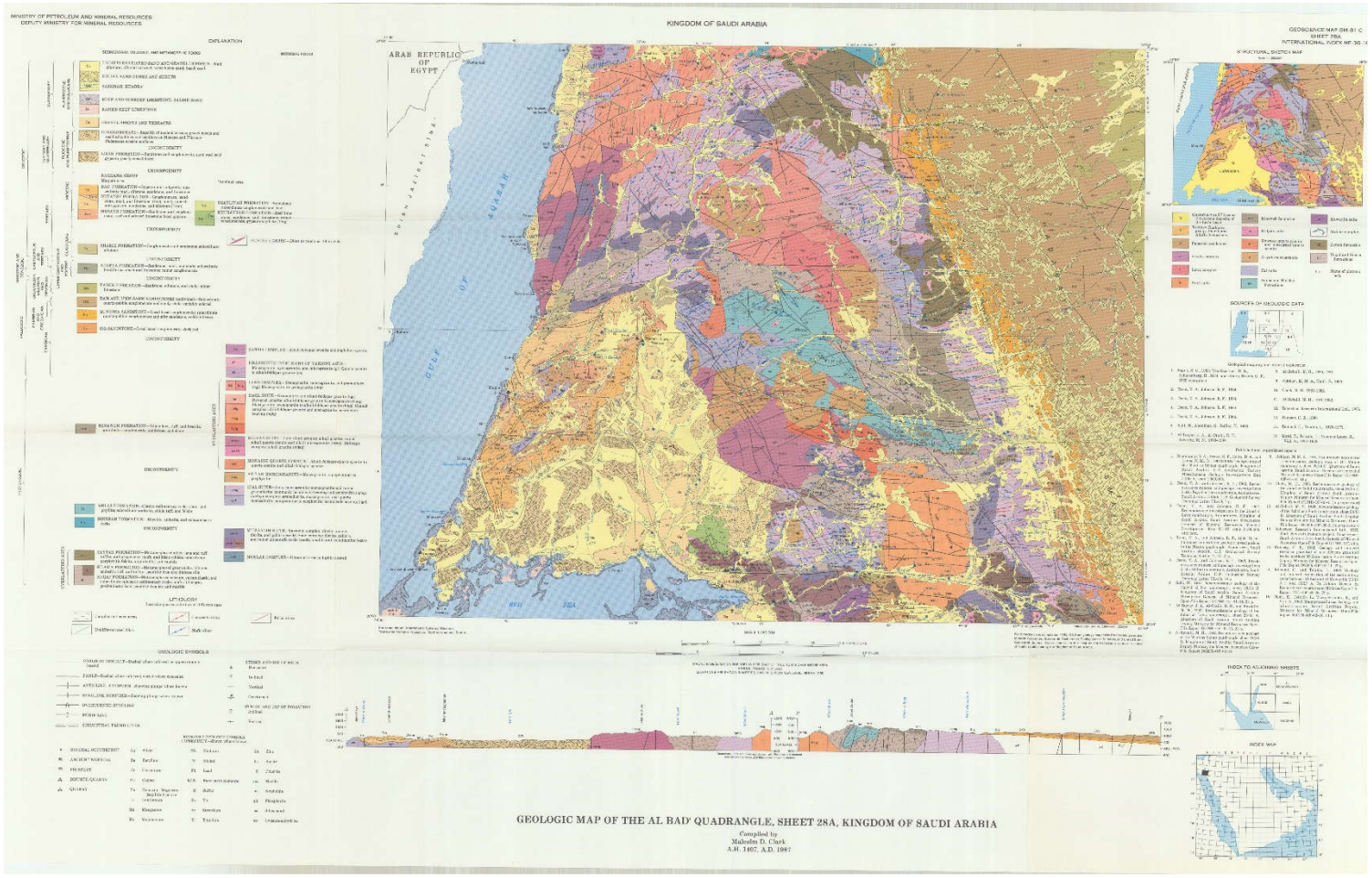

Figure 1.2: Geological map of the Al Bad' quadrangle (Midyan region), sheet 28A, NW Saudi Arabia. (Clark,1986)

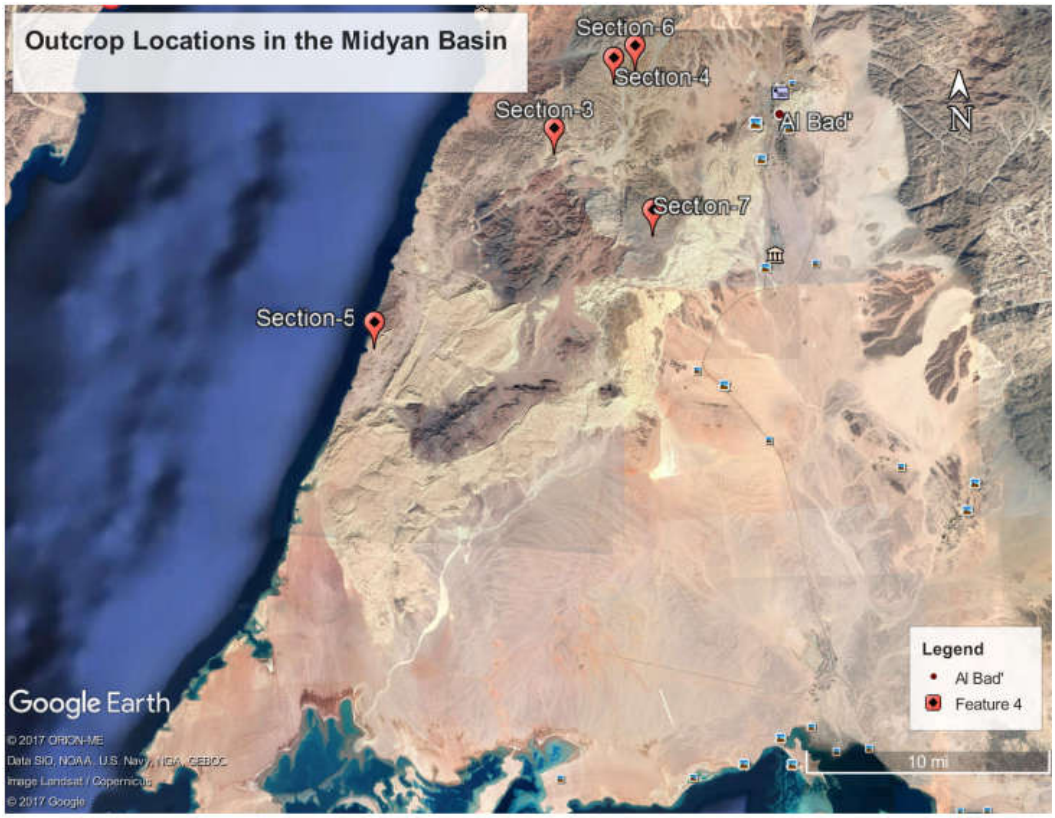

Figure 1.3: Location of representative outcrops of the Burqan Formation in the Midyan region, NW Saudi Arabia (Courtesy to Google Earth Pro ®).

1.3 Research Objectives

The main objective of the project was to enhance the understanding of the distribution of reservoir quality within the sediments of the Burqan Formation in the Midyan Basin. To achieve this objectives, the following targets were set:

1) Identification and description of different lithofacies and related petrographic and diagenetic alternations of Burqan Formation in Midyan region from different parts of the basin.
2) Interpretation of the diagenetic and depositional processes of the various lithofacies.
3) Reconstruct the diagenetic history of the sediments of the Burqan Formation, to develop the paragenetic sequence showing the timing of various phases of diagenesis.

The aforementioned analysis aims to evaluate the reservoir potential of Burqan Formation in the subsurface.

1.4 Research Approach

This research project involves fieldwork and laboratory analysis. A reconnaissance fieldwork of two weeks was conducted in the Midyan Basin to understand the distribution of different lithofacies and to select well-exposed outcrops to collect representative samples for detailed sedimentological studies.

In 2015-16, two other fieldworks were carried out in different parts of the Midyan Peninsula to measure and describe the selected stratigraphic sections in detail. More than 200 representative rock samples were collected from sandstone and mudstone intervals

from five stratigraphic sections to evaluate the impact of lithological variations, diagenesis and geochemical parameters on reservoir quality of the Burqan Formation.

The research plan to achieve the aims of this research is as follows:

1. A thorough review of the available published literature regarding the reserach conducted in the Midyan region.
2. Carrying out the fieldwork in the Midyan Peninsula to analyze the distribution of various lithofacies, selection and detailed description of well-exposed outcrops, interpretation of depositional processes of each lithofacies based on the distinguished features such as bed thickness, vertical grain size profile and sedimentary structures (Figure 1.4), characterization of architectural elements as well as collecting representative samples.
3. Thin section preparation for all the samples to conduct petrography, and electron microprobe analysis to better understand the mineralogy of framework components, altered grains and various diagenetic cements.
4. Petrographic studies involve the Modal Analysis by counting 300 points on each thin section to determine the mineralogical contents and textural relationship, geometry and distribution of various cements and porosities within the rock samples.
5. Selection of representative samples for geochemical analysis such as XRD, SEM and electron microprobe analysis to characterize the detrital and diagenetic components as well as to understand the timing of diagenesis within the Burqan Formation.

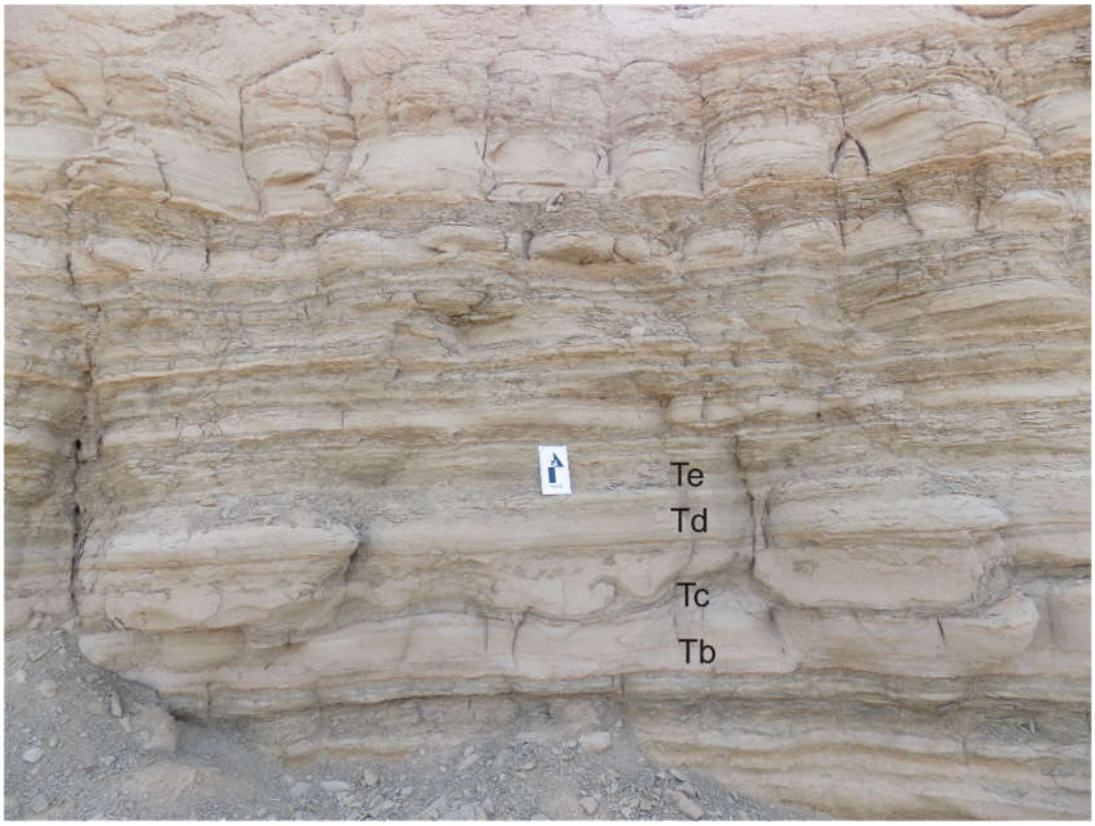

Figure 1.4: Field photograph showing sedimentary structures observed in Nutaysh Member of the Burqan Formation located on the west side of the Burqan valley.The outcrop shows the typical divisions of the Bouma Sequence.

2 LITERATURE REVIEW

2.1 Geologic Background

Reviewing the published literature related to Miocene successions of Saudi Arabian part of the Red Sea reveals the presence of limited documented research. For instance, describing different lithofacies, their depositional processes and impact of diagenesis on reservoir quality of the Burqan Formation is poorly understood in the Midyan region. The sedimentary successon on the western coast of the Red Sea is almost same as in the Midyan Basin (Dullo et. al., 1983). However, the correlative sedimentary succession on Sanai Peninsula in Egypt which was deposited under similar geologic and tectonic history is well explored. The lower part of the Rudeis Formation of Egypt is regionally equivalent to the Burqan Formation of Saudi Arabia (Bayer *et al.*, 1988; Hughes and Johnson, 2005) (Figure 2.1).

The early Miocene Burqan Formation in the Midyan Basin inhibits two members. The lower Nutaysh member is dominated by conglomerates and sandstones while the upper member consists of mud-rich sediments of the Subayti member (Figure. 2.2). The Burqan Formation was deposited in a submarine fan environment. These submarine fan deposits are stratigraphically sandwiched between underlying shallow marine carbonate deposits of the Musayr Formation and the overlying evaporite deposits of the Kial Formation of the Maqna group. The name of the Burqan Formation was derived from the exploration well drilled by Auxerap-Tenneco in Burqan Field located offshore in the Red Sea (Hughes and Johnson, 2005).

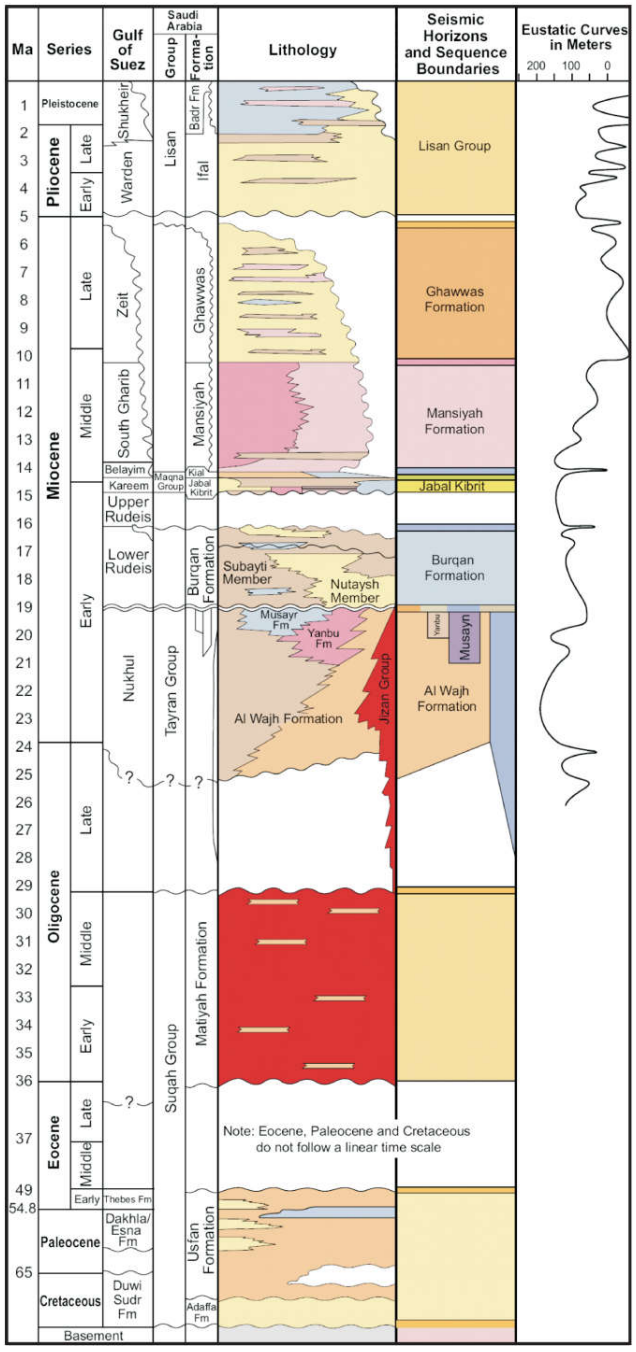

Figure 2.1: Generalized stratigraphic column of different lithostratigraphic units of Saudi Arabian Red Sea region and neighboring Gulf of Suez (Hughes and Johnson, 2005). The Burqan Formation of Saudi Arabia is correlative to the Lower Rudeis Formation of Gulf of Suez, Egypt.

The age assigned to the Burqan Formation ranges from Late Aquitanian to Early Burdigalian based upon the calcareous nano-fossils and index planktonic foraminifera (Hughes and Johnson, 2005).

2.2 Tectonic Evolution of the Midyan Basin

The rifting phase which created the Gulf of Aden and the Red Sea occurred since Permian time. It began with the break-away of Gondwana from Pangea along the continental margins of the Paleotethys and Neotethys Ocean (Stampfli *et al.*, 2001). The actual rifting in the Red Sea dates back to 34-33 Ma (Figure 2.3) (Lyberis, 1988; Hughes and Johnson, 2005), which is evidenced by syn-rift basalts that were encountered during drilling in Jeddah and could be dated to be between 34 and 33 Ma. Similarly, late Oligocene nanno-fossils have been encountered within the early syn-rift section during offshore drilling in the Red Sea (Hughes and Johnson, 2005).

Three major structural episodes controlled the development of the Midyan Basin through time (Stampfli et al., 2001; Bosworth et al., 2005). Mantle upwelling initiated the rifting along the Red Sea, which increased the movement of Arabian Plate in NE direction resulting in subduction along the Zagros Mountains. At approximately 5 Ma, the counterclockwise rotation of the Arabian Plate resulted in the formation of the Gulf of Aqaba/Dead Sea strike slip fault and rifting along the Gulf of Aden. Finally, drifting of the Arabian plate continued along with seafloor spreading in the Red Sea during Pliocene to Pleistocene times (Polis *et al.*, 2005; Tubbs *et al.*, 2014).

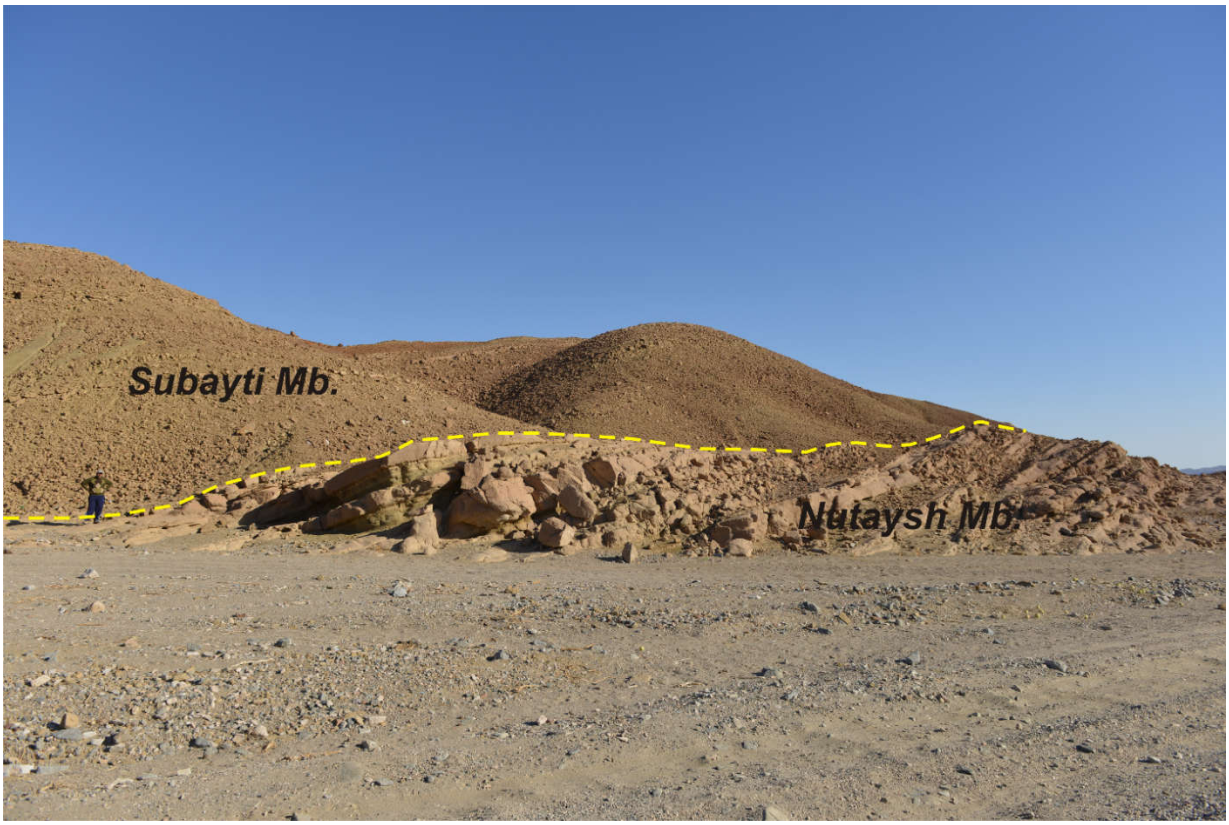

Figure 2.2: Field photograph showing the lower sand-dominated Nutaysh member (right) and the upper, shale-dominated, Subayti member as found in section 4 in the central part of the Midyan Basin. Person as scale.

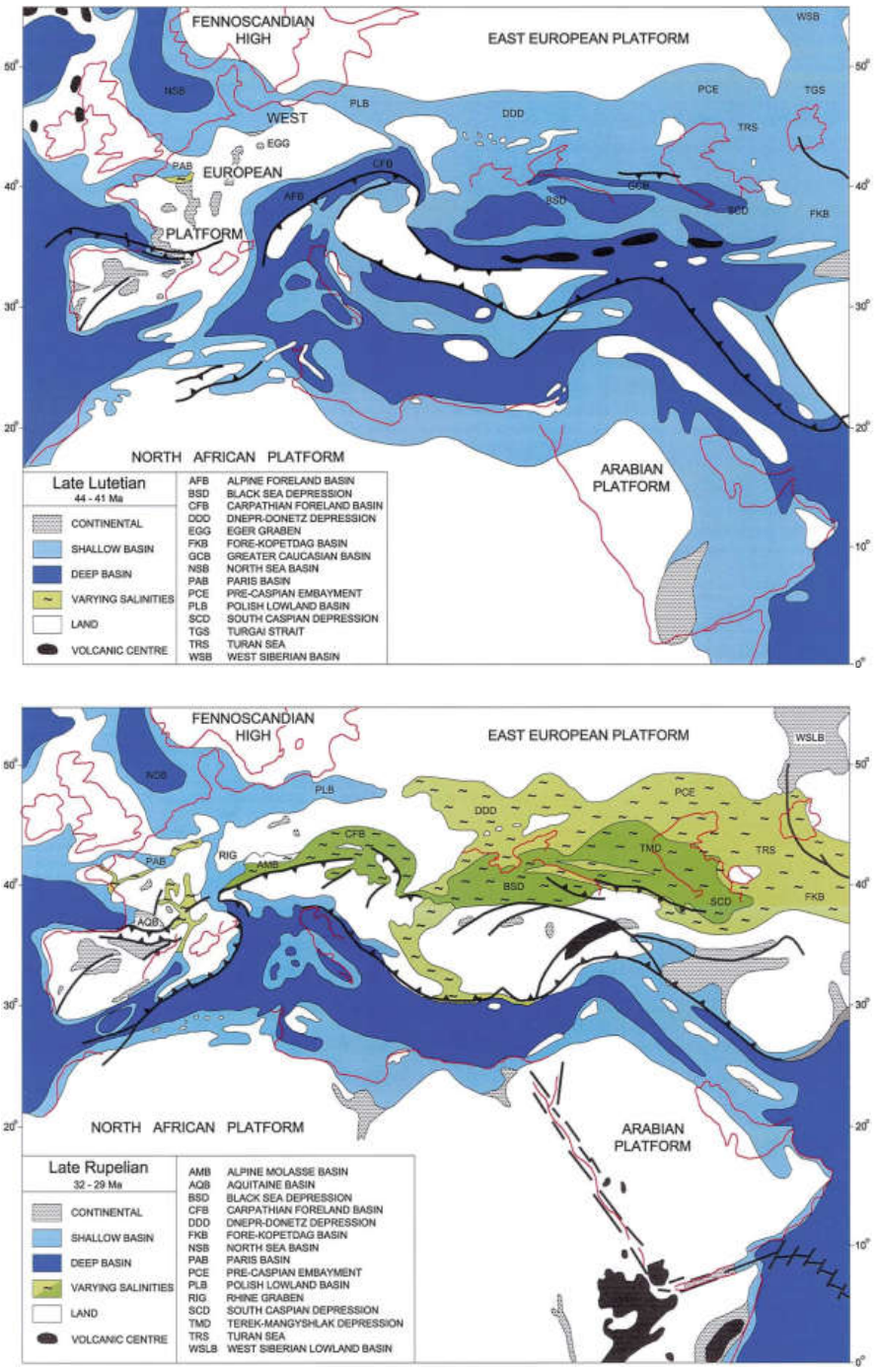

Figure 2.3: The paleogeographic reconstruction maps show the separation of the Arabian Platform from African Plate during the Late Rupelian (32-29 Ma; Early Oligocene). Red lines show the plate boundaries whereas bold black lines mark the major fault zones (Meulenkamp and Sissingh, 2003).

2.3 Tectonic Elements of the Midyan Peninsula

The Midyan Peninsula is bounded to the west by twenty six kilometers (26 km) wide pull-apart basin situated in the Gulf of Aqaba. The Dead Sea Transform Fault is acting as the bounding fault marking western border of the Midyan Basin. The northern and eastern sides of the Midyan Basin are bounded by normal faults along Proterozoic basement rocks. In the south, the Midyan basin is bordered by the Red Sea. The rift bounding master faults trending NW-SE correspond to the orientation of the Red Sea rifting while the NE-SW trending faults follow the trend of Dead Sea-Gulf of Aqaba transform fault (Figure 1.1). Additionally, several fault trends have been observed in the Midyan basin which follow a NE-SW trend aligned with the older Najd Fault System (Bayer *et al.*, 1988; Tubbs *et al.*, 2014) (Figure. 1.1).

2.4 Stratigraphy of the Saudi Arabian Red Sea

There are six sub-basins along the Saudi Arabian Red Sea margin starting with the Midyan sub basin in the north to the Jizan coastal plains in the south. The age of the lithostratigraphic units deposited in these sub-basins range from Cretaceous to Pleistocene. The sedimentary successions rest on Proterozoic Basement rocks. The sedimentary units have been divided into pre, syn and post rift sediments (Hughes and Johnson, 2005).

2.4.1 Proterozoic Basement

The oldest units exposed as rift basin margins are Proterozoic Basement rocks which are ultramafics, metasedimentary, metavolcanics and granitic in compostion. These basement rocks contain rhyolite, basalt and dolerite dikes (Figure 2.4). According to Gardner *et. al.*

(1996), these basement rocks originate back to a volcanic arc, 600 Ma to 700 Ma in age. Exploration drilling revealed the fractured nature of the igneous basement. The granitic composition of the igneous basement indicates that originated from continental rifting instead of spreading along the oceanic crust (Bosworth, 1993; Sultan *et al.*, 1993).

2.4.2 Pre-Rift Successions

The pre-rift sediments, the Suqah group, unconformably overly the Proterozoic Basement. The Mesozoic units were formally described for the first time by Clark *et al.* (1986). These sediments were deposited in both continental and marine environments (Bayer *et al.*, 1988). The first pre-rift unit is the Adaffa Formation, which consists of cross-bedded, yellow to reddish sandstones (Figure 2.5). A thin layer of conglomerates is present at the base of the sandstones and is composed of pebbles and cobbles derived from the Proterozoic basements and older Phanerozoic sedimentary rocks. The depositional environment of the Adaffa Formation is interpreted as a "fluvial system" based on the presence of phosphate nodules in shale-rich layers, fining upward succession along with the nature of cross-bedding found in the strata. The age assigned to the Adaffa Formation is Upper Cretaceous based on the presence of microfossils, turtle plates and bones of Sauropod dinosaurs (Hughes and Johnson, 2005). The Usfan Formation is the second pre-rift siliciclastic succession consisting of shallow marine sediments. Lithologically, the Usfan Formation consist of sandstone, marly limestone, conglomerates and coquinas. The lower and upper contacts of the Usfan Formation with the Adaffa Formation and the volcanics of the Matiyah Formation are unconformable respectively. The sediments of the Usfan Formation

are Cretaceous to Paleogene in age, which is based on the presence of specific shark teeth and molluscs (Hughes and Filatoff, 1995; Hughes and Johnson, 2005).

Figure 2.4: Field photograph showing the Proterozoic basement in the Midyan Basin. The igneous basement is intruded by dark colored dolerite and basaltic dikes.

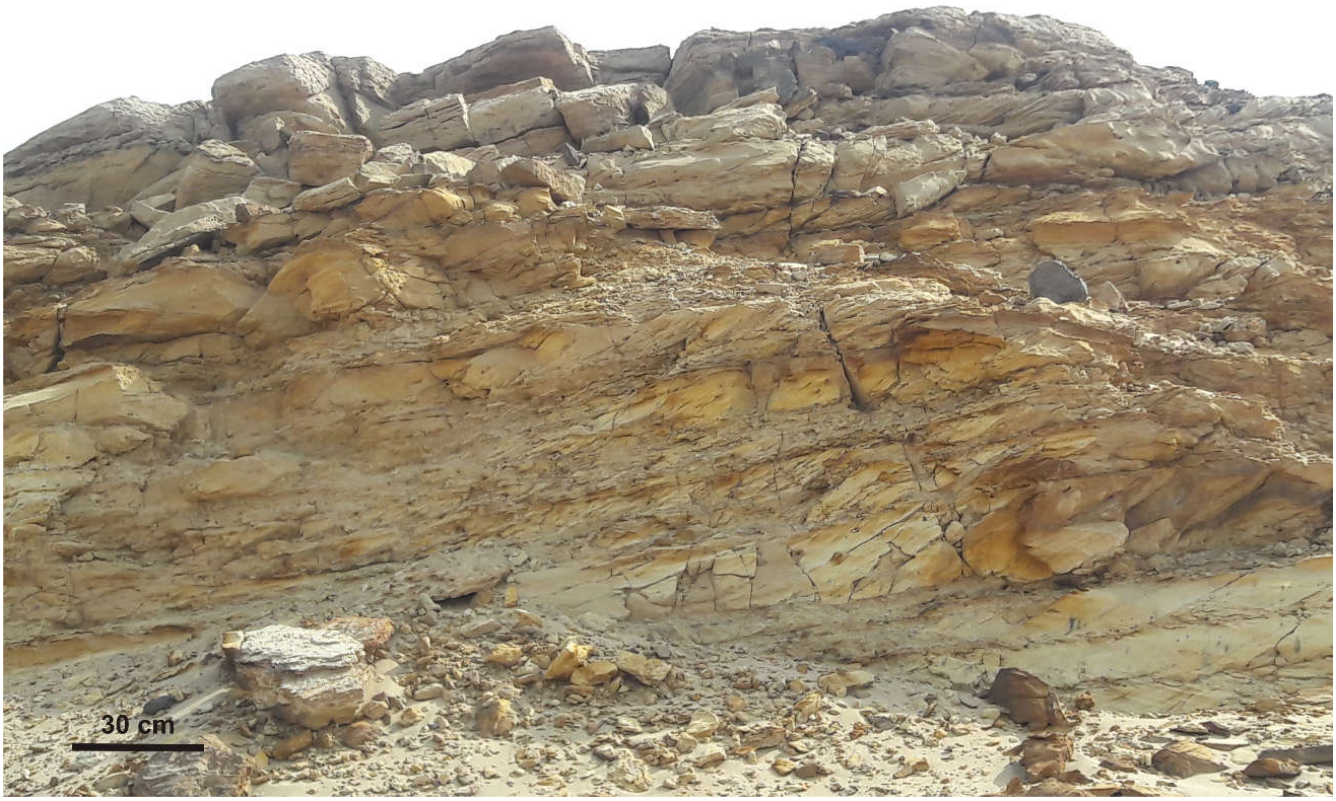

Figure 2.5: Outcrop of cross-bedded sandstone of the Upper Cretaceous Adaffa Formation in the Midyan region.

2.4.3 Syn-Rift Successions

The Neogene syn-rift sedimentary succession exhibits significant lithological heterogeneity. These sequences were formally described and subdivided into lithostratigraphic units for the first time by Dullo *et al.* (1983) and later the lithological nomenclature was revised in the Midyan region by Clark *et al.* (1986). The Tayran Group comprises the Al Wajh, Musayr and Yanbu Formations which unconformably overlie the volcanics of the Matiyah Formation (Hughes and Filatoff, 1995; Hughes and Johnson, 2005). The earliest Miocene sandstone of the Al Wajh Formation exhibit the first syn-rift

sedimentary succession deposited in a marginal marine environment. The Al-Wajh Formation consists of red colored siliciclastic succession devoid of fossils. The mineral composition and proximity to the igneous basement suggests that it was derived from the erosion of basement rocks. The Al Wajh Formation conformable overlies the Yanbu Formation in the Midyan region. At some localities, the Al-Wajh Formation is unconformably overlain by the shallow marine carbonates of the Musayr Formation or deep marine sediments of the Burqan Formation. An Early Miocene age has been assigned to the Al-Wajh Formation based on the presence of pollens. The middle sedimentary unit of the Tayran Group, the Yanbu Formation, shows evaporites (anhydrite, halite with minor shale). These thick early Miocene evaporites were deposited in locally restricted onshore basins. Its contact with the sediments of the Al-Wajh Formation is conformable while the upper contact with the Burqan Formation is unconformable. Based on the stratigraphic position above the Al-Wajh Formation and the presence of palynoflora found in Yanbu Formation, an Early Miocene is attributed to these sediments. The Musayr carbonates form the youngest sedimentary succession of the Tayran Group. This formation shows mixed carbonate-clastic deposits with basal calcareous sandstone overlain by grain/pack/wackestone. These deposits are rich in macrofossils such as oysters and index micro fossils such as *Miogypsina* sp. and *Miogypsinoides* sp. Based on the presence of Miocene index fossils, an Early Miocene age is assigned to the sediments of the Musayr Formation (Hughes and Filatoff, 1995; Hughes and Johnson, 2005).

During the early Miocene, deep marine turbidites forming the Burqan Formation were deposited in response to rapid subsidence of the Midyan basin. Lithologically, the Burqan Formation consists of the lower massive sand and conglomerate-dominated Nutaysh

member and an upper planktonic foraminifera bearing mud-rich Subayti member deposited in a deep marine submarine fan environment (Hughes and Johnson, 2005; Abdullatif and Olagoke, 2010; Al-Ramadan et. al., 2013) (Figure 2.2). The sandstone units of the Burqan Formation are friable in nature. The informal name recorded in an unpublished Saudi Aramco reports for the Burqan formation is *"Globigerina marls"*. The Burqan Formation has a lower and upper unconformable contact with the sediments of the Tayran and Maqna Group (Jabal Kibrit Formation and Kial Formation), respectively. An Early Miocene age has been given to the Burqan Formation due to the presence of index calcareous nannofossils and planktonic foraminifera (Hughes and Filatoff, 1995; Hughes and Johnson, 2005).

The syn-rift Maqna Group consists of the older Jabal Kibrit Formation of early to middle Miocene age and the younger Middle Miocene Kial Formation. The sedimentology of Wadi Waqb member of Jabal Kibrit Formation has been previously described in several studies (Dullo et. al., 1983; Clark, 1986; Hughes and Johnson, 2005; Hussain and Al-ramadan, 2009; Hughes, 2014). Koeshidayatullah *et al.* (2016) described the depositional cyclicity and complex internal architecture of the carbonate platform deposits of Wadi Waqb member in the Midyan Basin. The sediments of the Kial Formation represent evaporite deposits with gypsum and anhydrite acting as a seal in the central part of the Midyan basin. The sediments of the Maqna group outcrop along the eastern and western borders of the Ifal Plain in the Midyan Peninsula. The upper contact of the Kial Formation is conformable with the overlying sediments of the Mansiyah Formation. The Maqna Group unconformably overlies the clastic deposits of the Tayran Group. Because of local palaeotopographic variations the upper part of this group might be missing. Due to the

changes in the palaeotopography of the faulted blocks, the Mansiyah Formation at places rests unconformably upon the Proterozoic Basement (Hughes and Johnson, 2005).

The Ghawwas Formation is the youngest siliciclastic-evaporite succession of the syn-rift system. It is composed of carbonates, evaporites deposited in restricted environments, minor claystone and conglomeratic sandstone. It is unconformably overlain by the sediments of the post-rift Lisan Group. Its depositional environment was interpreted as marginal marine to shallow marine environments (Hughes and Johnson, 2005).

2.4.4 Post-Rift Successions

The post-rift stage sediments are represented by the Lisan Group that consists of siliciclastic deposits of the Ifal Formation and carbonate deposits of the Badr Formation. This group contains sediments deposited in a fluvial system that was active during the opening of Gulf of Aqaba during the early Pliocene. Based on the stratigraphic position in the outcrops above the Ghawwas Formation, Pliocene to Pleistocene ages are assigned to the Lisan Group (Purser, Philobbos and Soliman., 1990; Hughes and Filatoff, 1995; Hughes and Johnson, 2005).

3 RESULTS

3.1 Facies Analysis

Total of five (5) stratigraphic sections are made by detailed description of the Nutaysh Member of the Burqan Formation in the Midyan region for detailed sedimentological studies. These sections are located near the northern, eastern, central and southwestern margins of the Midyan Basin (Figure 1.1 & Figure 1.3). The stratigraphic sections were selected to identify the variability in the facies deposited in the Midyan Basin. The facies scheme used for facies analysis is based on Pickering *et. al.,* 1986. Each main class of the lithofacies (i.e; Facies-A) is identified based on grain size variations while sub-class is identified by the internal disorganized (A1) or organized structure (A2) of its constituent sedimentary beds. The described facies within the Burqan Formation include facies class-A consists of gravel and pebble size sediments, facies class-B consists of sand-sized grains, facies class-C shows interbedded sand-mud intervals whereas facies class-E consists of mud and clays (Pickering *et al.*, 1986). Facies Class-D has not been observed in the described outcrops. Total thirteen (13) sub classes of lithofacies has been identified. The detailed description of characteristic features of each lithofacies in each measured stratigraphic section is explained below.

3.1.1 Stratigraphic Section 3

The stratigraphic section-3 is located NNW of Al Bad' town (loc: 28°28'14.4" N, 34°51'09.3" E) (Figure 1.3). Mixed siliciclastic-carbonate lithofacies are present in the upper part of this section, which have not been observed at any other locality in the Midyan region. The presence of the carbonate unit will help to understand the paleotopography of the basin during the deposition of Nutaysh member of the Burqan Formation. The eastern side of the hill consists of this outcrop has NS trending fault and the carbonate units are absent on the other side of the fault.

This stratigraphic section is 125 meters thick and composed of coarse-grained siliciclastic facies and upper mixed siliciclastic/carbonate to carbonate facies (Figure 3.6). The siliciclastic facies were deposited by variety of single of composite gravity driven processes including traction, debris flow and turbidity currents.

The contact between the underlying shallow marine carbonate deposits of the Musayr Formation and overlying coarser turbidite facies is unconformable. This contact is marked by the presence of strong erosional surface (Figure 3.1). This erosional surface is overlain by the 5-6 m thick poorly sorted conglomerate grading upward into very coarse-grained pebbly sandstone. Above the sandstone unit, an approx. one meter thick light greenish gray shale is present. The first 115 m succession within section-3 consists of conglomerate, sandstone and two interbedded shale intervals. These successions are arranged in two fining upward sequences (Figure 3.2). Each sequence starts with a sharp scoured surface which is overlain by a conglomerate or pebbly sandstone unit. The conglomerates usually occur as lenses at the base of the channels which are up to 7 m thick, massive, laterally

continuous and internally graded layers (Figure 3.3). The pebbles have been largely derived from the igneous basement. Clasts derived from the Musayr limestone were observed at few places.

The conglomerates grade upward into the sandstones, which form the primary part of section-3. The thickness of sandstone units range from 10 to 15 meters and show a gradual decrease in bed thickness and grain size upward. The main part of the interval is composed of parallel planar-bedded, coarse-to medium-grained, well-sorted and friable sandstone which is overlain by thin-bedded, fine-to very fine-grained and bioturbated sandstone. The topmost 15 m thick sandstone is massive, partly thick-bedded, coarse-to medium-grained, well sorted, friable, and strongly bioturbated by vertical burrows (Figure 3.4).

The carbonate unit succeeds the bioturbated sandstone unit and is 11.5 m thick. The lower 1.5 m contains broken echinoid shells. The overlying unit is 10 m thick and consists of limestone interbedded with gray to cream colored calcareous mudstone and shale. The limestone is completely made up oyster shells (Figure 3.5).

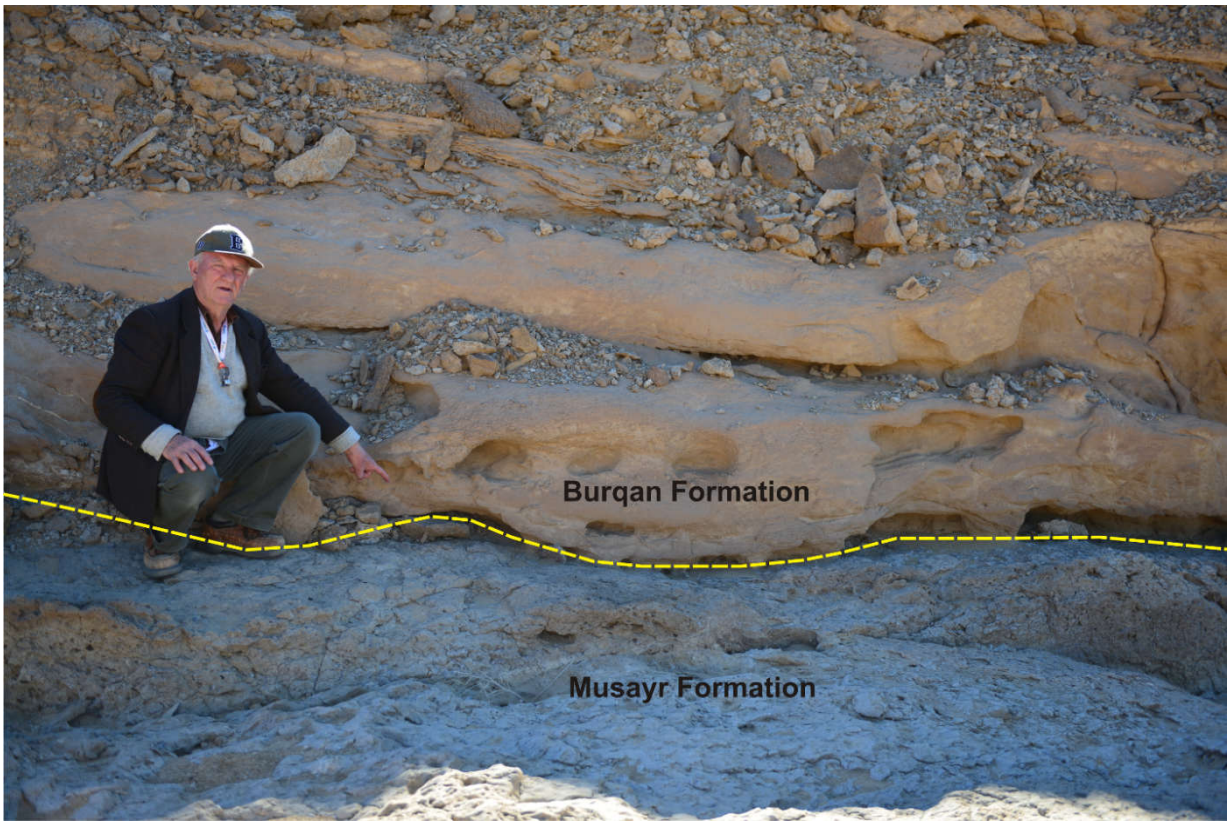

Figure 3.1: Field photograph showing the erosional, unconformable contact between the sediments of the Musayr Formation and the Burqan Formation at the base of Section-3.

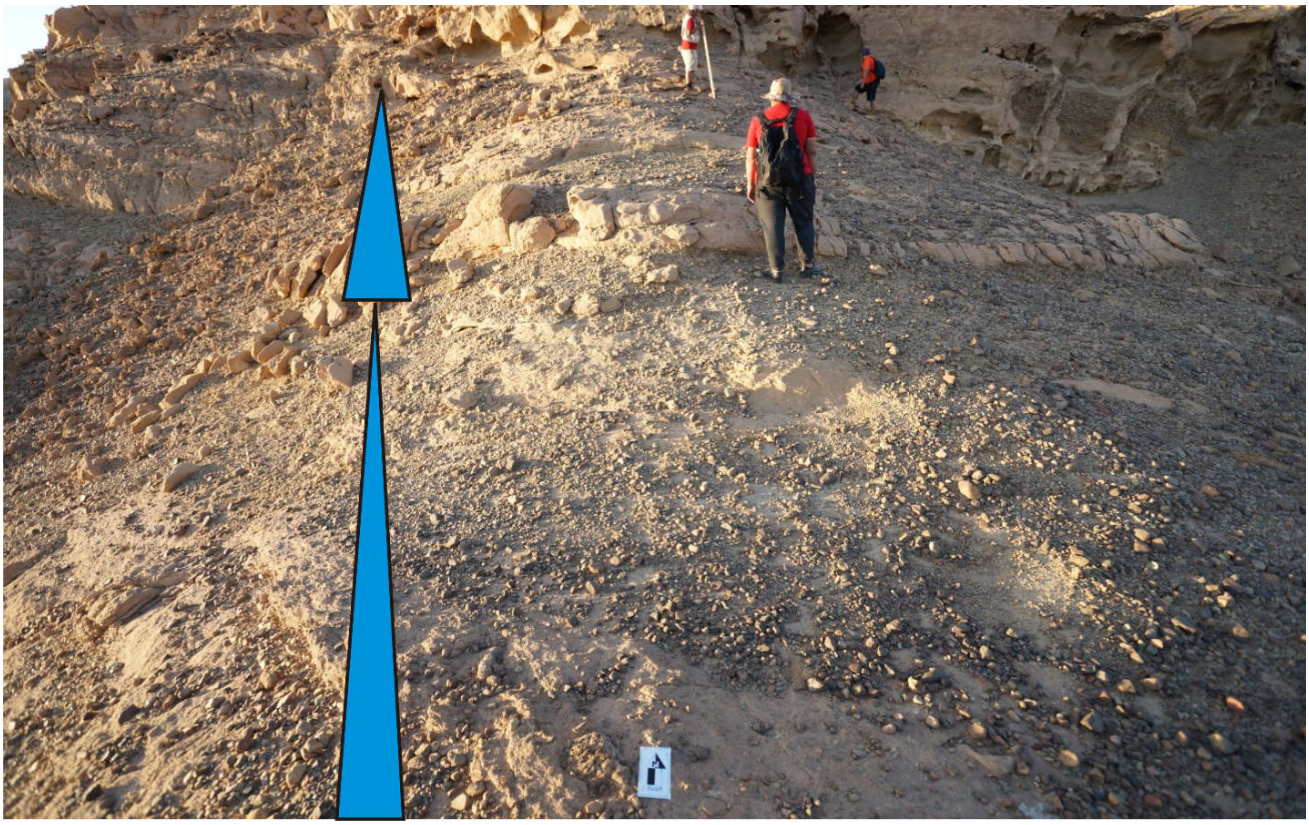

Figure 3.2: Field photo showing two fining and thinning upward sequences (blue traingles) in the first 115 meters of stratigraphic section-3.

Figure 3.3: Field photograph showing a lenticular shaped conglomerate base lag unit of a submarine fan channel.

Figure 3.4: Field photo showing the upper part of the Section-3. Massive, friable, medium to coarse-grained and bioturbated sandstone unit of the Burqan Formation. Hammer for scale.

Figure 3.5: Field photograph showing the lower sandstone unit containing abundant reworked shells of sand dollar (Echinoderms-yellow arrows) and oysters (red box) and overlying oyster bearing, cream colored thick limestone unit. Hammer for scale, 30 cm.

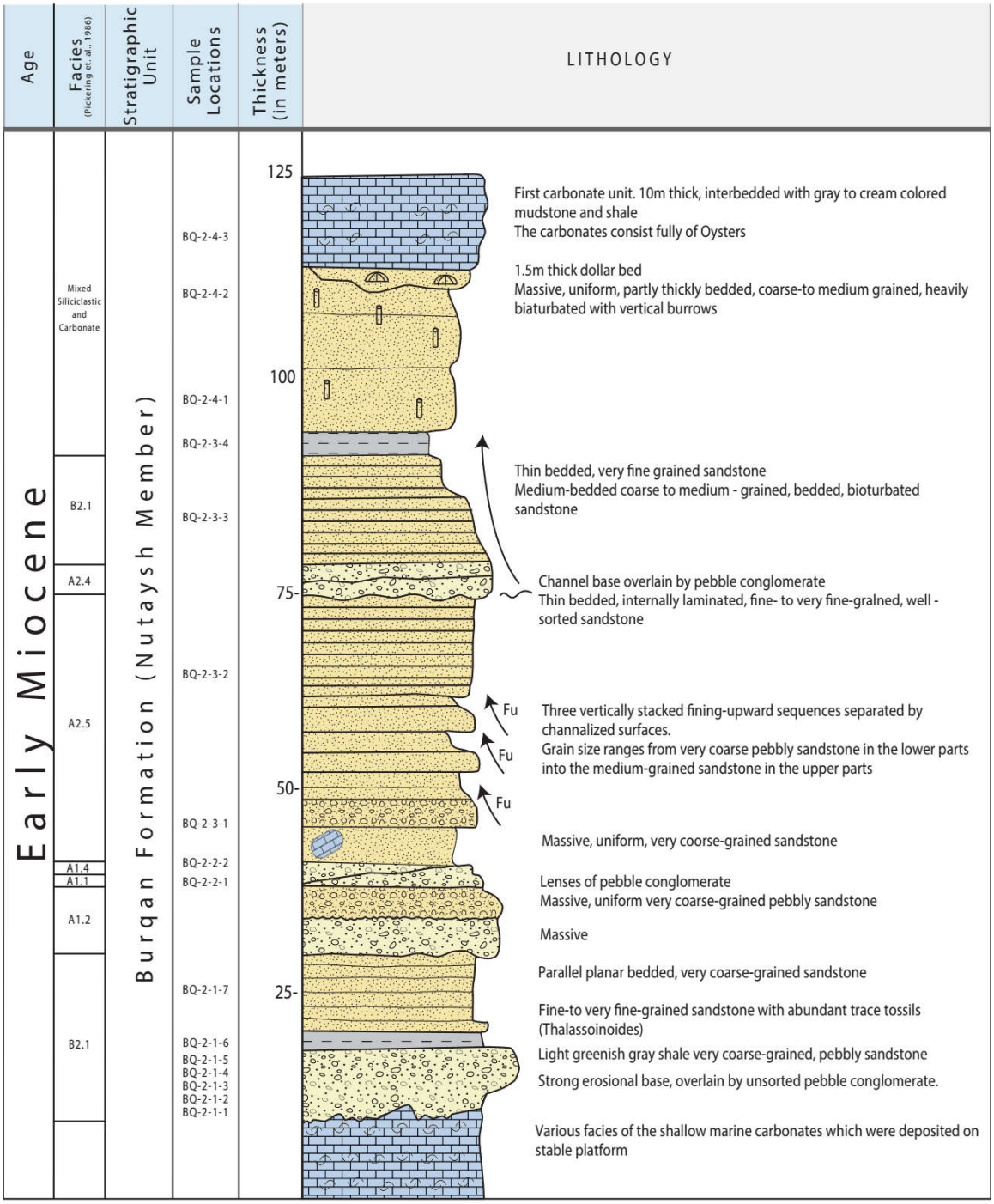

Figure 3.6: Detailed stratigraphic and sedimentological section-3 of the Burqan Formation in Midyan basin, NW Saudi Arabia.

:

3.1.2 Stratigraphic Section 3

Table 1: Summary of lithofacies description identified in stratigraphic section-3 of the Burqan Formation in Midyan Basin.

Facies	Field Photos
Mixed Siliciclastic and Carbonate Channelized sandstone units are medium to finegrained with intensely burrowed and bioturbated. Broken fragments of echinoderms (sand dollar) are abundant in sandstone units. These sandstone units show characteristics honeycomb weathering style as shown in figure. Carbonate unit is massive and cream to white in color.	

B2.1 Parallel Stratified Sands

Very coarse to pebbly sandstone with few scattered cobbles. Bed thickness is medium to thick. Base of the unit is strongly erosive. No clear grading of grain size is present.

A2.4 Graded Stratified Gravels

Thickly bedded, poorly sorted, gravely sandstone units. Normal grading is prominent with cobbles and pebbles at the base. Multiple cycles of normal grading are present within single thick bed.

A2.5 Stratified Pebbly Sands

Medium to thin bedded, poorly sorted, very coarse to pebbly sandstone with grain size decreases towards the top. Bed are 15 to 30 cm thick. Bounding surfaces are relatively flat.

A1.4 Disorganized Pebbly Sands

Very poorly sorted, very coarse to pebbly sandstone unit with few cobbles. Sand acts as matrix between the clasts. Bed lacking in any internal organization or grading. Lower bounding surface is irregular in nature. Clasts shows no imbrication or preferred orientation.

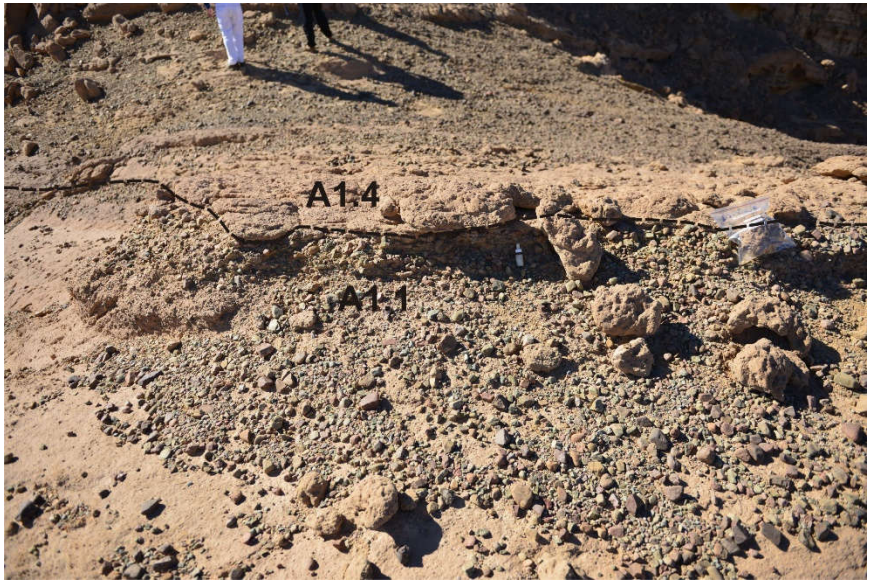

A1.1 Disorganized Gravels

Coarse-grained, very poorly sorted, mainly clast supported gravels showing no organization of clasts. Bed is lenticular in shape with maximum thickness of 15 cm in the center while thickness decreases on either sides. Base of the bed appears flat while the top surface is irregular in nature. Shape of the clasts ranges from angular to moderately-rounded while compositionally clasts are igneous in nature.

A1.2 Disorganized Muddy Gravels

Very poorly sorted, matrix supported muddy gravels without any internal organization, structure or grading. Grain size ranges from clay as matrix and coarse-grained to pebbles and cobbles in size for clasts. Composition of clasts is mainly igneous. Bed shows lenticular shape instead of uniform thickness. Bed has medium thickness with erosive base cutting the underlying sandy unit.

B2.1 Parallel Stratified Sands

Very coarse to pebbly sandstone with few scattered cobbles. Bed thickness is medium to thick. Base of the unit is strongly erosive. No clear grading of grain size is present.

3.1.3 Stratigraphic Section 4

The stratigraphic Section 4 of the Burqan Formation represents the distal and basinal facies of the submarine fan environment (loc: 28°30'54.0" N, 34°53'41.6" E) (Figure 1.3). This section covers all the architectural elements of a prograding submarine fan system. The coarsening- and thickening upward sequences in the lower parts of the succession and the fining- and thinning-upward sequences are well exposed in this measured section (Figure 3.9). The base of the section is faulted. The Nutaysh Member is overlain by the massive, green, gypsiferous shales of the Subayti Member.

This section covers 650 m of the Nutaysh Member and 5.0 m of the Subayti Member (Burqan Formation). The Nutaysh Member is composed of a 575 m thick coarsening and thickening upward sequence in the lower part that is overlain by a 75 m thick fining- and thinning-upward sequence. There is a sharp boundary present between these two different sequences. The first coarsening upward sequence is 130 m thick and consists of 50 m green colored basinal shale facies, gradually overlain by interbedded sandstone and shale sequence with classical turbidites of the mid-fan region. Sandstones are thin-bedded, fine- to very fine-grained in the lower parts, medium-grained in the middle parts and medium- to fine-grained in the upper parts. Normal grading and horizontal burrows are common sedimentary structures (Horizontal Burrows: Figure 3.7).

The second coarsening upward sequence is 180 m thick. The lower 30 m consists of green, massive, pelagic shales of basinal facies, gradually overlain by the distal turbidites. The 150 m thick classical turbidites in the upper part of this sequence consist of regularly

alternating, sharp or erosional based, thin-bedded, medium-to very fine-grained (graded bedded), bioturbated sandstones and green shales.

The third coarsening upward sequence is 185 m thick and consists of 25 m of interbedded green shale and thin-bedded, very-fine-grained bioturbated sandstone, distal turbidite facies. The shale to sand ratio in this sequence is 4:1. Upper 160 m thick section shows a interbedded sandstone and shale sequence almost in equal proportions. The top of the section is cut by the recent wadi (flow direction is from N40W to SE direction) and covered by the gravel and gravelly sand deposits of the braided stream system. The sandstones units have sharp base, thin-to medium-bedded, but clearly thicker than the sandstone units of the lower sections. It indicates the progradation of submarine fan.

The upper 75 m of the section consists of fining-and thinning-upward sequences deposited in the mid-fan area. Four laterally and vertically stacked sequences occur in this part of the section. The sandstones layers in this sequence act as the best reservoir bodies within the Burqan Formation. The first fining-and thinning-upward parasequence is 14 meter thick and its base (loc: (28°30’59.5” N, 34°53’43.4” E) is sharp and erosional. The lower 5 m shows massive-to thick bedded, very coarse-grained pebbly sandstone with igneous (mainly granitic) pebbles. The middle part of the section is 6 m thick and consists of medium-bedded, coarse-to fine-grained (gradually fining upward in grain size), well-sorted and friable sandstone. Multiple grading is present within the sandstone units. The top of the sandstone is overlain by a 1.5-3 m thick interbedded shale and sandstone sequence with shale/sand a ratio of 3:1. The sandstones are thin-bedded, fine-to very fine-grained, and show graded bedding and bioturbation. The direction of the submarine channel is from N40E to SW direction.

Figure 3.7: Horizontal burrows on top of medium grained sandstone unit in section-4.

The succeeding fining-and thinning-upward parasequence is 9 m thick and starts with a sharp and irregular surface at its base. The section consists entirely of a gradually fining-upward sandstone unit. The lower 3 m is medium-bedded, coarse-grained, trough cross-bedded, well-sorted and friable. Upper 6 m is thin-bedded, medium-to fine-grained, moderate-to well-sorted, bioturbated and friable. Lower and upper sandstones show multiple graded-bedding. The overlying 6 m thick section is composed of green shale and includes one horizon of brown colored, transported coral head limestone blocks (Figure 3.7).

The green shale unit is overlain by a 11 m thick channel complex, consisting of 3 or 4 vertically and laterally stacked channels. There are erratic boulders on the surface of the

outcrop. In each channel the sandstone beds thin upward and at the same time their grain size becomes finer. Each channel laterally pinches out against the green shales. The grain size and bedding thickness of the sandstones show lateral fining-and thinning. The beds are amalgamated towards the deepest parts of the channels. The channel geometry is well exposed in their transverse section providing reliable information about the direction of sediment transport. The palaeocurrent measurements of the channel axis indicated that the sediments were transported from N30E, N35E and N34E to a SE direction. The channel-fill sandstones are very good reservoir facies for HC accumulation.

The channel complex (loc: 28°31'04.6" N, 34°53'45.2" E) is overlain by 17.5 m thick unit of shale (70%) interbedded by thin-to medium bedded, fine-to very fine-grained, graded bedded and bioturbated sandstone. The fourth progradational sequence, forming the uppermost part of the Nutaysh Member is 22 m thick and shows a continuous fining upward sequence. This sequence has a sharp base. The lower 10 m thick interval is massive- to thick bedded, coarse-to very coarse-grained, well sorted, friable and shows well-developed multiple graded bedding. This interval consists of vertical and lateral stacked small sized channels. Pockets of green shale are preserved between the channels. The palaeocurrent direction measured from the number of channel axis indicated sediment transport direction as N30E to SW. Upper 12 m thick section consists of medium-to thin-bedded, medium-to fine-grained, graded-bedded, well sorted, friable sandstone. There are common vertical and horizontal burrows.

The overlying Subayti Member consists of greenish gray to green colored, massive gypsiferous shale to mudstone. The contact between the sandstone-dominated Nutaysh

Member and the shale or gypsiferous mudstone dominated Subayti Member is sharp and can easily be recognized (Figure 2.2).

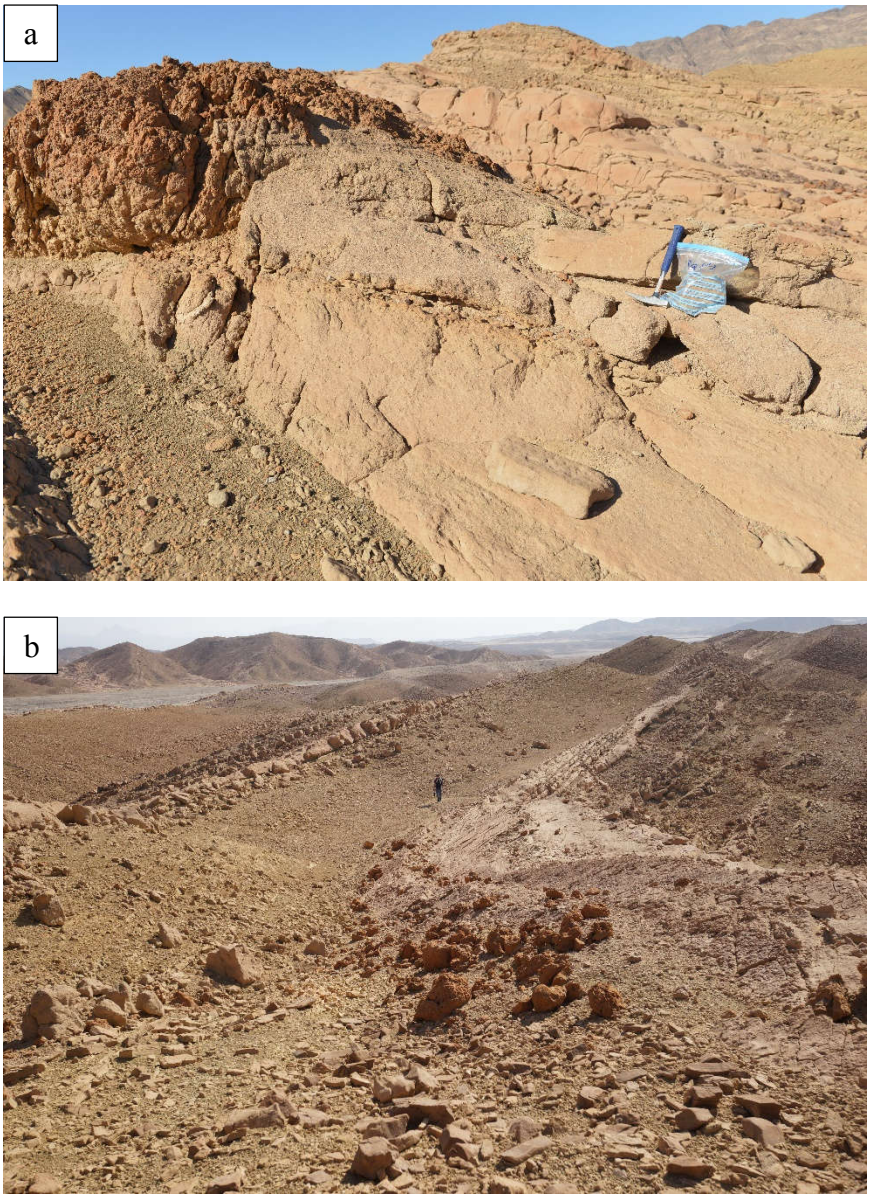

Figure 3.8: a) Field photo showing in-situ large transported coral head limestone boulder within the sandstone unit. (b) Field photograph showing several eroded and scattered coral head limestone pieces presumably derived from large coral head boulder.

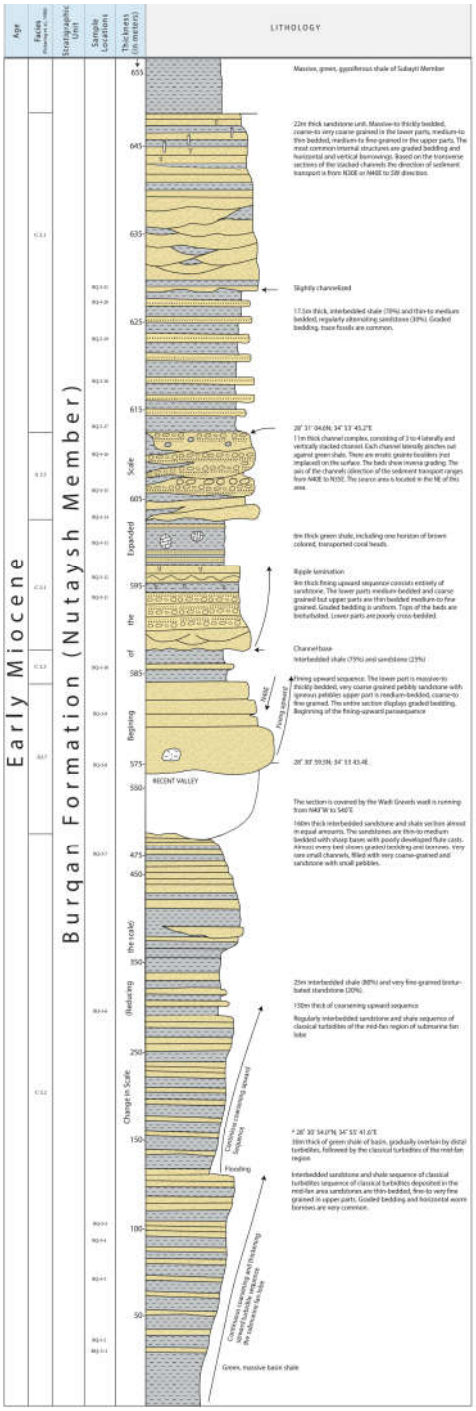

Figure 3.9: Detailed stratigraphic and sedimentological section-4 of the Burqan Formation in Midyan basin, NW Saudi Arabia.

3.1.4 Stratigraphic Section 4

Table 2: Summary of lithofacies description identified in stratigraphic section-4 of the Burqan Formation in Midyan Basin.

Facies	Field Photo
Subayti Member (Greenish Shale) Basinal shales of Subayti member are lying above the channelized sandstone units interbedded with shale. **C2.1 Very Thick to Thick Bedded Sand-Mud Couplet.** Massive laterally and vertically stacked, channel shaped sandstone units are present with thin interbedded shale units. The grain size ranges from very coarse to pebble size sand within sandstone beds. Multiple normal grading is present within massive unit.	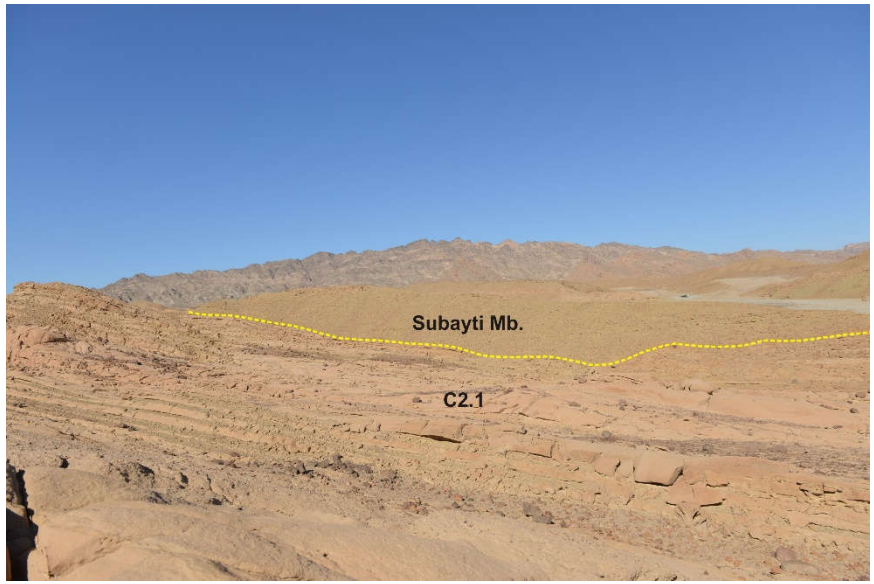

A lenticular shaper massive sandstone unit deposited inside a channel.

Eroded granitic boulders derived from nearby exposures are scattered on the surface of the outcrop of facies C2.1.

A2.2 Inversely Graded Gravels

Sandstone units are thick bedded with channel-shaped. Grain size ranges from very coarse to gravel size sand grains as tracing from bottom to the top of the unit. Inverse grading is the characteristic feature of these facies.

Upper sandstone unit of Amalgamated channelized sandstone units. Channelized body pinches on both sides against green shale. Coarse grained pebbly sandstone unit. No grading of grain size is present.

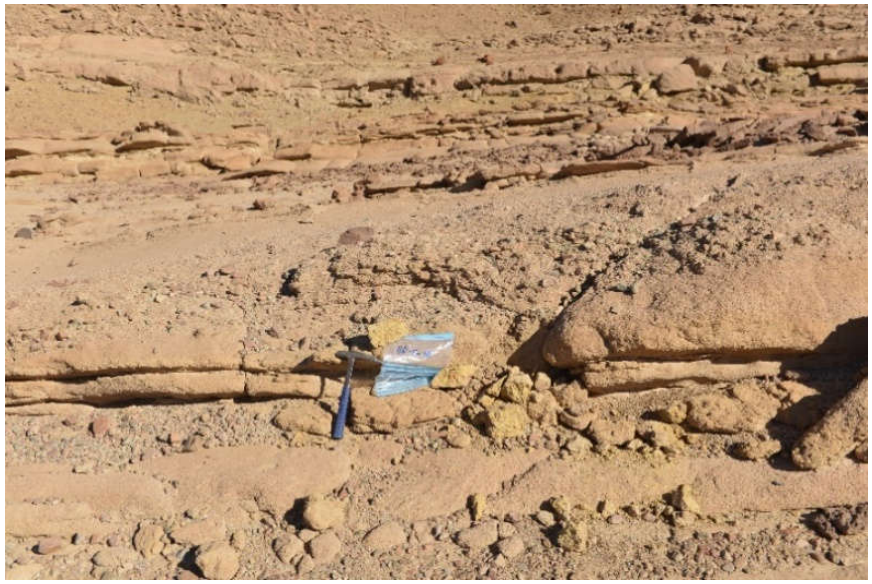

Amalgamated channel shaped sandstone units. Channelized body pinches on both sides against green shale. Coarse grained pebbly sandstone unit. No grading of grain size is present.

C2.1 Very thick/thick-bedded sand-mud couplets

These facies contains thin shale interval interbedded with beds of medium to coarse grained sandstone units. Sandstone beds show normal grading and ripple lamination. In situ transported coral heads and a piece of petrified wood are present along one horizon.

Ripple lamination is present in a sandstone unit within facies C2.1.

This unit shows normal grading with mud near the top.

Petrified wood piece was found within facies C2.1, lying perpendicular to the channel axis of the massive channel shaped sandstone units.

Vertical burrows are present on top of the structure-less, coarse to medium grained very poorly sorted sandstone units.

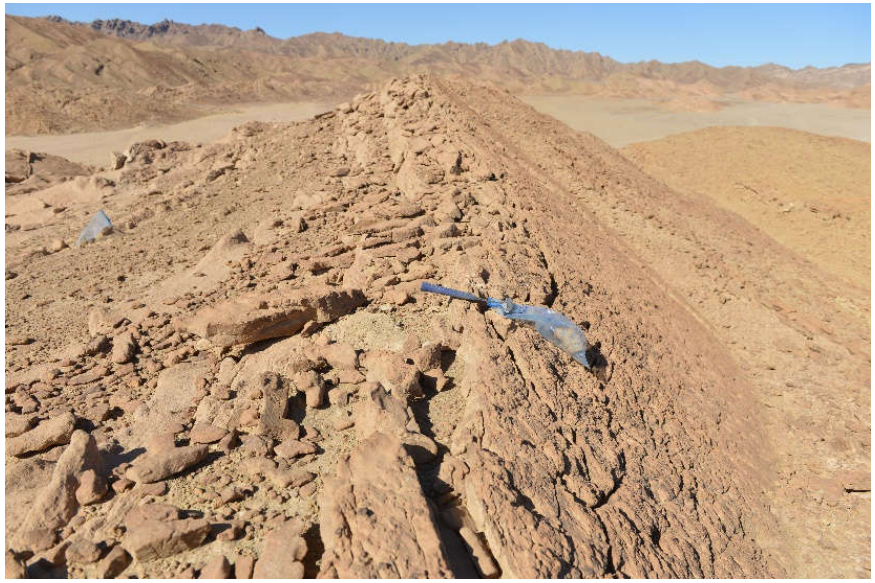

Erosive base of the bed. Medium to thick bedded, Normally graded.

Very poorly sorted, very coarse to coarse grained pebbly sandstone.

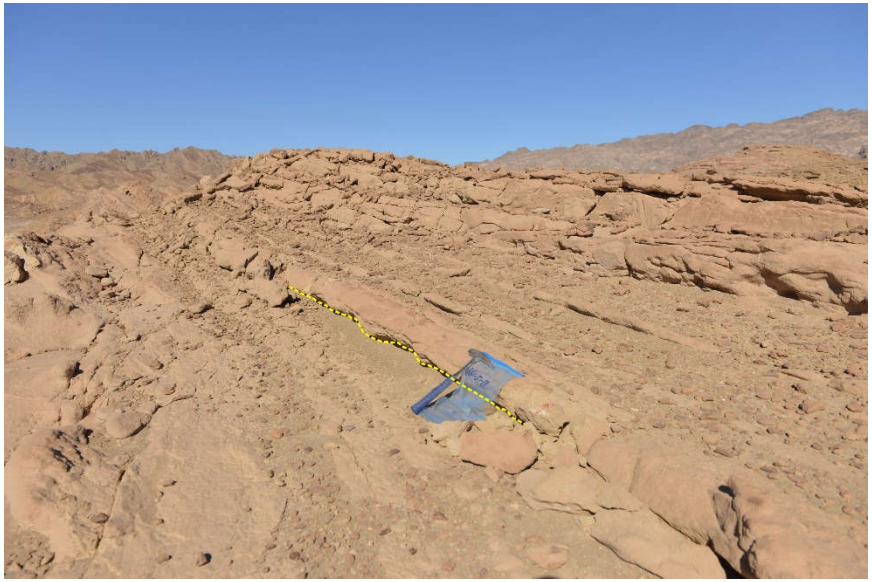

C2.3 Thin Bedded Sand-Mud Couplet

Lower part: Medium to very fine grained medium bedded sandstone unit. Poorly sorted with minor matrix content. Beds show normal grading.

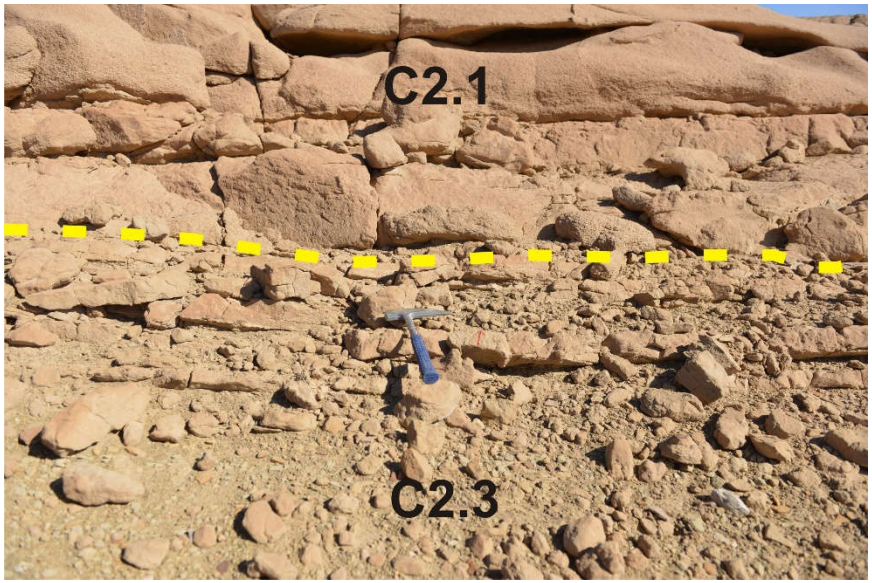

Close up view of upper part of facies A2.7 showing thick bedded sandstone unit with clear normally grading. Grain size ranges from very coarse to pebble in diameter. These sandstone units contain very low angle cross stratification in the upper part of the unit.

A2.7 Stratified Pebbly Sandstone Facies

Stratified, Poorly sorted, very coarse grained pebbly sandstone, multiple layers of normal grading massive to thickly bedded sandstone layer. In situ scattered cobbles are also present the base of normally graded layer.

C2.2 Very Thick to Thick Bedded Sand-Mud Couplet

Fining upward sequence:

The lower part of this fining upward sequence consist of medium to coarse-grained, very poorly sorted, medium bedded sandstone units interbedded with shale intervals. Normally grading is common in sand units. The lower interface of the sandy unit is irregular. Horizontal burrows (thalassinoides) are present on top of sandy units (Figure 3.6).

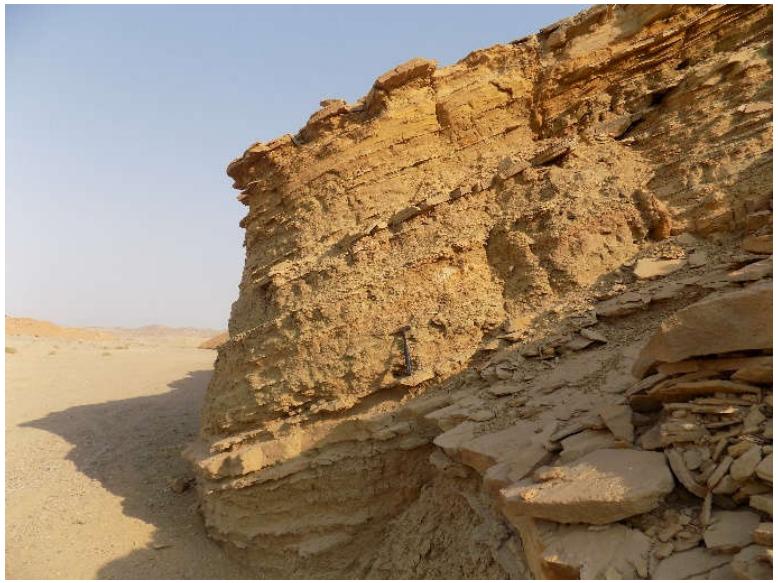

The upper part of this fining upward sequence shows very fine grained sandstone.

3.1.5 Stratigraphic Section 5

This stratigraphic section is located (28°21'00.4" N, 34°43'37.9" E) in the south of Magna town along the coastal highway (Figure 1.3). The total thickness of this section is 636 meters and it consists of coarsening upward sequences present in the lower part of the section while fining upward sequences in the upper part of the section (Figure 3.21).

The lowermost coarsening-and thickening upward sequence is 50 m thick (Figure 3.10). Its lower 28 m consists of greenish gray, massive shale while in the upper parts less than 5% of the sequence consists of thin-bedded, very fine-grained and bioturbated sandstones. The upper part of this sequence shows regularly interbedded, thin-bedded, medium-to fine-grained, graded bedded, and bioturbated sandstone (60%) and greenish fissile shale (40%). This interbedded lithofacies shows a transition to a sequence with classical turbidite facies. The sandstones (80-90%) are medium-to thick-bedded, coarse-to fine-grained (mostly medium-grained), graded bedded, well sorted and bioturbated (Figure 3.11, 3.12). The shales occur as thin beds between the sandstone beds.

The second coarsening and thickening-upward progradational sequence is overall 155 meters thick. The lower 101 m consists of greenish shale with thin beds of sandstone while the upper 54 m consists of sandstone and shale sequence. The thickness of the sandstone units increases towards the top of this sequence. The sandstones are thin- to medium-bedded, fine- to very fine-grained, show grading, and are bioturbated (Figure 3.13 & 3.14). The surface of the outcrop has erratic granitic boulders.

Figure 3.10: Field photograph showing basal coarsening upward sequence in measure section 5 along the coastal road south of Maqna. Jacob staff (1.5 m) is used as a scale in the middle of the photograph.

Figure 3.11: Field photo showing the normal grading in the sandstone unit of first coarsening upward sequence of measured section 5. Pencil Scale = 14cm.

Figure 3.12: The field photo showing the burrowed and bioturbated lower surface of sandstone unit within the first coarsening upward sequence of section-5 in the Midyan region. Pencil Scale = 14cm.

Figure 3.13: Field photo of second coarsening upward sequence of section-5 in the Midyan region. The thickness of sandstone units is increasing as we move to the top of the sequence. Jacob Staff (1.5 m) is taken as a scale.

Figure 3.14: Field photo of a normally graded bed within second coarsening upward sequence in section-5. Pencil Scale = 14cm.

The section between 203 m and 636 m consists of vertically and laterally stacked fining- and thinning-upward and coarsening- and thickening upward sequences. The first fining and thinning upward sequence is 66 m thick. Its lower 24 m is composed of massive- to thickly-bedded, coarse- to very coarse-grained pebbly sandstone, friable and shows inverse graded-bedding (Figure 3.15 & 3.16). This coarse-grained lithofacies is gradually overlain by the 42 m thick, interbedded sandstone and shale sequence of (Figure 3.17). The sandstones are thin-bedded, fine-to very fine-grained, with graded-bedding and the sediments are bioturbated. Individual beds are 10-32 cm thick and show horizontal burrows on their top surfaces. The shale beds are greenish gray or green colored and range in thickness from 5 to 10 cm.

The second fining and thinning-upward sequence is 45.70 m thick and consists of a 39.70 m thick, vertically and laterally stacked channel-fill sequence. Each channel fines upward from coarse-grained pebbly sandstone to medium-grained sandstone. However, the gray shale is deposited between the channel-fill sandstones. The uppermost part of the sequence is overlain by the 6 m thick interbedded sandstone and shale of the classical turbidite facies (Figure 3.18).

The third fining-and thinning-upward sequence is 32.40 m thick and starts with a strongly erosional channel base. The lower 22.40 m thick section is a channel-fill sequence, consisting of medium to thin-bedded, fine to very fine-grained, well-sorted and friable sandstone. The overlying 10 m is composed of regularly interbedded sandstone and shale representing the classical turbidite facies.

Figure 3.15: Field photo showing the massive sandstone unit in the lower part of the first fining upward sequence of section-5. Jacob Staff (1.5 m) is used as a scale.

Figure 3.16: Field picture showing inverse grading in massive sandstone unit of first fining upward sequence of section-5. Jacob Staff (1.5 m) is used as a scale.

Figure 3.17: Field photo showing the interbedded sand-shale interval of classical turbidites above the fining upward sequence in section-5.

Figure 3.18: Field photo of fining and thinning upward sequence within section-5 in Midyan region (Person for scale).

The fourth sequence starts with erosional base (Loc: 28°21’10.9” N, 34°43’54.4” E) and has overall thickness of 27 meters. The grain size ranges from coarse- to very coarse-grained, multiple-graded friable sandstone with scattered small pebbles and granules. This section is overlain by the 18 m thick regularly interbedded sandstone and shale sequence.

The fifth fining upward sequence is about 60 m thick. Lower 10 meters of this sequence consists of 6 m coarse to very coarse-grained, unsorted pebbly sandstone of debris flow deposits. It is overlain by 4 m thick medium-bedded, coarse- to medium-grained, graded-bedded, well-sorted, friable sandstone. The upper 50 m thick section consists of vertically and laterally stacked channel-filled sandstones. There are erosional remnants of shale beds between the channels. This interval is very thickly bedded, coarse to medium-grained and show well developed multiple graded-bedding (Figure 3.19).

In this upper part, two coarsening and thickening-upward sequences occur. The lower sequence is almost 50 m thick. The lower 10.5 m section shows light gray to green colored massive shale and includes one single granite block (loc: 28°21’10.9” N, 34°43’54.4” E). The overlying unit is 16 m thick and consists of thin- to medium-bedded, fine- to medium-grained, graded bedded sandstone with thin beds of shale. The upper part of the sequence is 23.5 m thick, light brown, very thick-bedded, coarse- to very coarse-grained (partly pebbly), multiple graded bedded sandstone. Upper progradational sequence is 21.5 m thick. Its lower part is 8 m gray-green shale. Its upper part is 13.5 m thick, thin-bedded, fine-to very fine-grained bioturbated sandstone.

Figure 3.19: A closer view of a sandstone unit showing grain size variations (Multiple grading) within a sandstone unit. The smaller grains are present at the base and top of the unit while coarse grains are concentrated in the middle of the sandstone unit. Hammer 30 cm for scale.

The overlying 49 m thick interval consists of interbedded sandstone and shale sequence. It is not regularly interbedded. Green, massive shale intervals range from 4 to 10 m in thickness. The sandstone beds range from 1.5 m to 4.5 m in thickness. This 4.5 m thick sandstone unit shows a fining upward grain size variations.

The uppermost part of the measured section 5 is 14 meters thick and consists of 2.5 m thick green shale overlain by the 11.5 m is composed of green shale interbedded with thin-bedded, fine-to very fine-grained and bioturbated sandstone. A 2.5 meters thick lenticular sandstone unit with mud clasts concentrated near its base is present at the bottom of this part (Figure 3.20).

Figure 3.20: Field photo of the uppermost sequence of the section-5. The lenticular sandstone units have mud intraclasts (red arrows) near its base.

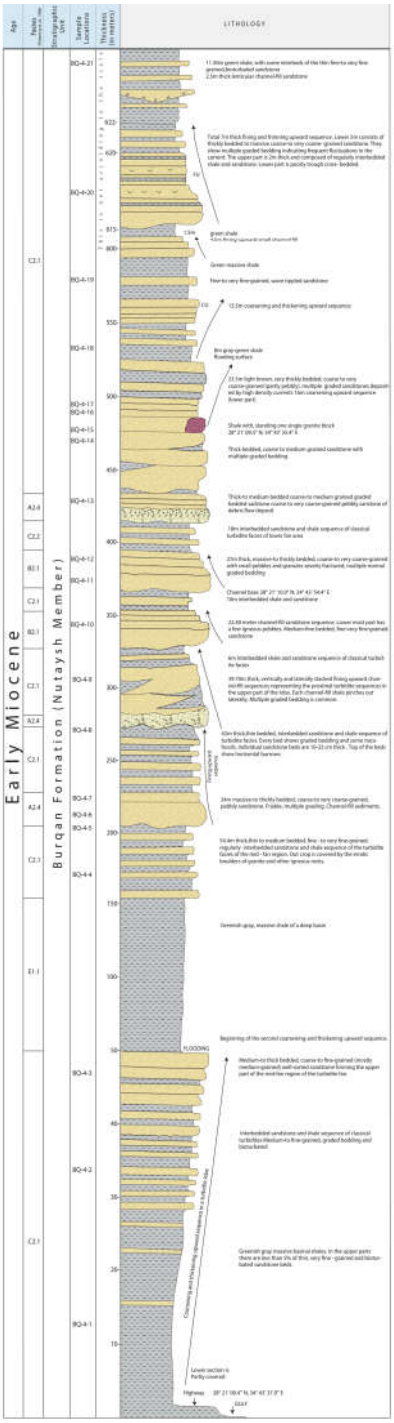

Figure 3.21: Detailed stratigraphic and sedimentological section-5 of the Burqan Formation in Midyan basin, NW Saudi Arabia.

3.1.6 Stratigraphic Section 5

Table 3: Summary of lithofacies description identified in stratigraphic section-5 of the Burqan Formation in Midyan Basin.

Facies	Field Photos
C2.1 Very thick to thick-bedded Sand-Mud Couplet Bed thickness ranges from 10 cm to more than 30 cm. Bed thickness and shape of each sandy unit is inconsistent. Sandstone units are poorly sorted with well-developed normal grading. Grain size ranges from medium to pebble size. Thickness of sandstone units increases as we move in the upper part of this facie. Usually base of the bed is erosive while the upper bounding surface is relatively flat in sandy units. Beds amalgamate laterally into shale or sandy units.	

A large igneous boulder deposited in sand-mud matrix within Facies C2.1.

A2.4 Graded Stratified Gravels

Massive to thickly bedded, coarse to very coarse-grained with small pebbles and granules. Beds are severely fractured. Multiple normal grading is present in medium sandy units while massive beds do not show any grading or sorting. Lower bounding surface of massive beds are usually irregular while upper surfaces are flat.

B2.1 Parallel Stratified Sands

Massive to thickly bedded, coarse to very coarse-grained with small pebbles and granules. Beds are severely fractured. Multiple normal grading is present in medium sandy units while massive beds do not show any grading or sorting. Lower bounding surface of massive beds are usually irregular while upper surfaces are flat.

C2.1 Very thick to thick-bedded Sand-Mud Couplet

Bed thickness ranges from 15 cm to more than 30 cm. Bed thickness and shape of each sandy unit is inconsistent. Sandstone units are poorly sorted with well-developed normal grading. Grain size ranges from medium to pebble size. Thickness of sandstone units increases as we move in the upper part of this facie. Usually base of the bed is erosive while the upper bounding surface is relatively flat in sandy units. Beds amalgamate laterally into shale or sandy units.

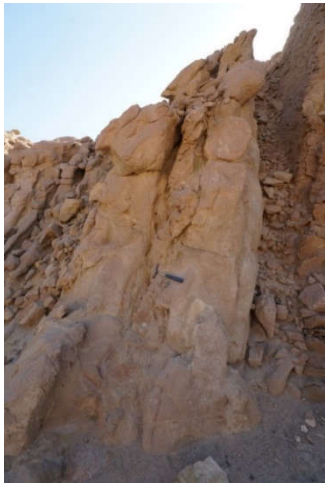

A2.4 Graded Stratified Gravels

Thickly bedded, poorly sorted, gravely sandstone units. Normal grading is prominent with cobbles and pebbles at the base. Multiple cycles of normal grading may occur within massive sand unit. Base of the unit is erosive in nature while upper surface shows nearly flat or irregular nature.

C2.1 Very thick to thick-bedded Sand-Mud Couplet

Bed thickness ranges from 15 cm to more than 30 cm. Bed thickness and shape of each sandy unit is inconsistent. Sandstone units are poorly sorted with well-developed normal grading. Grain size ranges from medium to pebble size. Thickness of sandstone units increases as we move in the upper part of this facie. Usually base of the bed is erosive while the upper bounding surface is relatively flat in sandy units. Beds amalgamate laterally into shale or sandy units.

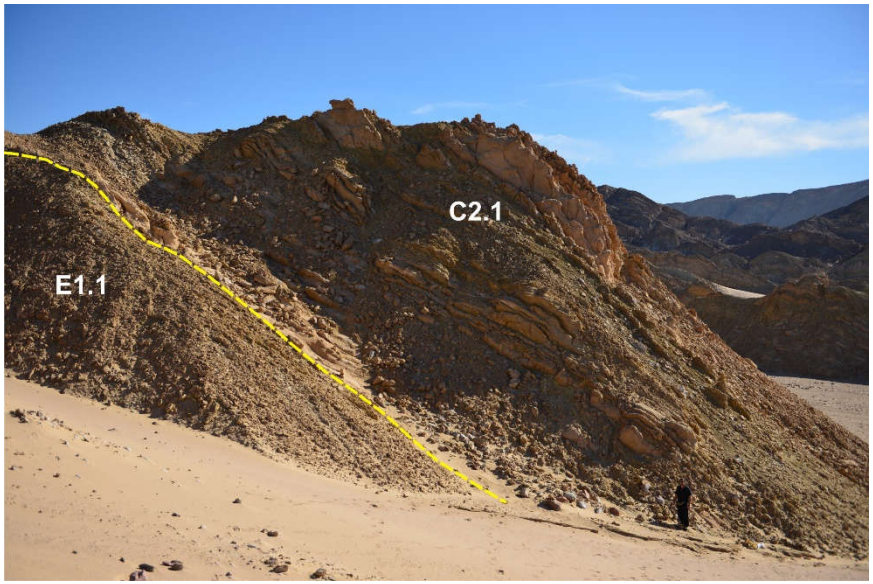

E1.1 Structureless Mud

Weathered greenish brown colored fissile shale. No clear bedding is present.

C2.1 Very thick to thick-bedded Sand-Mud Couplet

Bed thickness ranges from 15 cm to more than 30 cm. Bed thickness and shape of each sandy unit is inconsistent. Sandstone units are poorly sorted with well-developed normal grading. Grain size ranges from medium to pebble size. Thickness of sandstone units increases as we move in the upper part of this facie. Usually base of the bed is erosive while the upper bounding surface is relatively flat in sandy units. Beds amalgamate laterally into shale or sandy units.

Field photograph showing well-developed normal grading with pebbles near the base and coarse grained sand grains near the top

Field Photograph showing bioturbation at the base of massive sandstone unit within Facies-C2.1

3.1.7 Stratigraphic Section 6

Stratigraphic section 6 is measured close to the northern margin of the Midyan Basin (loc: 28°31'21.4" N, 34°54'35.9" E) (Figure 1.3). The Nutaysh member of the Burqan Formation is 260 m thick and is composed mainly of coarse-grained sandstone and conglomerates (Figure 3.27). The base of the section is not exposed. The lower part of the Nutaysh Member consists of small cycles of coarsening and thickening upward sequences. The middle and upper parts consists of interbedded sand-shale sequences. The bedding thickness and grain size of the sandstones and pebbles gradually increase upward in coarsening upward sequences. Two coarsening-and thickening-upward sequences were encountered.

The lower sequence is 7 m thick and consists of 1.5 m green shale, gradually overlain by the 5.5 m thick interbedded sandstone (90%) and shale (10%) sequence. Graded-bedding and bioturbation are the most common sedimentary structures in the sandstone beds. (Figure 3.22)

The second coarsening-and thickening-upward parasequence is 37.5 m. There is no shale facies at the base of this parasequence. The lower 18 m is composed of regularly interbedded sandstone (80%) and shale (20%). Graded bedding, bioturbation and bottom structures (mainly flute and groove casts) are common. The overlying 9.5 m thick section consists entirely of medium-to thick-bedded, medium-to coarse-grained, well-sorted and friable-to weakly cemented sandstone having excellent reservoir quality. There are common *Ophiomorpha* burrows.

The overlying classical turbidite facies of the mid-fan region of the submarine fan environment is 30 m thick and consists of regularly interbedded shale (60%) and sandstone (40%). The sandstones are sharp-based. The most common sedimentary structures are normal grading, wave-ripples, bioturbation and some turbidity currents generated bottom structures (Figure 3.23, 3.24).

The regularly interbedded sandstone and shale sequence of classical turbidites are overlain by the fining-and thinning-upward sequences. The first sequence is 17 m thick. The lower 9 m section is a massive bedded, coarse-to very coarse-grained conglomeratic sandstone overlain by the medium-grained bioturbated sandstone. This channel-fill conglomeratic sandstone unit is overlain by 8 m thick green, massive and partly laminated pelagic shale.

The main part of the stratigraphic section 6 consists of 125 m thick coarsening and thickening-upward sequence Lower 50 m section is medium-bedded (occasionally thin-bedded), medium to fine-grained, moderate-to well-sorted, normally graded and horizontally burrowed sandstone. The sandstone is interbedded with 0.3-0.5 m thick greenish gray bioturbated shale beds. There some occasional lens or wedge-shaped small channel-filled sandstones. The rare pebbles fill the deepest parts of these channels. (Figure 3.25)

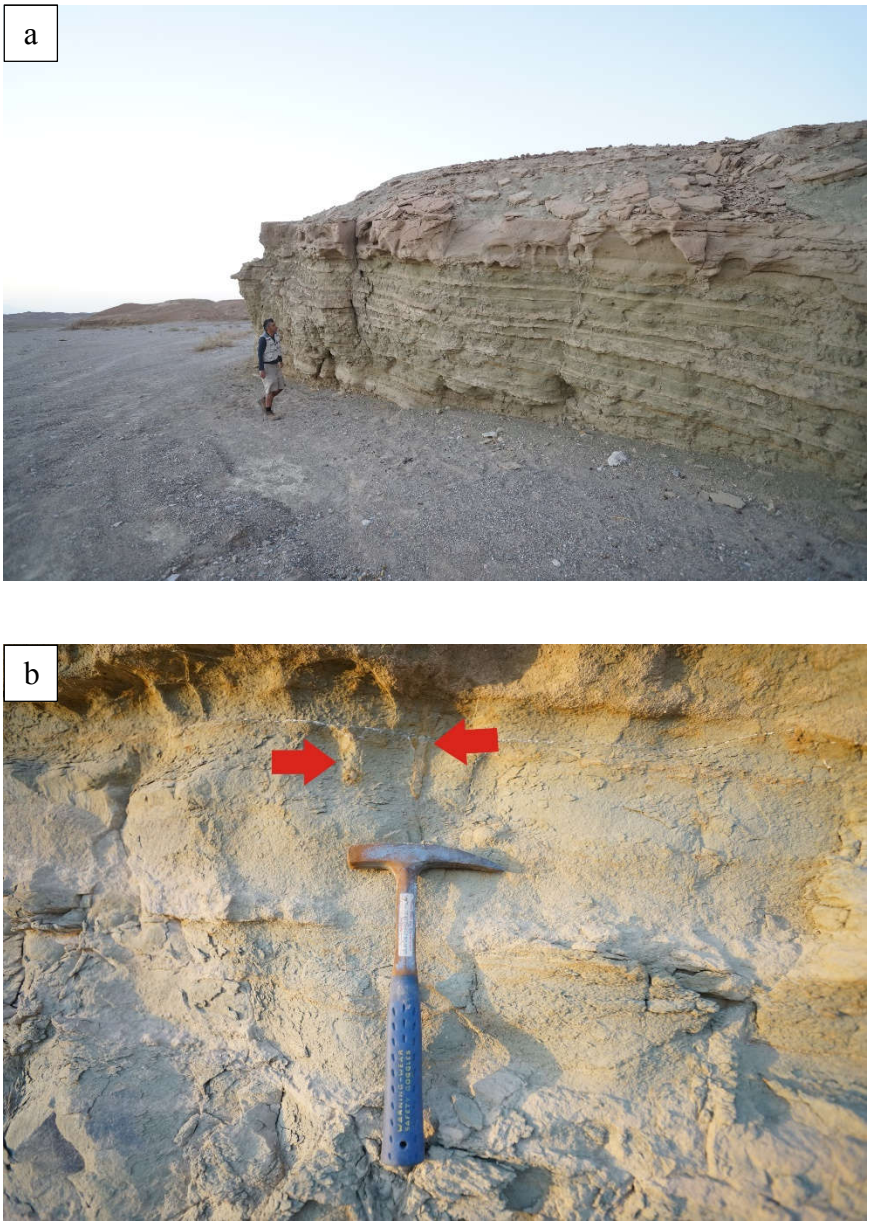

Figure 3.22: a) Field photograph showing the first coarsening upward, progradational sequence of measure section-6. Person as Scale. (b) Field photo showing vertical burrows in the upper part of the sequence. Hammer (30 cm) as scale.

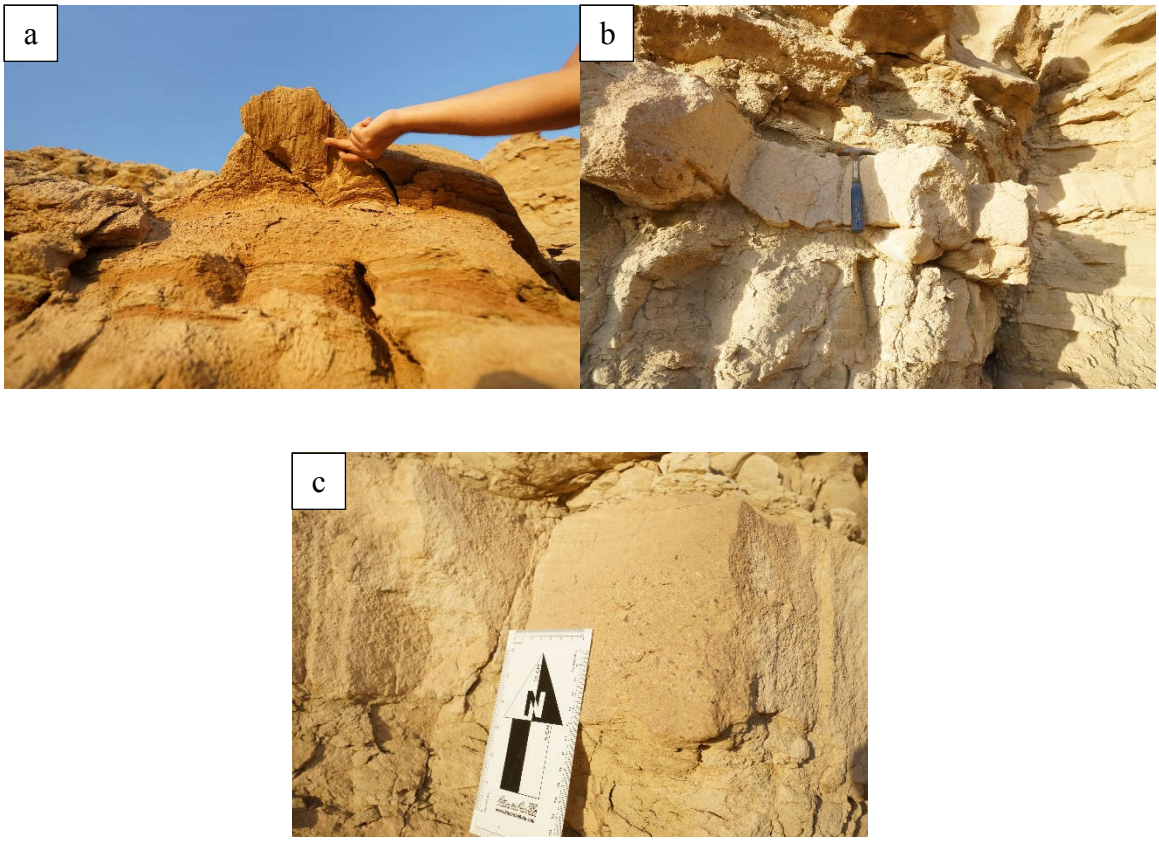

Figure 3.23: Field photographs showing common sedimentary structures observed in section-6. a) Groove casts. (b) Flute marks. (c) Normal grading T_a, T_b.

Upper 75 m thick section is distinctly coarser in grain size and bedding thickness is thicker. This section consists of vertically and laterally stacked channel fill sandstones. The size of the channels increases upward. Small pebbles occupy the deepest parts of the channels. The abundance and size of the pebbles increase upward. The pebbly sandstone facies gradually fines upward into the massive-to thickly-bedded, coarse-to medium-grained sandstone. Inverse grading is present in the thick sandstone units (Figure 3.26). The lenticular shale beds are preserved between the channels. These sediments were deposited in the highly channelized uppermost part of the submarine fan environment.

Top of the measured section is 59 m thick and consists almost entirely of conglomerate deposited in a submarine canyon cutting the uppermost part of the submarine fan. The lower 20 m thick section is massive, small-to large pebbles and unsorted conglomerates (Figure 3.25). The conglomerates are overlain by the 5 m thick horizontal-bedded pebbly sandstone. The overlying 34 m thick section shows no sign of stratification, consisting of massive-to very thickly-bedded, very poorly-sorted. The matrix is pebbly sandstone. Some parts show reverse grading.

The conglomerates and conglomeratic sandstones of Nutaysh Member are overlain by the Subayti Member. It consists of light gray-to greenish gray, massive looking shale, cut with the secondary gypsum.

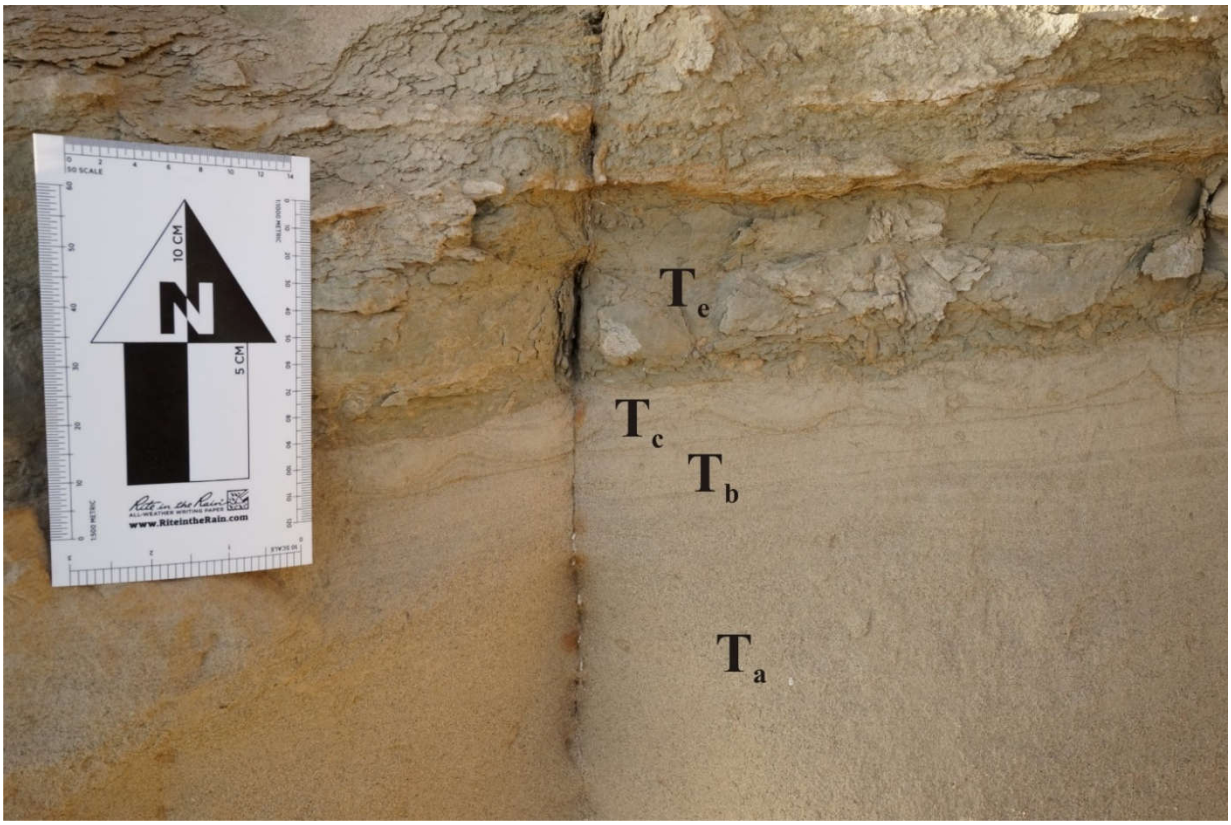

Figure 3.24: Field photograph showing divisions of classical Bouma Sequence within measured section 6. **T_d** division may have been eroded before the deposition of **T_e**.

Figure 3.25: Field photo is showing lenticular, channel filled pebbly sandstone deposited in the deepest part of the channel.

Figure 3.26: Field photo showing inverse grading from base of the unit to the middle and then grain size decreases towards the top of this thick sandstone unit in section-6.

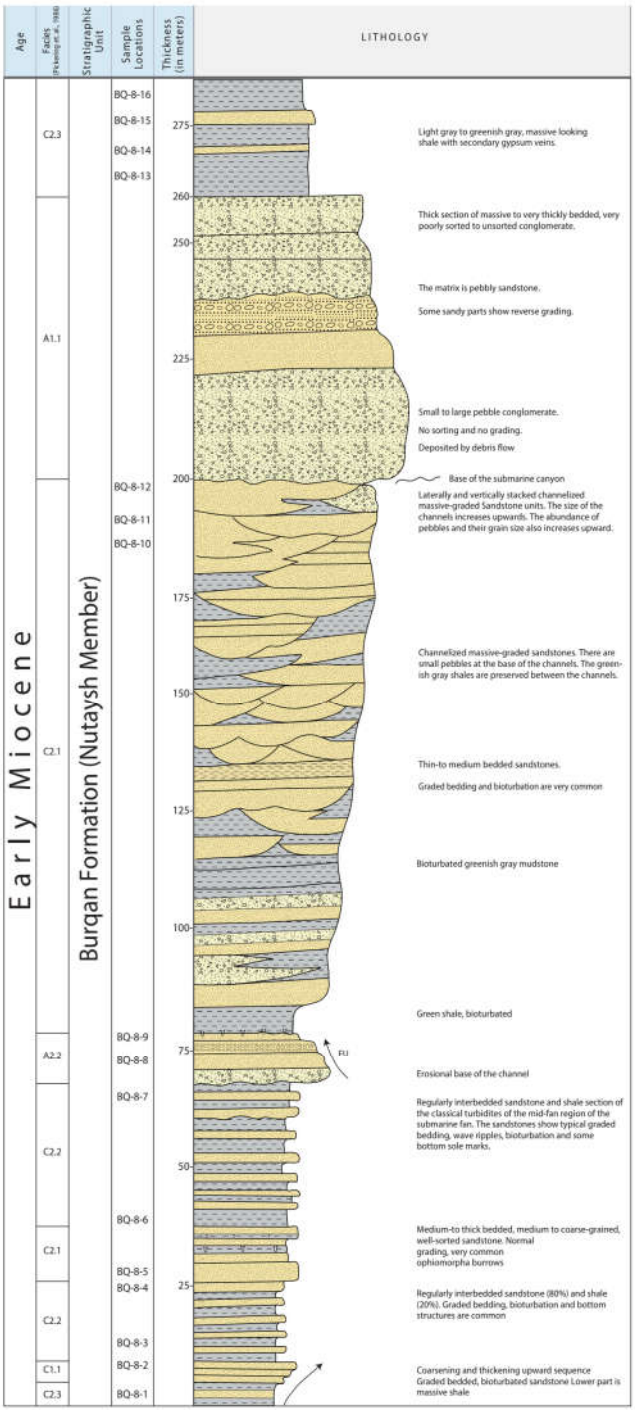

Figure 3.27: Detailed stratigraphic and sedimentological section-6 of the Burqan Formation in Midyan basin, NW Saudi Arabia.

3.1.8 Stratigraphic Section 6

Table 4: Summary of lithofacies description identified in stratigraphic section-6 of the Burqan Formation in Midyan Basin.

Facies	Field Photos
C2.3 Thin Bedded Sand-Mud Couplet Oftenly, these facies contains Tbcde divisions of bouma sequence. Sandstone units show normal grading. Bed thickness is less than 10 cm in these facies.	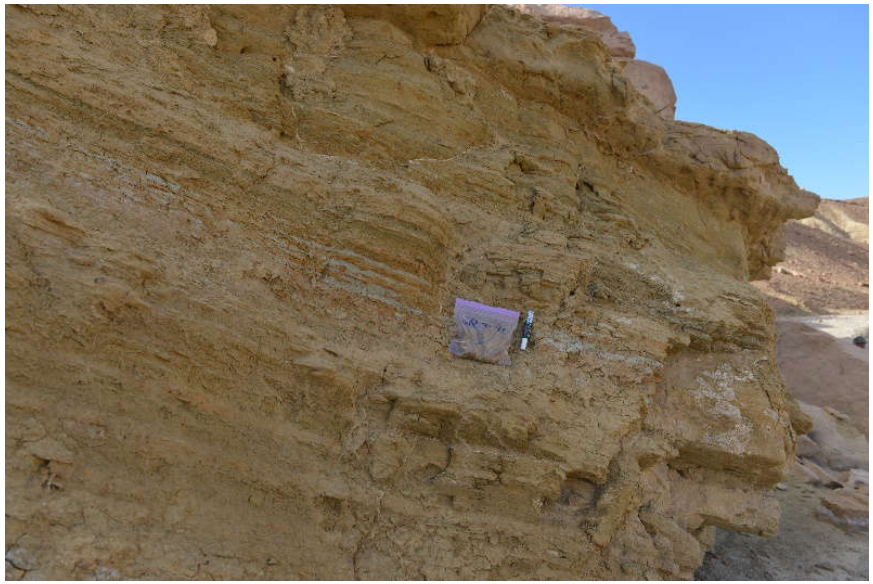

A1.1 Disorganized Gravels

Small to large sized pebbles and cobbles without sorting and grading. Pebbles show imbrication. Bounding surfaces are flat in medium to thick beds while base of massive beds is erosive. These deposits shows both clast and matrix supported properties. Clast are moderately rounded.

Field photo showing the lower part of facies A1.1.

C2.1 Very Thick to Thick Bedded Sand-Mud Couplet

Very thick to thick bedded, poorly sorted sandstone beds with well-developed normal grading. Tabc are present in sandstone beds. Sole markings such as Load casts and tool marks are also present. Lower surface of the sandstone beds is mostly irregular while upper surface usually shows flat nature. Beds shows lateral amalgamation with other sandy units.

A2.2 Inversely Graded Gravels

Thick bedded, poorly sorted, medium to very coarse grained pebbly sandstone shows inverse grading. Base of the unit is erosional in nature. Inverse grading is overlain by a cycle of normal grading.

C2.2 Medium Bedded Sand-Mud Couplet

Very thick to thick bedded, poorly sorted sandstone beds with well-developed normal grading. Tabc are present in sandstone beds. Sole markings such as Load casts and tool marks are also present. Lower surface of the sandstone beds is mostly irregular while upper surface usually shows flat nature. Beds shows lateral amalgamation with other sandy units.

C2.1 Very Thick to Thick Bedded Sand-Mud Couplet

Very thick to thick bedded, poorly sorted sandstone beds with well-developed normal grading. Tabc are present in sandstone beds. Sole markings such as Load casts and tool marks are also present. Lower surface of the sandstone beds is mostly irregular while upper surface usually shows flat nature. Beds shows lateral amalgamation with other sandy units.

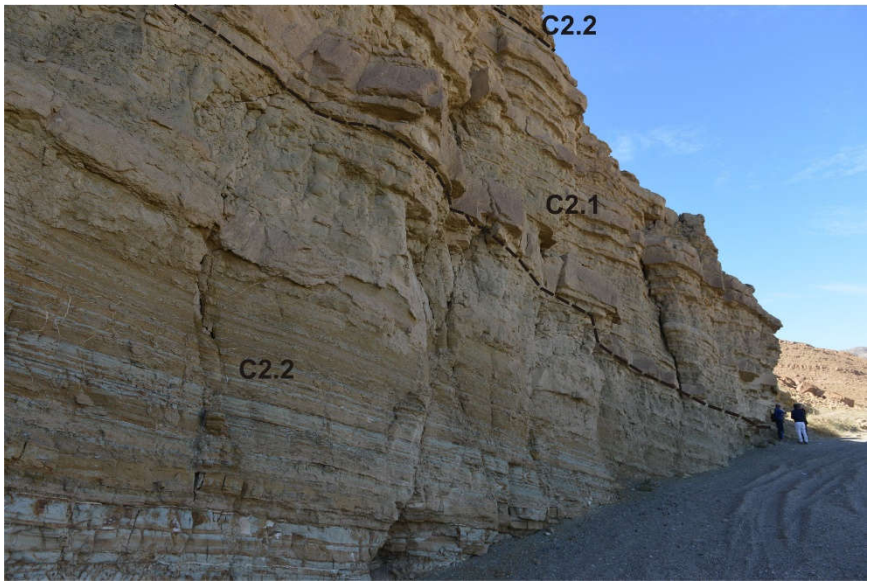

C2.2 Medium Bedded Sand-Mud Couplet

Medium to coarse-grained, very poorly sorted, medium bedded sandstone units interbedded with shale intervals. Normally graded sand units. Lower bounding surface of sandy unit is mostly irregular.

Ta, Tb, Tc and Te divisions of Bouma Sequence Associated with facies C2.1.

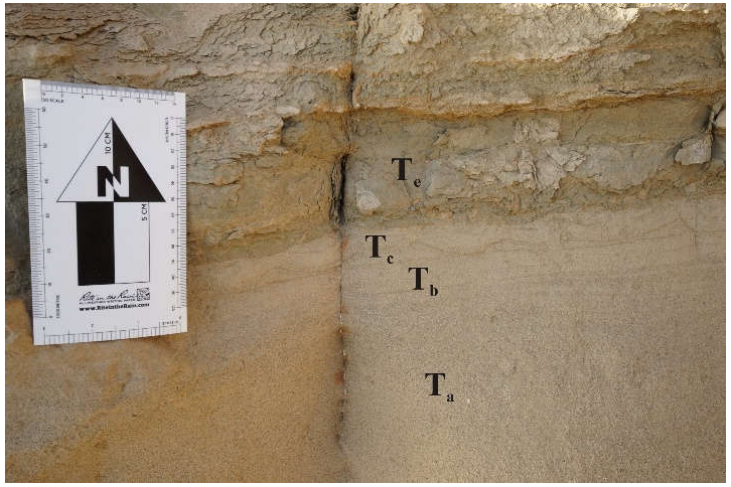

Td is missing or may have been eroded before the deposition of Te.

A sandstone unit showing erosive base and flute marks within facies C2.1.

Tool marks are present at the base of a sandstone unit in facies C2.1.

C1.1 Poorly sorted muddy sand

Thickness of beds ranges from 15 cm to 30 cm. Medium to fine grained, poorly sorted lower bed with erosive base. Mud intraclasts are concentrated near the base of the bed. Plane parallel lamination T_b is present in the upper part of the lower unit. Upper bed is poorly sorted and ungraded sandstone unit with scattered mud intraclasts occurring at different levels. Lower bounding surface is irregular in nature while upper surface is relatively flat.

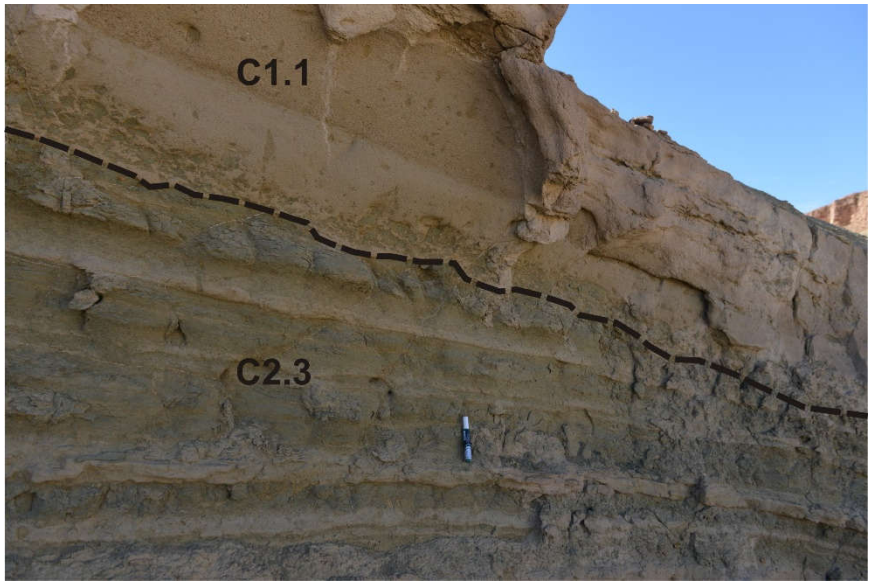

C2.3 Thin Bedded Sand-Mud Couplet

These facies contains Tbcde divisions of bouma sequence. Sandstone units show normal grading. Bed thickness is less than 10 cm in these facies.

Field photograph is showing typical Bouma sequence Tb, Tc, Td, Te present in the lower part of the facies C2.3.

Ta is missing here.

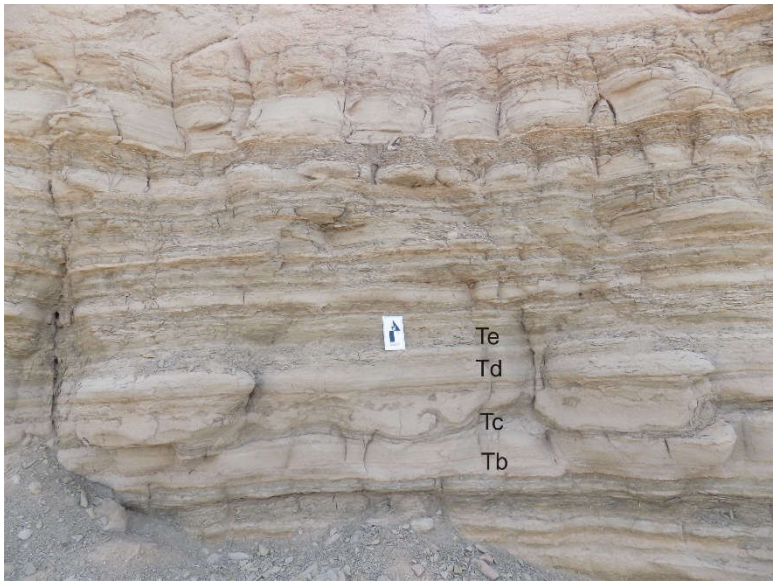

3.1.9 Stratigraphic Section 7

The stratigraphic section 7 is located on (loc: 28°25’07.9” N, 34°55’14.3” E) close to a NE-SW trending normal fault (Figure 1.3) (Figure 3.28). In the high area the Neoproterozoic granitic basement and the overlying Musayr Formation is exposed. The Al Wajh Formation is preserved locally on the irregular topographic surface of the granitic basement.

The measured section 7 is 80 m thick and consists of three fining-and thinning upward sequence (Figure 3.28). The bedding thickness and grain size decreases upward in this section. The lowermost sequence is 31 m thick and cuts deeply into the underlying greenish gray to green shale. It is covered with thin layer of igneous pebble conglomerate. This unit also consists of 5 to 10 m thick, vertically stacked channel-fill sandstones. The grain size in these channel-fill bodies shows upward fining trend. The conglomerate layer is covered at the base of the sandstone units. Middle parts of the section are thick-to medium-bedded, poorly trough cross-bedded, poorly sorted and friable or weakly cemented. Almost every bed shows graded bedding indicating successive stages of high density turbidity currents. Upper 10 m thick section is medium-to thin-bedded and show horizontal and vertical burrows. The sandstone unit is covered by the 2-3 m thick interbedded sandstone shale sequence.

The second fining upward sequence starts with another irregular erosional surface. It is 13.5 m thick channel-fill sequence. The lower half is thickly-bedded, coarse-grained, graded bedded and show poorly developed trough cross-bedding. The upper half is medium-to thin-bedded, fine-to very fine-grained, well-sorted, bioturbated and friable.

Overlying 16.5 m thick section is composed of bluish gray massive shale, partly covered with thick soil.

The uppermost fining-and thinning-upward sequence is 15 m thick. Lower 5 m thick sandstone is coarse-to medium-grained, well-sorted and friable. The top surfaces are bioturbated. The sandstone beds show graded bedding from coarse grained to finer sand. The upper 10 m section is thin-bedded, fine-to very fine-grained, wave-rippled, bioturbated and calcite cemented sandstone. The top of the measured section is overlain by the cream colored, massive, gypsiferous shales of the Subayti Member.

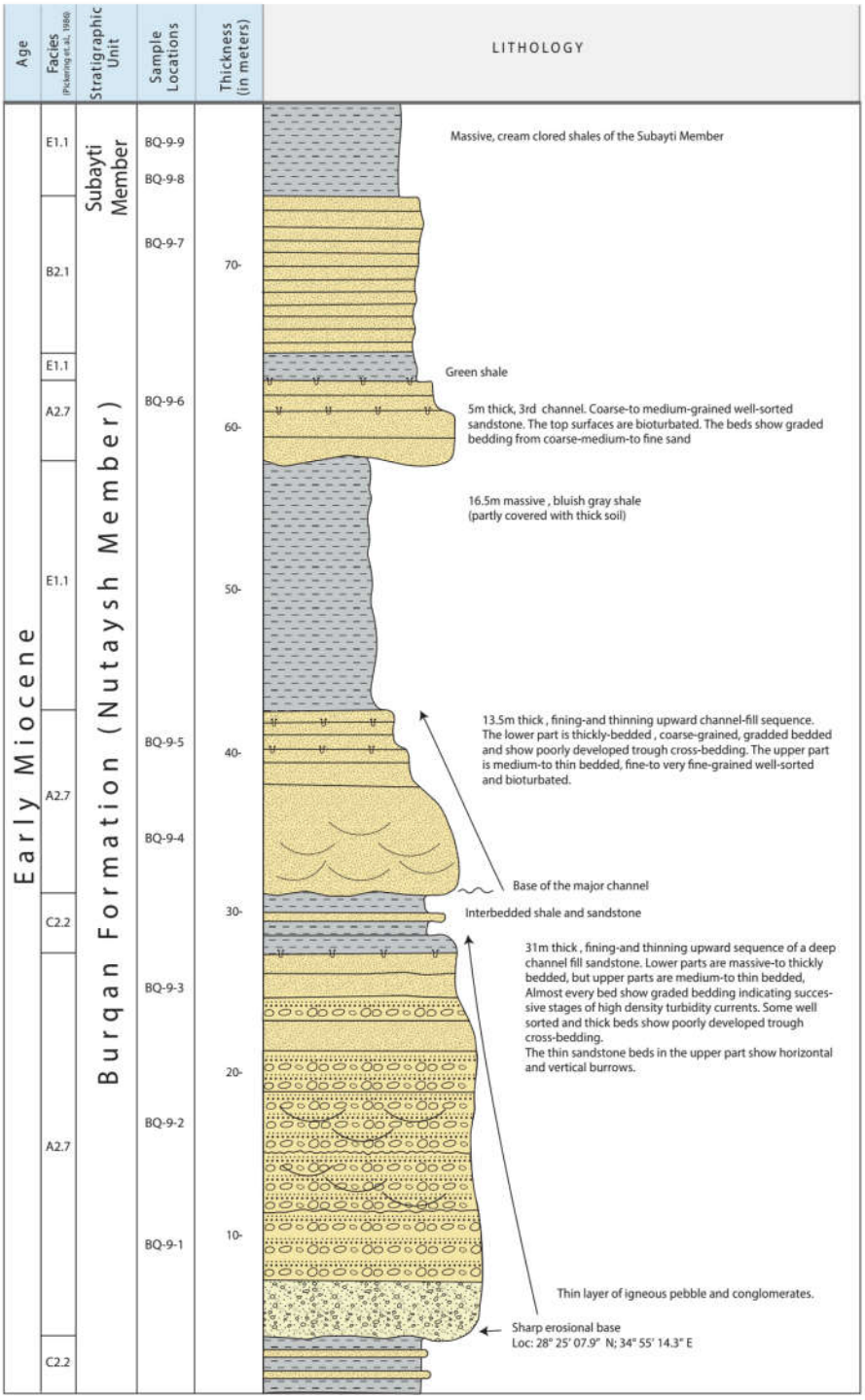

Figure 3.28: Detailed stratigraphic and sedimentological section-7 of the Burqan Formation in Midyan basin, NW Saudi Arabia.

3.1.10 Stratigraphic Section 7

Table 5: Summary of lithofacies description identified in stratigraphic section-7 of the Burqan Formation in Midyan Basin.

Facies	Field Photos
B2.1 Parallel Stratified Sands Medium to thick bedded, poorly sorted, coarse to medium grained sandstone units. Normal grading is present in some beds while few thick beds are ungraded. Upper bounding surfaces are relatively flat while lower surfaces show erosive nature. **E1.1 Structureless Mud** Weathered greenish brown colored fissile shale. No clear bedding is present	

A2.7 Normally Graded Pebbly Sands

Lower beds are massive to thickly-bedded with channelized shape. Upper beds are medium to thin bedded and changes into C2.2 Facies upward. Every bed shows normal grading. Massive beds shows multiple cycles of normal grading with thin layer of igneous pebbles or conglomerates at the base and grain size changes up to coarse sand towards the end of cycle. Base of this facies is erosional in nature. Some thick beds also show poorly developed trough-cross bedding. Thin sandstone units near the top of this facie are affected by horizontal and vertical burrows. Plane parallel stratification is also present at some intervals above the base in thick sandstone units.

C2.2 Medium Bedded Sand-Mud Couplet

Sand beds have thickness ranges from less than 10 cm to 30 cm. Sandstone units shows normal grading. Grain size ranges from medium to coarse grained, poorly sorted sand with few scattered pebbles. Lower bounding surface of the beds are sometime irregular to flat. But upper surfaces are flat in nature

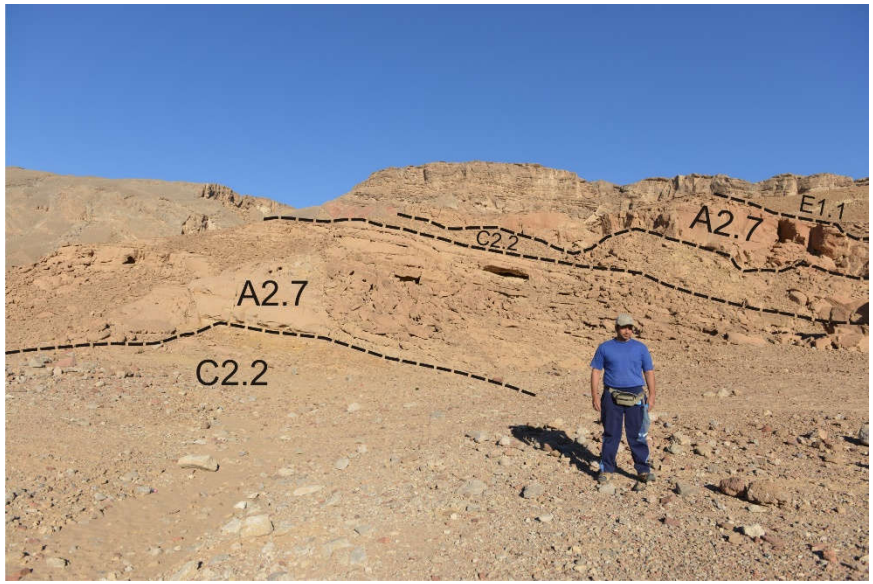

3.2 Petrology

More than 200 rock samples from sandstone and mudstone units were collected from the five measured sections. Majority of sandstone samples are friable in nature, therefore, these samples were impregnated with blue epoxy resin before mounting them on the glass slide to prepare their thin section. Total 150 thin sections were prepared and studied while seventy representative thin sections were selected and thoroughly examined for modal analysis by using petrographic microscope. 300 points were counted for each thin section by using the Gazzi-Dickenson's Point Counting approach (Gazzi, 1966; Dickinson, 1970). The result of modal analysis reveals the textural characteristics, mineralogical and diagenetic composition of sandstone samples taken from Nutaysh member of the Burqan Formation in the Midyan region. The summarized results of modal analysis are presented in Table-6. Different types of detrital grains were distinguished based on the differences in their optical properties under the transmitted light microscope. Meanwhile, the optical photomicrographs were captured at different scale of magnification to record the compaction, sorting, framework grains and different diagenetic features present in each sample.

Petrography, Provenance and Modal Analysis Results

The detrital composition and quality of the siliciclastic sedimentary reservoirs is governed by numerous geological factors such as the tectonic activity in the source region, climate, composition of the parent rock, erosion and weathering rates in the source area, sediment transport, diagenetic effect and many more (Dickinson and Suczek, 1979; Suttner *et al.*,

1985; McLennan *et al.*, 1993; Osae *et al.*, 2006; Al-Ramadan *et al.* 2013; Ikhane *et al.,* 2014). The mineralogical composition, texture and authigenic minerals have direct influence on the reservoir properties such as porosity and permeability of sediments during and after the deposition. For instance, the reduction in permeability can be caused by the precipitation of diagenetic clays such as smectite and kaolinite by decreasing the size of pore throats which in turn reduce the quality of the reservoir (Pettijohn, Potter and Raymond Siever, 1972). Therefore, petrographic studies will not only aid us in determining the provenance of the rock but will also assist in determining sequence of diagenetic events controlling the reservoir quality of the Burqan Formation.

3.2.1 Provenance

As the nature and quantity of cement and matrix within pore spaces are the function of diagenesis similarly the ratio of framework grains depends largely on the provenance (Dickinson, 1970). The reservoir quality of a sandstone is independent of the proportion of framework grains rather it mainly relies upon textural characteristics of detrital components. However, the detrital minerals of different compositions respond differently under different diagenetic conditions and show variable porosity reduction rates as burial depth changes. For instance, feldspars are less stable minerals and more susceptible to chemical alteration than quartz and hence experience more dissolution at shallower depth. This dissolution may cause the growth of authigenic cements or matrix with increasing depth that may result in considerable porosity loss. Likewise, rock fragments are more prone to be crushed or deformed due to increase in overburden pressure which also leads

to porosity reduction. Therefore, knowing the provenance and proportion of detrital components is vital to determine the reservoir quality of siliciclastic reservoirs. (Dickinson and Suczek, 1979)

The provenance classification for sandstone samples of the Burqan Formation shows that majority of them were derived from transitional continental blocks and recycled orogenic terranes. Some quartz rich samples fall in the category of craton interior terrain (Figure 3.31). The petrographic analysis reveals that the Burqan Formation has large plutonic rock fragments, heavy minerals like zircon and rutile, chert and limestone fragments as well as sutured or deformed polycrystalline quartz grains. Quartz is a useful indicator of provenance and it is used to infer the nature of metamorphic rocks in the source area (Basu *et al.*, 1975).

3.2.2 Petrography

The petrography of examined sandstone samples shows very poor to moderate sorting (Figure 3.29). According to the Folk's Classification of sandstone, the sandstone samples are arkosic, sub-arkosic to lithic arkose in composition as shown in the following ternary plot (Figure 3.32). The facies-wise ternary plots have been generated for each individual stratigraphic section to see the compositional variations within all facies (Figure 3.33). The average percentage composition of major framework grains is $Q_{71}F_{21}L_{8}$. The size of framework grains ranges from medium grained to pebbly in feldspar rich sandstone samples as compared to quartz rich samples which consists of very fine to coarse-grained mineral grains. The framework grain types observed in selected thin sections include

monocrystalline and polycrystalline quartz (Q_m, Q_p), K-feldspar (orthoclase and microcline), Plagioclase (albite) and lithic fragments (sedimentary, plutonic/volcanic and metamorphic origin), biotite and heavy minerals such as rutile and zircon (Figures 3.29, 3.30, 3.34, 3.35, 3.36, 3.37). The percentage of monocrystalline quartz is higher than polycrystalline quartz. Undulatory quartz grains exists in several samples but their occurrence is less in number than non-undulatory quartz grains. Chert was included in sedimentary rock fragments. Matrix content is relatively higher in siltstones and feldspar rich sandstones in comparison with the quartz rich sandstones (Figure 3.38). The matrix generally consists of detrital clay and serecite mica that is crushed between the framework grains. Mud intraclasts are also present as pseudo-matrix in few thin sections (Figure 3.39)

3.2.3 Texture

The sorting in majority of the sandstone samples collected from the Burqan Formation ranges from very poorly sorted to moderately sorted sandstones. The grain has angular to sub-angular shape (Figure 3.29). The grain size of sandstone samples varies from very fine sand to very coarse sand to pebble in size. The porosity types observed in sandstone samples include intergranular, intragranular fracture and dissolution porosities. The thin section of friable sandstones shows little to no cement therefore the major porosity type in these thin sections is primary or intergranular porosity (Figure 3.37), While the lithified samples contain carbonate and iron oxide or pyrite cements, therefore, the main porosity type in these thin sections is secondary or intragranular fracture and dissolution porosities (Figures 3.34, 3.35, 3.36, 3.38). Based on the modal analysis, low matrix content is present

in sandstone samples ranges from 0.1 to 2 percent while the matrix content in siltstones is as high as 14.5 percent. Two major pore filling cements are present such as the calcite and hematite cement. In some thin sections, Fe-dolomite and dolomite cements are also present along with the calcite cement.

3.2.4 Composition

Modal analysis reveals that quartz is the abundant framework grain with average 71 percent among feldspar (21%) and lithic fragments (8%). Q_m is more abundant than Q_p. Few quartz grains show inherited quartz overgrowth instead of in situ quartz overgrowth. The boundary of quartz overgrowth shows small pits and signs of erosion (Figure 3.44). The shape of the quartz grains ranges from angular to sub-rounded while grain size ranges from very fine to coarse grained overall. Some quartz grains show undulose extinction which may occur due to post-depositional processes such as diagenesis, folding and faulting near the provenance (Conolly, 1965).

The average percentage composition of feldspars is 21% by volume in all the samples. The shape of the feldspar grains ranges from sub-angular to sub-rounded while the size of individual feldspar grains ranges from very fine to very coarse grained in siltstone and sandstone samples respectively. Albite and orthoclase are the primary types of feldspars whereas microcline is present in small quantity in few thin sections. The process of sericitization has affected the surface of several plagioclase feldspar grains (Figure 3.29) Pertihitic texture is common on the surface of microcline and orthoclase feldspar (Figure 3.34b). Rock fragments are the least abundant framework grains (8%) in the studied thin

sections. All type of lithic fragments have been observed including sedimentary (chert, sandstone and limestone), igneous (plutonic & volcanic) and metamorphic rock fragments (Figures 3.29b, 3.35 b, 3.36 b, 3.46 b & d, 3.47 b & d).

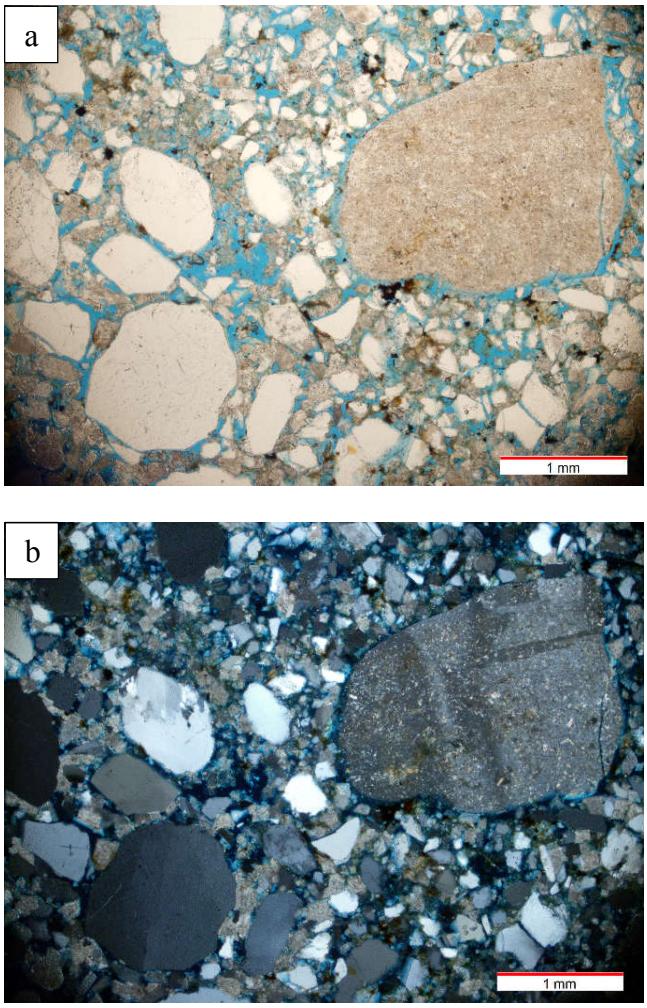

Figure 3.29: a) PPL-view (4X): Photomicrographs showing very poorly sorted and angular to sub-rounded framework grains. (b) XPL-view (4X): Majority of quartz grains are monocrystalline in nature. Undulose extinction in a large quartz grain lying in lower left corner is visible. Sericitization on the surface of large albite grain can be observed

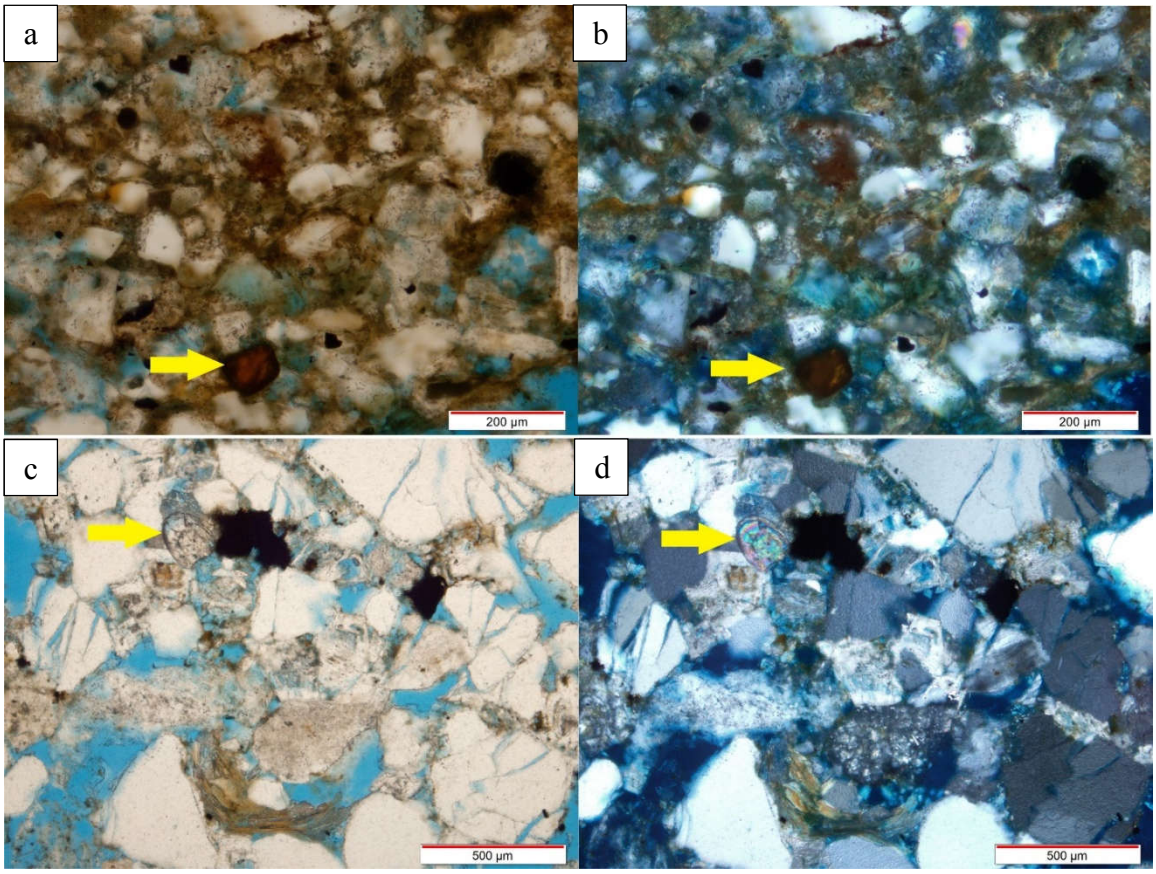

Figure 3.30: a & b) Magnification-20X: Optical micrographs showing the presence of rutile in siltstone sample. c & d) Magnification-10X: Heavy mineral zircon with very high relief and characteristic variegated color is present in a sandstone sample.

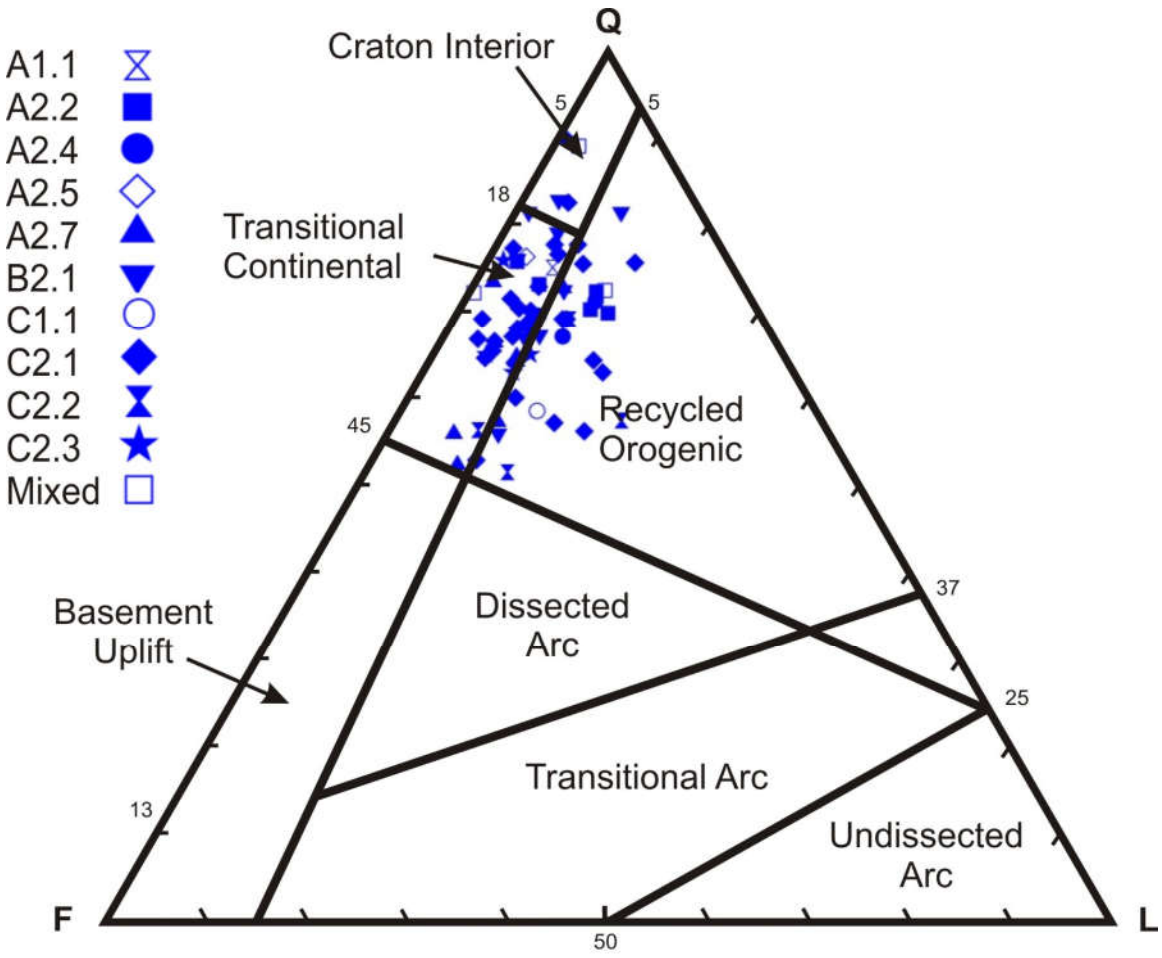

Figure 3.31: Compositional (QFL) plot showing different source terrains of Burqan Formation in the Midyan region.

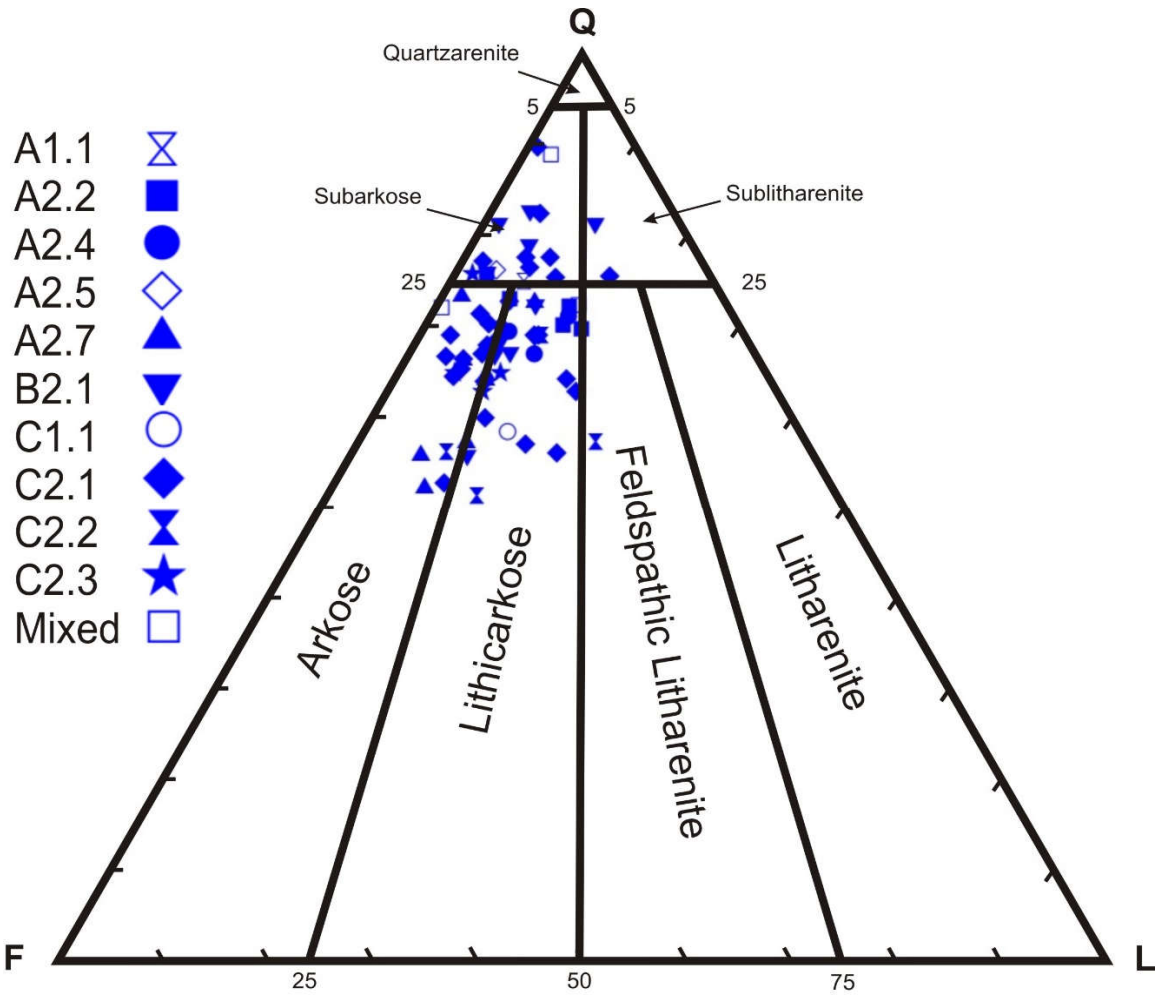

Figure 3.32: According to folk's classification of sandstones, the ternary plot of QFL showing that the sandstone samples are compositionally arkosic, sub-arkosic and lithic arkosic in nature (Modified after Folk, 1980).

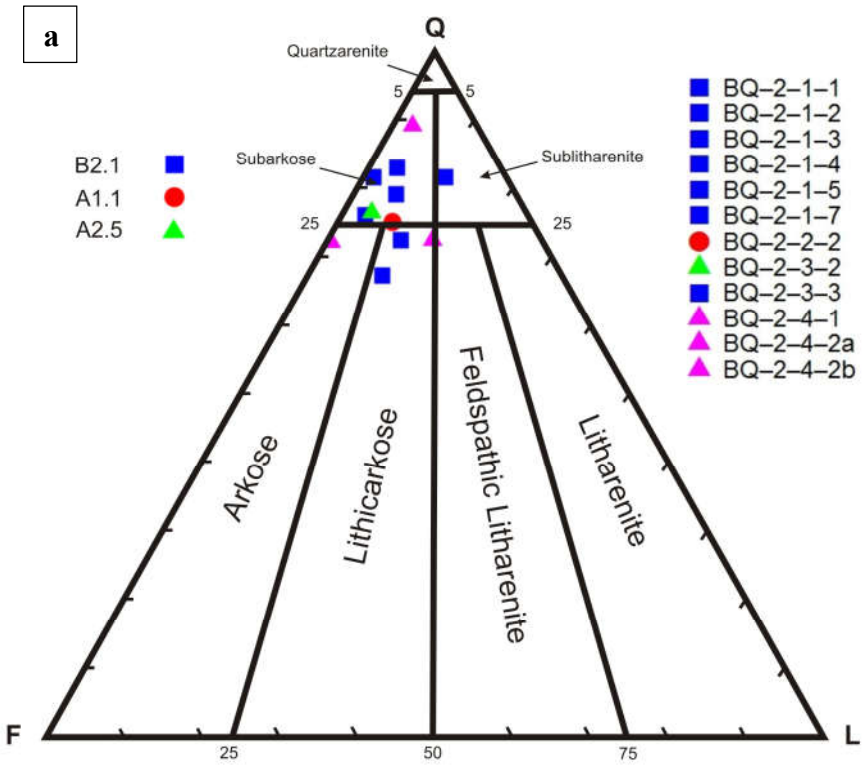
a
Q
Quartzarenite
5
5
Subarkose
Sublitharenite
25
25
B2.1
A1.1
A2.5
BQ–2–1–1
BQ–2–1–2
BQ–2–1–3
BQ–2–1–4
BQ–2–1–5
BQ–2–1–7
BQ–2–2–2
BQ–2–3–2
BQ–2–3–3
BQ–2–4–1
BQ–2–4–2a
BQ–2–4–2b
Arkose
Lithicarkose
Feldspathic Litharenite
Litharenite
F
L
25
50
75

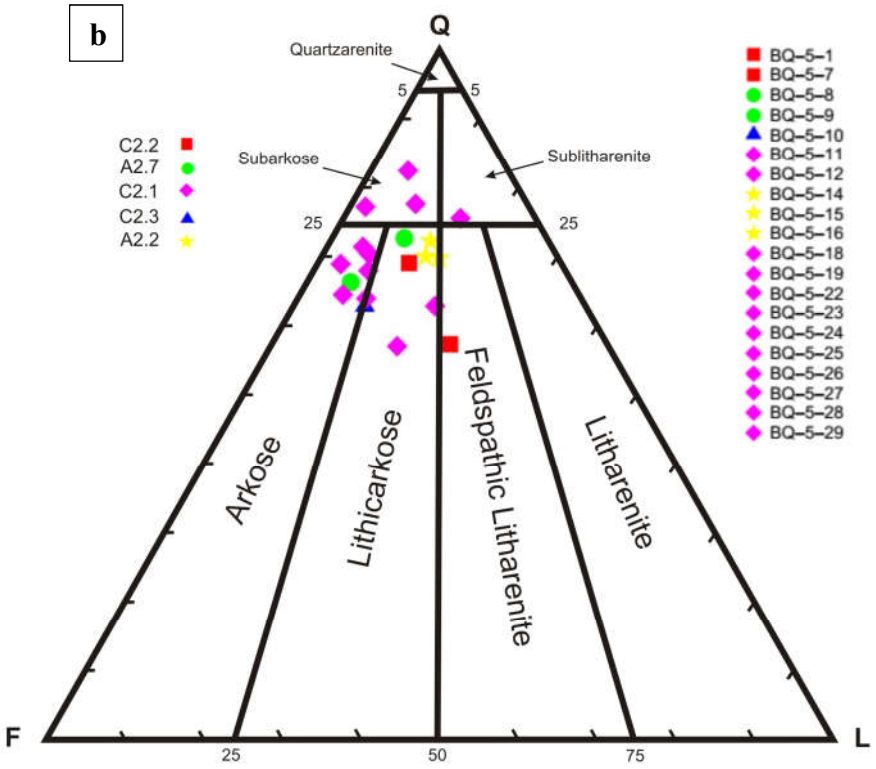
b
Q
Quartzarenite
5
5
Subarkose
Sublitharenite
25
25
C2.2
A2.7
C2.1
C2.3
A2.2
BQ–5–1
BQ–5–7
BQ–5–8
BQ–5–9
BQ–5–10
BQ–5–11
BQ–5–12
BQ–5–14
BQ–5–15
BQ–5–16
BQ–5–18
BQ–5–19
BQ–5–22
BQ–5–23
BQ–5–24
BQ–5–25
BQ–5–26
BQ–5–27
BQ–5–28
BQ–5–29
Arkose
Lithicarkose
Feldspathic Litharenite
Litharenite
F
L
25
50
75

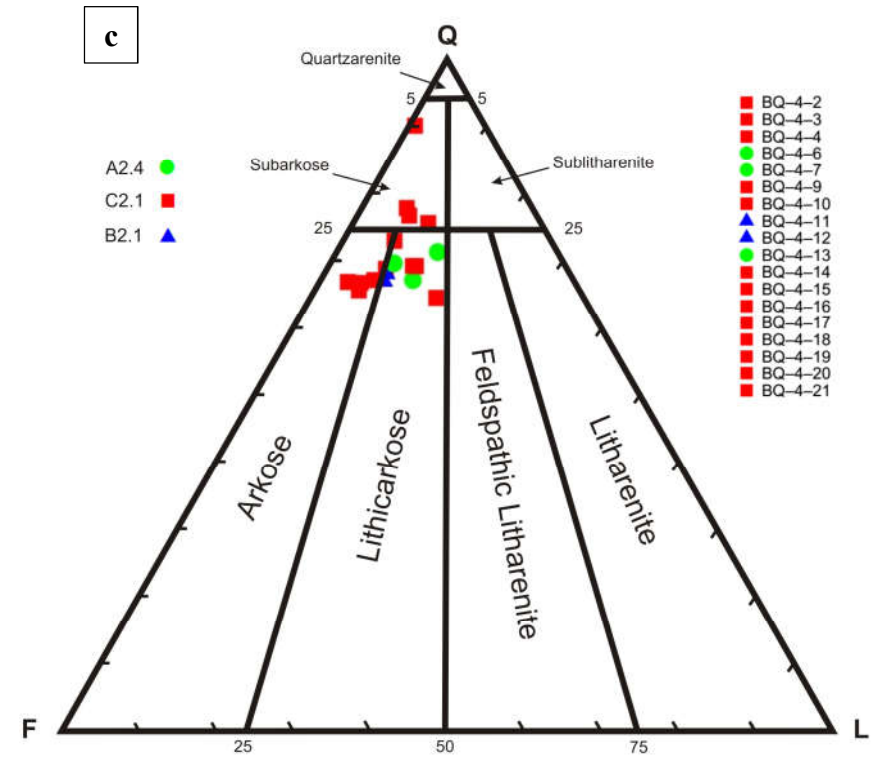
c
Q
Quartzarenite
5
5
Subarkose
Sublitharenite
25
25
A2.4
C2.1
B2.1
BQ–4–2
BQ–4–3
BQ–4–4
BQ–4–6
BQ–4–7
BQ–4–9
BQ–4–10
BQ–4–11
BQ–4–12
BQ–4–13
BQ–4–14
BQ–4–15
BQ–4–16
BQ–4–17
BQ–4–18
BQ–4–19
BQ–4–20
BQ–4–21
Arkose
Lithicarkose
Feldspathic Litharenite
Litharenite
F
L
25
50
75

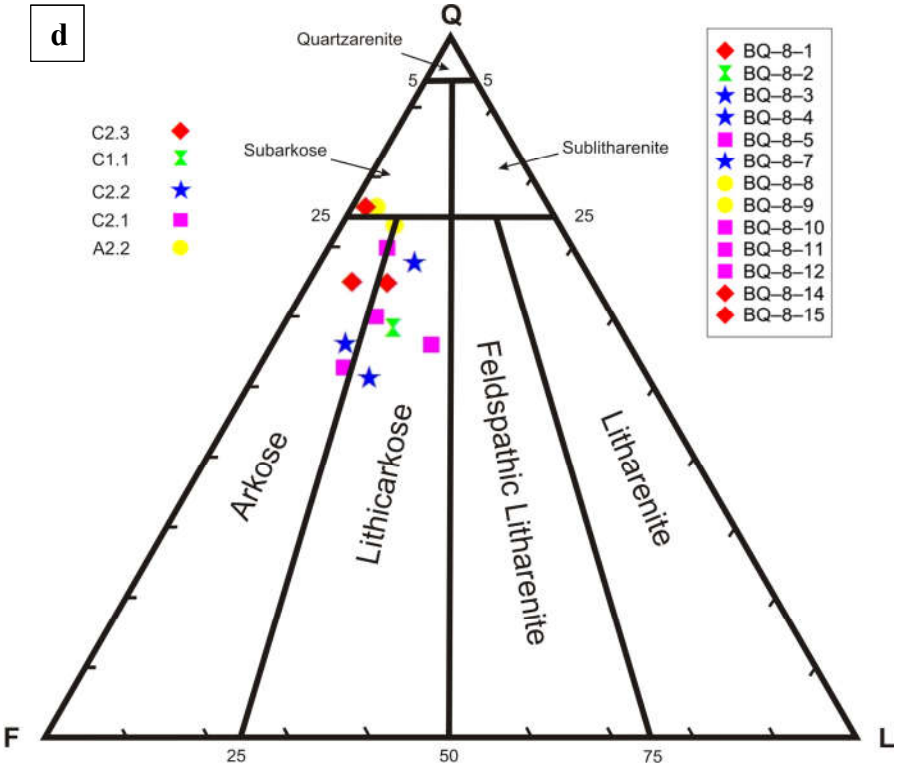
d
Q
Quartzarenite
5
5
Subarkose
Sublitharenite
25
25
C2.3
C1.1
C2.2
C2.1
A2.2
BQ–8–1
BQ–8–2
BQ–8–3
BQ–8–4
BQ–8–5
BQ–8–7
BQ–8–8
BQ–8–9
BQ–8–10
BQ–8–11
BQ–8–12
BQ–8–14
BQ–8–15
Arkose
Lithicarkose
Feldspathic Litharenite
Litharenite
F
L
25
50
75

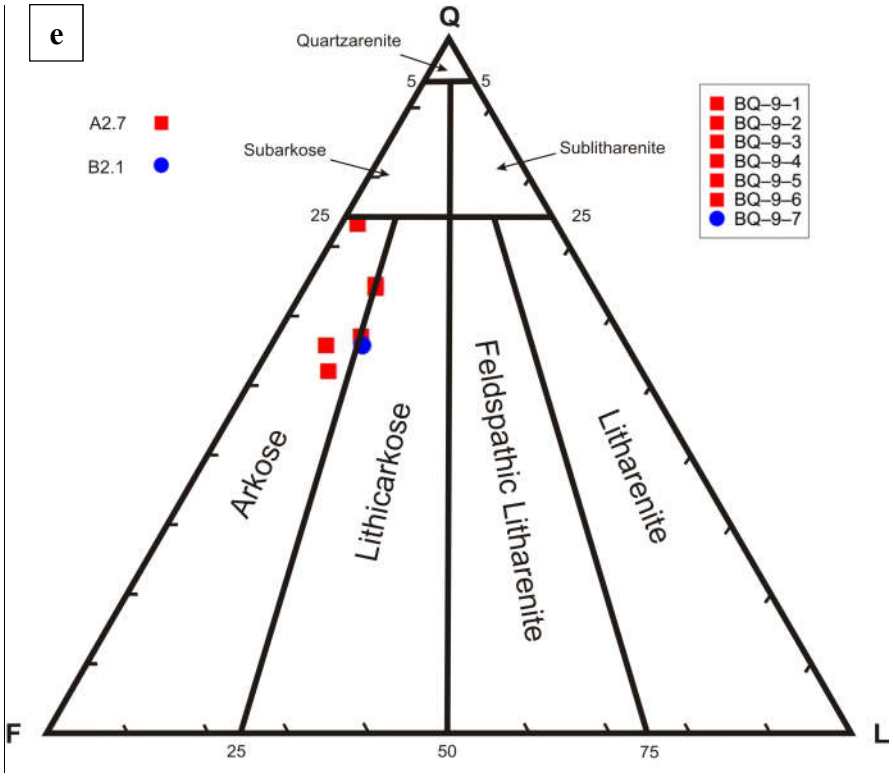

Figure 3.33: (a) Facies-wise ternary plot of Section-3, (b) Facies-wise ternary plot of Section-4, (c) Facies-wise ternary plot of Section-5, (d) Facies-wise ternary plot of Section-6, (e) Facies-wise ternary plot of Section-7. Facies-wise ternary plots of all stratigraphic sections are based on Folk's Classification.

Sample ID	Quartz	Feldspar	Lithics	Muscovite	Biotite	Dolomite	Calcite	Pyrite	Primary Porosity	Secondary Porosity	Heavy Minerals	Bioclasts	Kaolinite	Matrix Mud	Pickering Facies
BQ-2-1-1	58.1	11.3	4	N/A	3.3	N/A	N/A	1	14.3	3	0.7	N/A	3.3	1	B2.1
BQ-2-1-2	42.3	11	5.7	0	1.7	20	0	3	5.3	9	0.3	0	1.7	0	B2.1
BQ-2-1-3	40	8.3	0.6	0.6	3.3	21	2	10	13.6	0.6	0	0	0	0	B2.1
BQ-2-1-4	28.3	9	0.3	1.7	8.7	0	0	5.3	0	1.7	1.3	0	0	43.7	B2.1
BQ-2-1-5	54.5	5.3	7	0	0.3	14	1.3	3	13.6	1	0	0	0	0	B2.1
BQ-2-1-7	40.7	13.6	5.6	1.3	10.6	0	0	6	17.6	4	0.6	0	0	0	B2.1
BQ-2-2-2	46	11	4.3	0	3	0	0.7	2.7	14.3	10	0.7	0	5.7	1.6	A1.1
BQ-2-3-2	47.4	12.3	2.3	0.7	7.3	0	3	3	9	7	1.7	0	4	2.3	A2.5
BQ-2-3-3	53	8.7	2.3	0.3	2	16	1.7	2.7	6	7	0.3	0	0	0	B2.1
BQ-2-4-1	44.3	16.6	0.3	0.3	3	0	1	5.6	19.3	5.6	0.7	0	3.3	0	Mixed Siliciclastic and carbonate
BQ-2-4-2a	46.3	9	8.7	0	0.3	0	19.7	2.3	6.7	4.7	0.6	1.7	0	0	Mixed Siliciclastic and carbonate
BQ-2-4-2b	56	5.3	1.7	0	1.3	0	20	2	0.7	11.7	0	1	0.3	0	Limestone
BQ-4-2	64.7	6.7	0.7	0.3	0.3	0	7	3	8.3	8	1	0	0	0	C2.1
BQ-4-3	47.3	13.3	4.3	0	0.7	0	26.4	2	0	5	1	0	0	0	C2.1
BQ-4-4	47.6	14	7.7	0	0.7	0	17	2.3	8.7	1.7	0.3	0	0	0	C2.1
BQ-4-6	50.3	15.7	8.7	0	0	0	10.7	0.3	8.3	5.7	0.3	0	0	0	A2.4

BQ-4-7	46.7	10.3	8.7	0	0	0	0	0	30.3	3.7	0.3	0	0	0	A2.4
BQ-4-9	35.6	12.3	4	0	0	0	16	0.7	12.7	15.7	0	0	2.3	0.7	C2.1
BQ-4-10	44	9.4	3.3	0	0	0	16.4	0.3	6	9.7	0.3	0	2.3	0	C2.1
BQ-4-11	45.6	17	5.6	0	0.3	0	16	3.3	0.6	11.6	0	0	0	0	B2.1
BQ-4-12	46	16	5.7	0	0.7	0	21	0.7	7.6	2.3	0	0	0	0	B2.1
BQ-4-13	41.7	13.3	5	0	0	0	6.7	0	28.3	5	0	0	0	0	A2.4
BQ-4-14	37.3	15	3.7	0	0.3	0	37.3	0.7	1	4.7	0	0	0	0	C2.1
BQ-4-15	50.4	14.3	8.3	0	0.3	0	13.7	2	0	11	0	0	0	0	C2.1
BQ-4-16	51	10	6.7	0	1	0	18.7	1.3	2	9	0	0	0	0.3	C2.1
BQ-4-17	36.7	11	9.3	0.3	0.7	0	13	0.7	21.6	6.7	0	0	0	0	C2.1
BQ-4-18	42	18.7	2.3	0.3	1	0.7	14.3	3	3	14.7	0	0	0	0	C2.1
BQ-4-19	56.4	12.3	5	0	3	0	0	3.3	7	12.3	0.7	0	0	0	C2.1
BQ-4-20	41.7	18.3	3.7	0	1.3	0	31.7	0.3	0	3	0	0	0	0	C2.1
BQ-4-21	43.7	18.3	3.7	0.3	3.3	0	9.7	1.7	8	9.3	1	0	1	0	C2.1
BQ-5-1	35.4	12.3	14	0	1	0	24.3	3	0	8.7	1.3	0	0	0	C2.2
BQ-5-7	56	15.7	9.4	0.3	1.3	0	0	4.3	2.4	10.3	0.3	0	0	0	C2.2
BQ-5-8	52.3	13	6.7	0	1.3	0	0	1.3	16.7	8	0.7	0	0	0	A2.7
BQ-5-9	44	18.6	3.7	0.7	6	0	0	1.7	19	5	0	0	1.3	0	A2.7
BQ-5-10	41.3	18.3	6	0.7	3.7	0	1	4	11.7	12.3	0	0	1	0	C2.3
BQ-5-11	42.7	15.6	4.3	0	4	0	10	3	10	5.7	0.7	0	4	0	C2.1
BQ-5-12	41.6	16.6	1.7	0	2.7	0.3	22.6	4.6	0.6	9	0.3	0	0	0	C2.1

BQ-5-14	40.7	9.7	7.7	0.3	2	0	25	0.7	3	10.3	0.3	0	0.3	0	A2.2
BQ-5-15	49.3	10.7	10.7	0	1.3	0	0	1	21	6	0	0	0	0	A2.2
BQ-5-16	49.7	10.3	8.7	1	4.7	0	1	2.3	2.3	11.7	0.3	0	8	0	A2.2
BQ-5-18	45.7	15.3	3	0.7	5.7	0	16.3	4	1	7.3	0.7	0.3	0	0	C2.1
BQ-5-19	29.6	12.7	4	0.3	2.7	0	25.7	4	0	18.7	1.3	0.3	0.7	0	C2.1
BQ-5-22	50.6	6.3	10	0	4	0	3.7	4.7	1.3	18.7	0.7	0	0	0	C2.1
BQ-5-23	56.7	10.3	6	0.3	2	0	2.4	2.7	9.3	10.3	0	0	0	0	C2.1
BQ-5-24	62.7	9.6	3.6	0	2.6	0	0	2.6	11.3	7	0.6	0	0	0	C2.1
BQ-5-25	51.3	17.3	4.7	0	4.3	0	0	3.7	9	9.4	0.3	0	0	0	C2.1
BQ-5-26	50.7	13.7	1.3	0.3	8.7	0	0	8.7	4.3	12	0.3	0	0	0	C2.1
BQ-5-27	38.4	11.7	11.3	0	1.7	0	3.7	2.3	14.3	9	0	0	5.3	0	C2.1
BQ-5-28	43.6	20.3	3.7	0	0.7	0	15.7	3	10.7	2.3	0	0	0	0	C2.1
BQ-5-29	32	15	9	0	4	0	17	6.7	0	11.7	0.3	0	3.7	0.6	C2.1
BQ-8-1	40.4	18.3	3.3	0.3	8.7	0	11	8	0	10	0	0	0	0	C2.3
BQ-8-2	35.7	17	8.3	0.7	10	0	10	4.3	1	13	0	0	0	0	C1.1
BQ-8-3	41.3	25.6	6.7	0.7	3	0	0	8.7	0	13.7	0.3	0	0	0	C2.2
BQ-8-4	31	20.7	8.7	0.7	7.3	0	15	3.7	0	12.6	0.3	0	0	0	C2.2
BQ-8-5	33.7	23.3	6.7	0.3	5	10	5.7	4.3	0	11	0	0	0	0	C2.1
BQ-8-7	43	13	7.3	0	1.3	15.6	6	2.6	0	10.6	0.3	0	0.3	0	C2.2
BQ-8-8	44.4	12.3	4	0	4	0	15	3	0	16.3	0	0	1	0	A2.2
BQ-8-9	48.7	13.7	2	0.3	3	0	13	2	8	6.3	0	0.3	2.7	0	A2.2

BQ-8-10	42.3	20.7	7.7	0	2.3	0	0.3	3.3	11.3	8.3	0	0	3.7	0	C2.1
BQ-8-11	48.4	15.7	5	0	1.3	0	0	5.3	13.7	6.3	0.3	0	4	0	C2.1
BQ-8-12	35.4	15.3	12.3	0.3	0.7	0	10	1.7	8.3	11.7	0	0	4.3	0	C2.1
BQ-8-14	45	13.3	1	0.3	3.7	0	14	2.7	8.7	5.7	0.3	0	1.3	4	C2.3
BQ-8-15	37.7	14.7	5.7	0.3	4	0	4.4	4.7	15.3	10.3	0	0	1.6	1.3	C2.3
BQ-9-1	38.7	16.3	5.3	0	2.6	0.9	23	3.6	0	8	0.3	0	1.3	0	A2.7
BQ-9-2	39.4	13.3	1	0.7	4.3	0	28	6.3	0	6.3	0.7	0	0	0	A2.7
BQ-9-3	35.3	14.6	4.6	0.7	5.7	1.3	23.7	5.7	0	7.7	0.7	0	0	0	A2.7
BQ-9-4	31.3	23.3	5.3	0.7	8.3	0	0	6.7	18.7	4	0.7	0	1	0	A2.7
BQ-9-5	34.7	19.7	6.4	0	3	0	25	3	0	3.3	0.3	2.3	0.3	2	A2.7
BQ-9-6	33.3	22.3	4	0.7	4.7	0	22.7	5.6	0	5.7	1	0	0	0	A2.7
BQ-9-7	31.6	18.7	6.3	0.7	5.3	0	20	8	0	7.7	0.7	0	0	1	B2.1

Table 6: Summarized modal analysis (framework grain, diagenetic minerals, porosity types, bioclasts, matrix content, heavy minerals and Pickering Facies) of 70 representative sandstone and siltstone samples from Burqan Formation.

Sample ID	Quartz %	Feldspar %	Lithic Fragments %	Total (%)
BQ-2-1-1	79	15.5	5.5	100
BQ-2-1-2	72.4	18.2	9.4	100
BQ-2-1-3	81.4	17.2	1.4	100
BQ-2-1-4	74.5	24.5	1	100
BQ-2-1-5	81.4	8	10.6	100
BQ-2-1-7	67.2	23.2	9.6	100
BQ-2-2-2	75	18	7	100
BQ-2-3-2	76.3	20	3.7	100
BQ-2-3-3	82.8	13.5	3.7	100
BQ-2-4-1	72.1	27.3	0.6	100
BQ-2-4-2a	72.4	14.1	13.5	100
BQ-2-4-2b	89	8.4	2.6	100
BQ-2-5-1	79.2	12.8	8	100
BQ-2-5-2	85.4	8	6.6	100
BQ-2-5-3	79	14	7	100
BQ-2-7-1	66.5	15.9	17.6	100
BQ-2-8-1	58	33	9	100
BQ-2-9-1	75.5	16.5	8	100
BQ-2-10-1	62.9	33.5	3.6	100
BQ-2-11-1	88.7	9.4	1.9	100
BQ-2-11-2	85.6	9.8	4.6	100
BQ-2-11-3	85.8	11.5	2.7	100
BQ-2-11-4	78.7	11.8	9.5	100
BQ-2-12-1	75	19	6	100
BQ-2-12-2	80.3	13.3	6.4	100
BQ-2-12-3	84.1	12.2	3.7	100

BQ-2-12-4	84	9	7	100
BQ-4-2	89.8	9.3	0.9	100
BQ-4-3	72.8	20.5	6.7	100
BQ-4-4	69	20	11	100
BQ-4-6	67	21	12	100
BQ-4-7	71.1	15.7	13.2	100
BQ-4-9	68.6	23.7	7.7	100
BQ-4-10	77.6	16.5	5.9	100
BQ-4-11	66.8	24.9	8.3	100
BQ-4-12	68	24	8	100
BQ-4-13	69.5	22.2	8.3	100
BQ-4-14	67	26	7	100
BQ-4-15	69	19.6	11.4	100
BQ-4-16	75.4	14.8	9.8	100
BQ-4-17	64.3	19.3	16.4	100
BQ-4-18	66.7	29.6	3.7	100
BQ-4-19	76.5	16.7	6.8	100
BQ-4-20	65.4	28.8	5.8	100
BQ-4-21	66.5	28	5.5	100
BQ-5-1	57.3	20	22.7	100
BQ-5-7	69.1	19.3	11.6	100
BQ-5-8	72.7	18.1	9.2	100
BQ-5-9	66.3	28.1	5.6	100
BQ-5-10	62.9	28	9.1	100
BQ-5-11	68	25	7	100
BQ-5-12	69	28	3	100
BQ-5-14	70.1	16.7	13.2	100
BQ-5-15	69.8	15.1	15.1	100
BQ-5-16	72.3	15	12.7	100
BQ-5-18	71.4	24	4.6	100
BQ-5-19	64	27.3	8.7	100

BQ-5-22	75.6	9.5	14.9	100
BQ-5-23	77.6	14.2	8.2	100
BQ-5-24	82.5	12.7	4.8	100
BQ-5-25	70.3	23.7	6	100
BQ-5-26	77.2	20.8	2	100
BQ-5-27	62.9	19.1	18	100
BQ-5-28	64.5	30	5.5	100
BQ-5-29	57.1	26.8	16.1	100
BQ-8-1	65	29.6	5.4	100
BQ-8-2	58.5	27.8	13.7	100
BQ-8-3	56.2	34.8	9	100
BQ-8-4	51.4	34.3	14.3	100
BQ-8-5	52.8	36.7	10.5	100
BQ-8-7	67.9	20.5	11.6	100
BQ-8-8	73.1	20.3	6.6	100
BQ-8-9	75.7	21.2	3.1	100
BQ-8-10	60	29.2	10.8	100
BQ-8-11	70	22.7	7.3	100
BQ-8-12	56.1	24.3	19.6	100
BQ-8-14	75.8	22.5	1.7	100
BQ-8-15	64.9	25.3	9.8	100
BQ-9-1	64.1	27.1	8.8	100
BQ-9-2	73.3	24.8	1.9	100
BQ-9-3	64.6	26.8	8.6	100
BQ-9-4	52.2	38.9	8.9	100
BQ-9-5	57.2	32.4	10.4	100
BQ-9-6	55.9	37.4	6.7	100
BQ-9-7	55.8	33	11.2	100
Mean (%)	**70.5**	**21.3**	**8.2**	**100**

Table 7: The table showing average composition of major framework grains in all samples of the Burqan Formation.

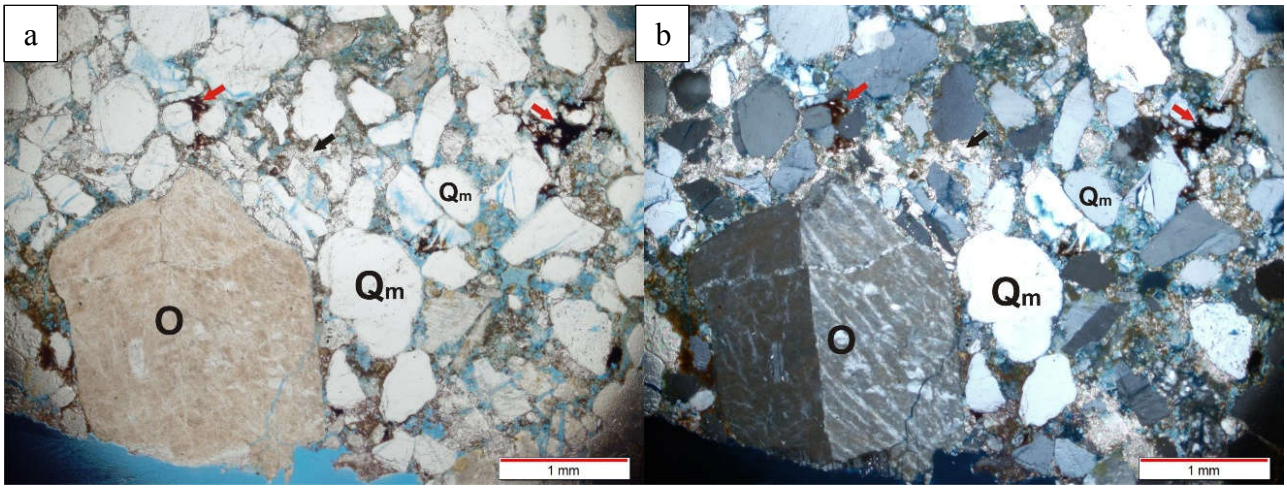

Figure 3.34: a) PPL-view (4X): Optical micrograph showing different framework grains, cement and porosity types. Q_m= monocrystalline quartz, O= Orthoclase, Red Arrows are showing hematite cement engulfing the calcite cement while black arrows are pointing towards calcite cement clogging the pores. (b) XPL-view (4X): Abundant monocrystalline quartz grains are present. The coarse grained orthoclase shows Carlsbad twinning and Perthitic texture.

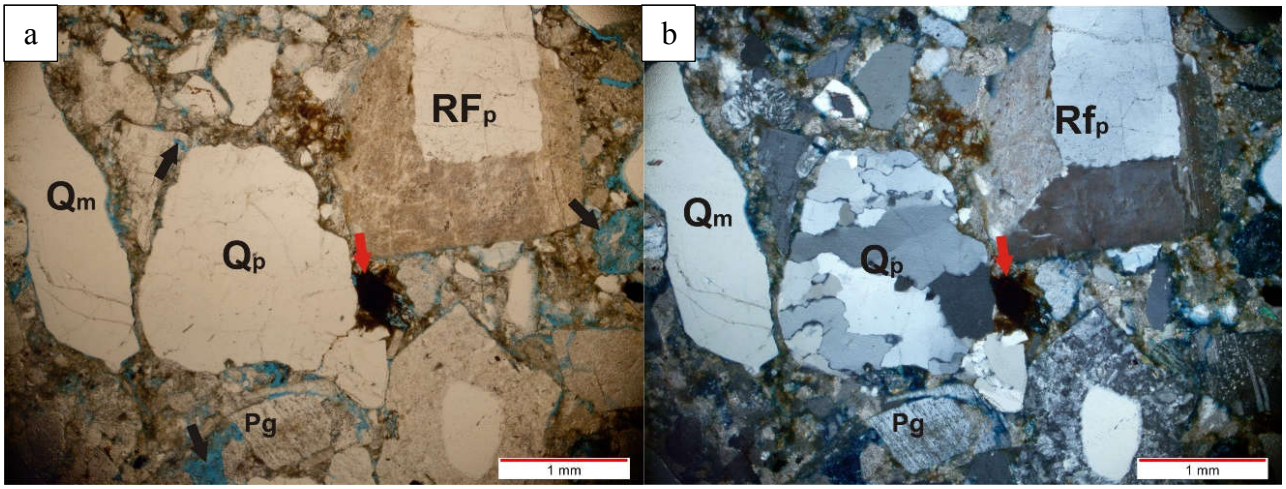

Figure 3.35: a) PPL-view (4X): Photomicrograph showing mono- and polycrystalline quartz and plutonic rock fragments. Red Arrow shows hematite cement while black arrows show secondary porosity (partial grain dissolution). (b) XPL-view (4X): Photomicrograph showing non-undulatory monocrystalline quartz crystal (Q_m) embedded next to polycrystalline quartz grain (Q_p) consists of several crystals. Plagioclase (P_g=Albite) shows characteristic polysynthetic twinning. A large plutonic rock fragment is also present. Red arrow indicates hematite cement.

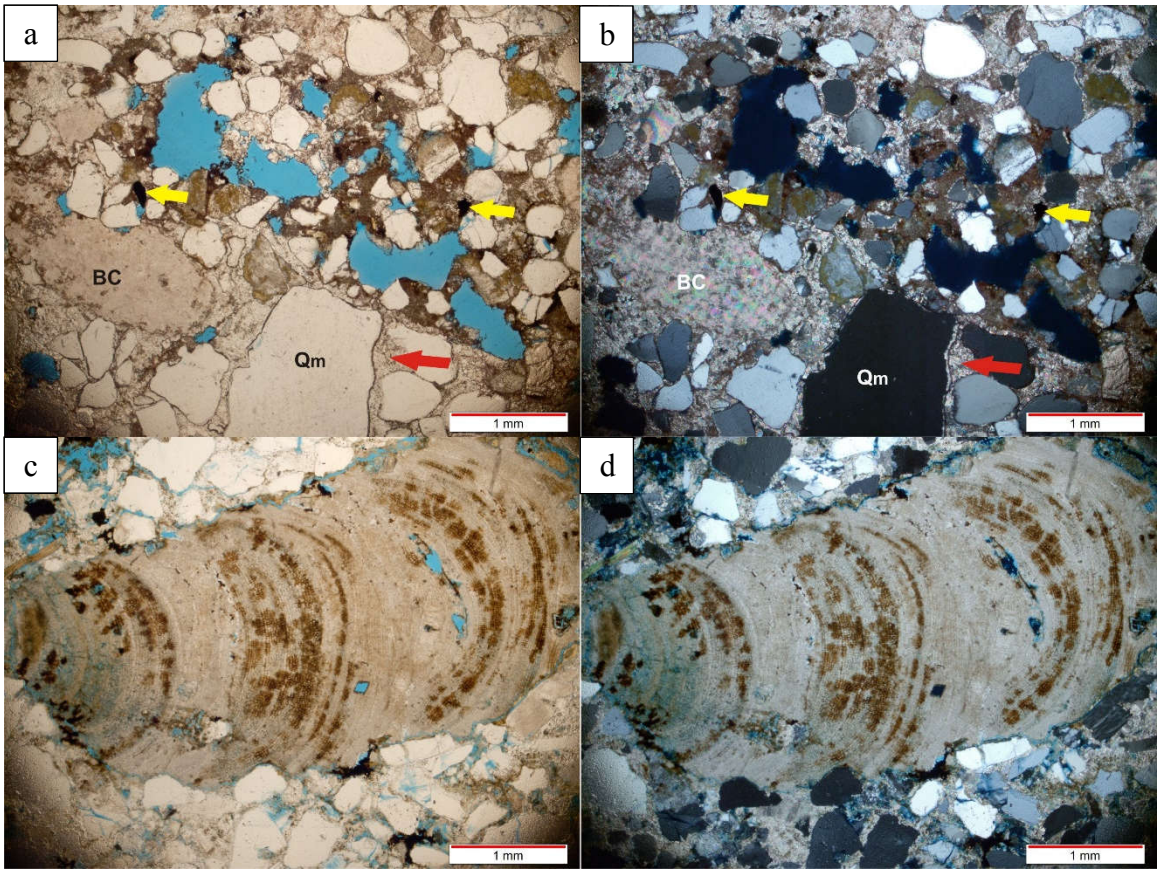

Figure 3.36: a) PPL-view (4X): Optical micrograph showing bioclast composed of calcium carbonate (BC). Red arrows indicate syn-depositional calcite cement while yellow arrows indicate patches of early diagenetic pyrite cement engulfed by calcite cement. Secondary porosity is visible which is created due to the dissolution of framework grains and cement. (b) XPL-view (4X): xnicol view of micrograph-a. (c) PPL-view (4X): Optical micrograph showing large piece of dolomitized red algae. Secondary porosity is shown by blue color. (d) XPL-view (4X): xnicol view of micrograph-c.

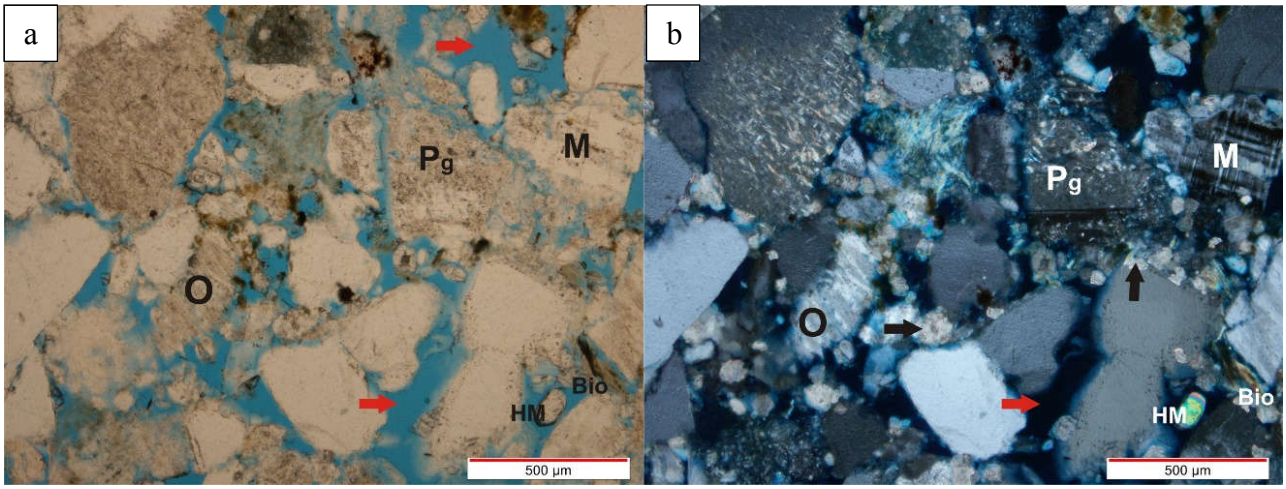

Figure 3.37: a) PPL-view (10X): Red arrows in optical micrograph are indicating towards high primary intergranular porosity. This is due to lack of sufficient cement. (b) XPL-view (10X): Photomicrograph showing Orthoclase grain (O) with perthitic texture, Plagioclase (Albite-Pg with multiple twinning) with tiny serecite mica flakes on the surface, Microcline (M) shows characteristics cross-hatch twinning. Black arrows indicate towards patches of calcite cement.

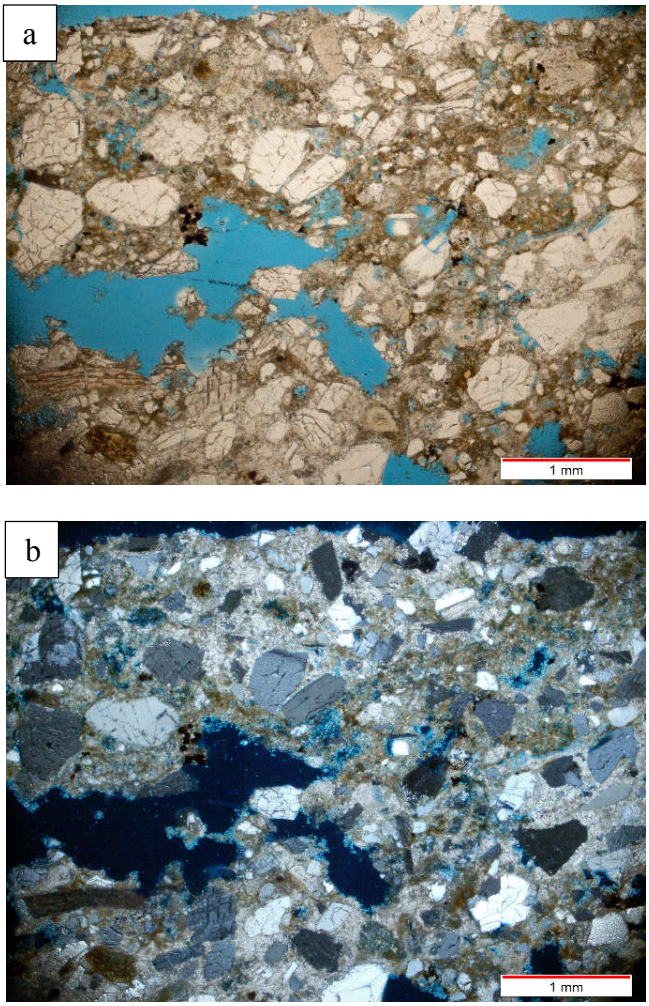

Figure 3.38: a) PPL-view (4X): Photomicrograph showing highly fractured quartz grain with argillaceous matrix between the grains. The primary cement between the grains is calcite. Sparse early diagenetic pyrite cement is also present. High secondary porosity (blue colored spaces) is visible due to the partial dissolution of framework grains and cement. (b) XPL-view (4X). Cross nicols view of optical micrograph-a.

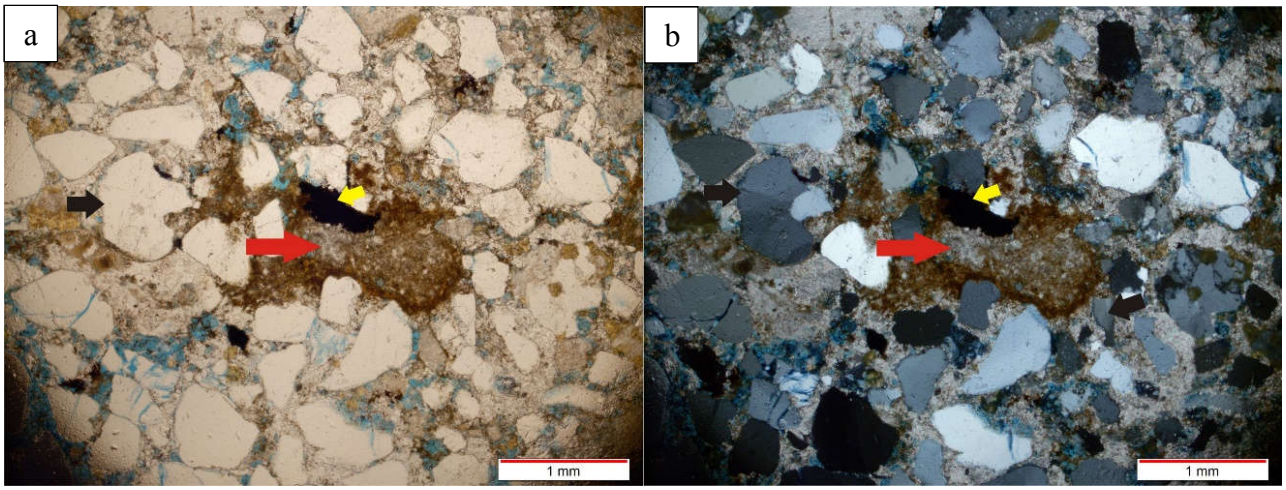

Figure 3.39: a) PPL-view (4X): Optical photomicrograph showing mud intraclast (red arrow) squeezed between quartz grains. (b) XPL-view (4X): Black arrows indicates towards undulatory quartz grains while yellow arrows are showing early diagenetic pyrite cement present as patches. Calcite cement is the major cement occluding all the primary pore spaces.

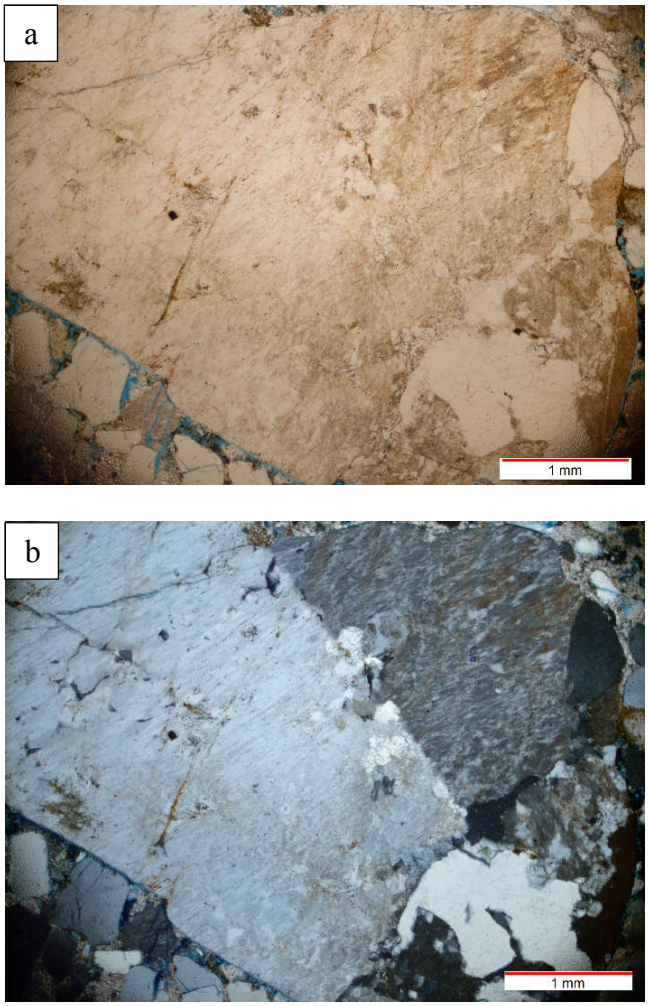

Figure 3.40: a) PPL-view (4X): Optical micrograph is showing a pebble of plutonic rock fragment. The size of the grain is larger than 4 mm and the grain boundaries are going out of the field of view. (b) XPL-view (4X): Crossed nicols view of optical micrograph-a.

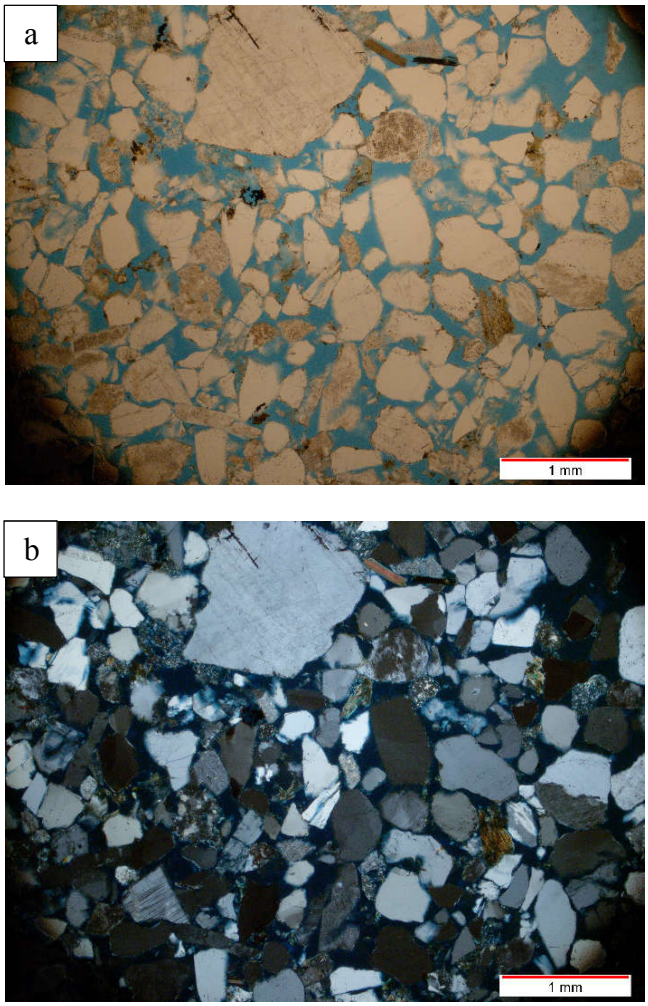

Figure 3.41: a) PPL-view (4X): Photomicrograph showing low compaction, high intergranular porosity in friable sandstone sample of Burqan Formation due to the absence of any cement. Only early diagenetic pyrite cement is present as small patches. (b) XPL-view (4X): Optical micrograph showing the relative abundance of monocrystalline quartz Q_m over polycrystalline quartz Q_p. Few detrital biotite mica grains are also present.

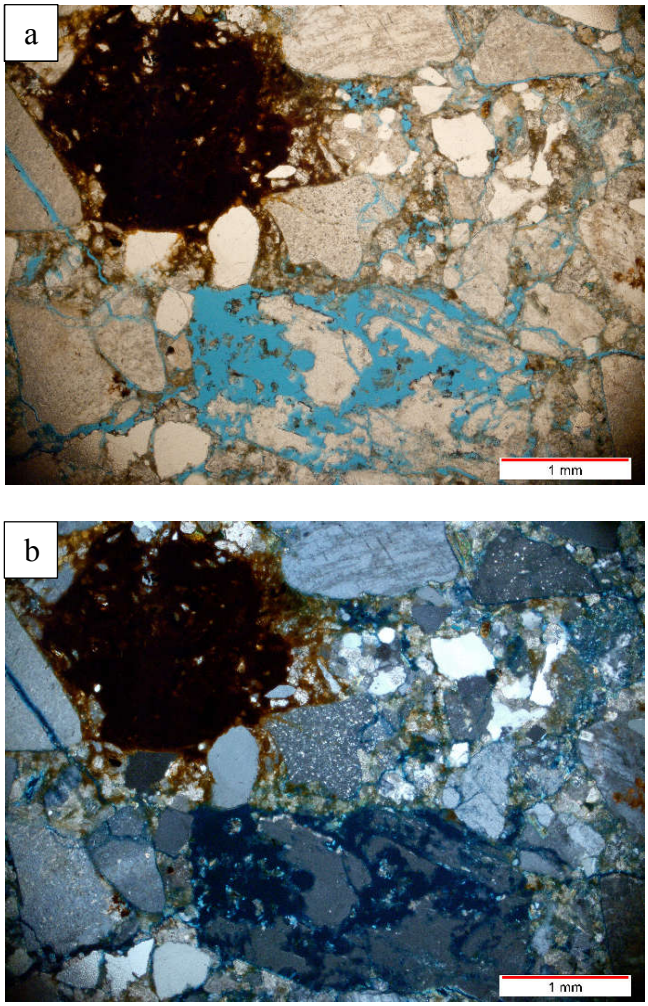

Figure 3.42: a) PPL-view (4X): Optical micrograph showing the secondary porosity created by partial dissolution of quartz grain and calcite cement. Similarly, fracture porosity is also visible near the left corner of the picture. Large patch of late diagenetic stage thick patch of hematite cement is present (b) XPL-view (4X): Optical micrograph showing abundant altered feldspar grains of different shapes and sizes.

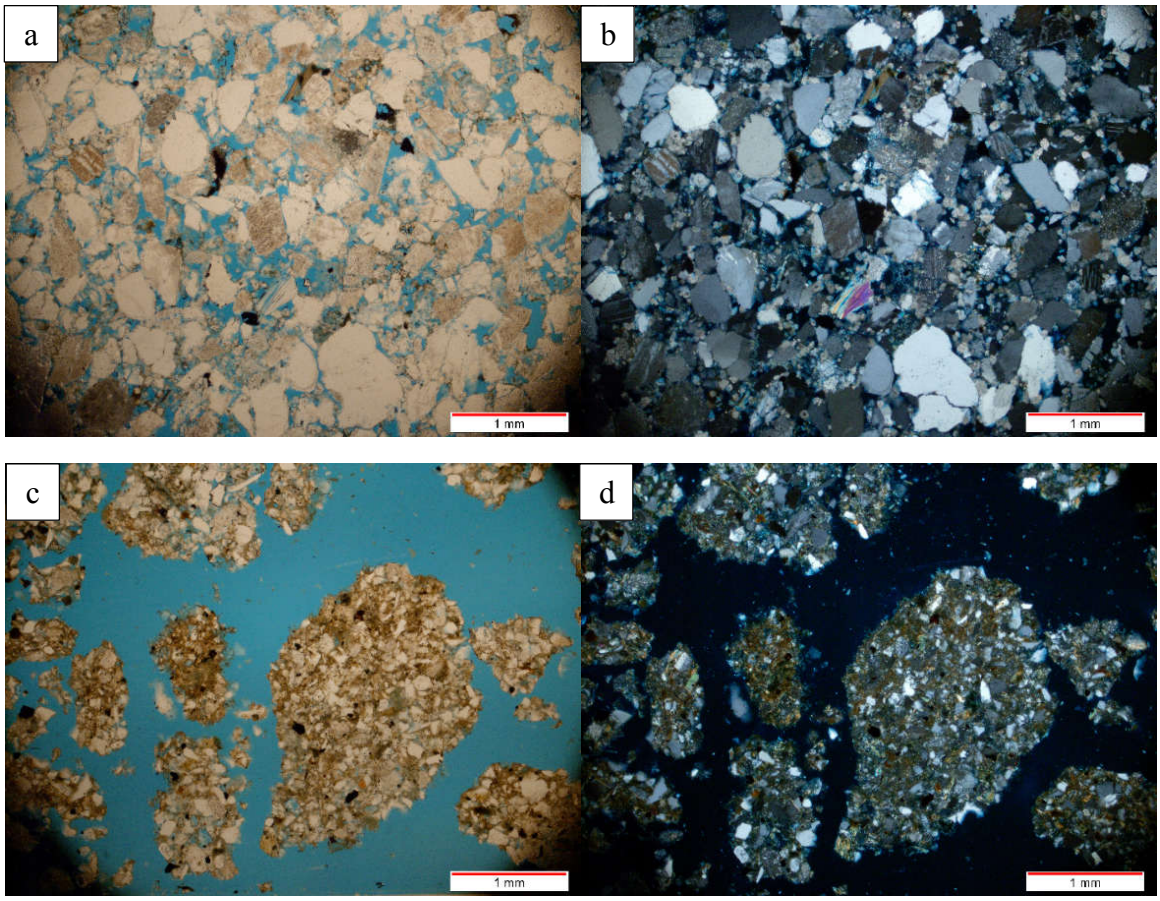

Figure 3.43: Photomicrographs showing the comparison between lowest matrix content in calcite cemented sandstone sample (a & b) and highest matrix in siltstone sample (c & d). Magnification-4X.

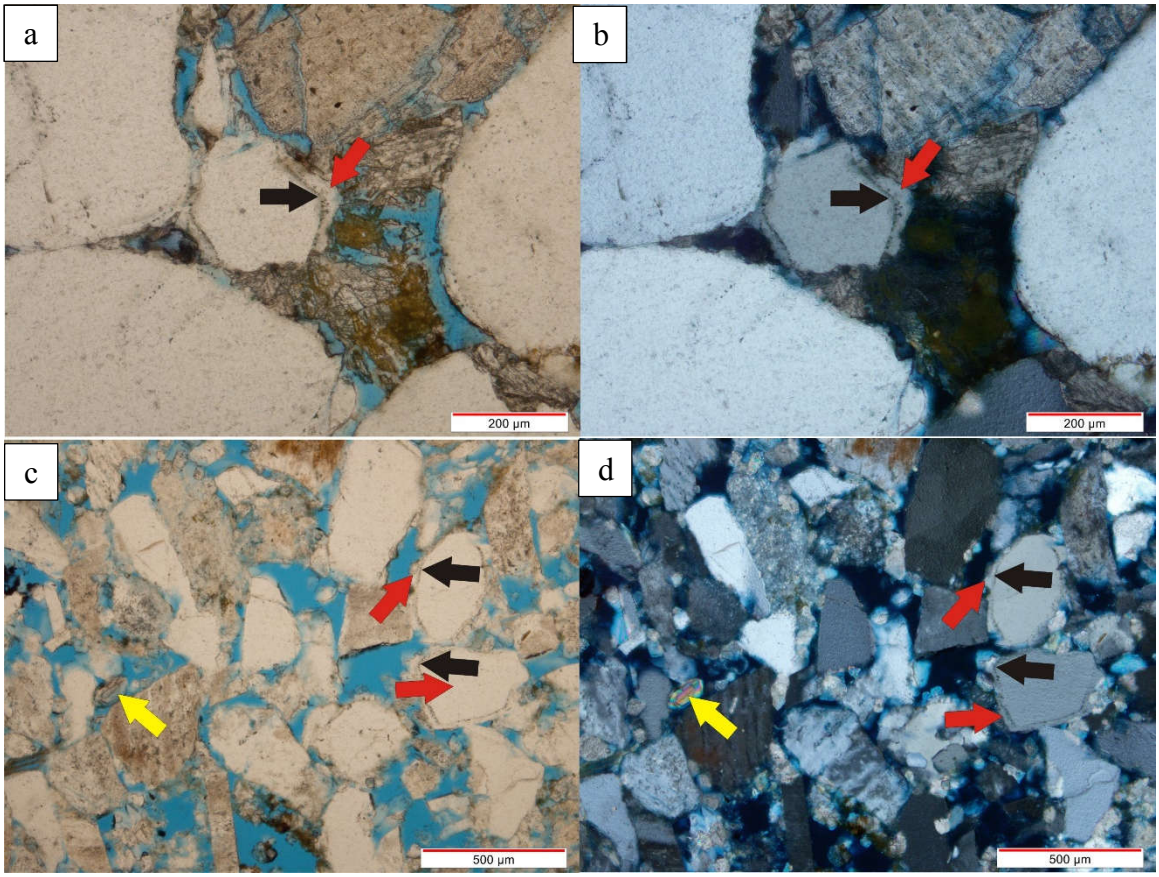

Figure 3.44: Photomicrographs showing the inherited quartz overgrowths. The thickness of overgrowth is variable and not euhedral around the grain showing its inherited nature. The black arrows indicate the dust line while red arrows show syntaxial inherited quartz overgrowths. Yellow colored arrows are indicating the presence of high relief Zircon (heavy mineral) grain in (c) and (d). a &b has 20X magnification. c & d has 10X magnification.

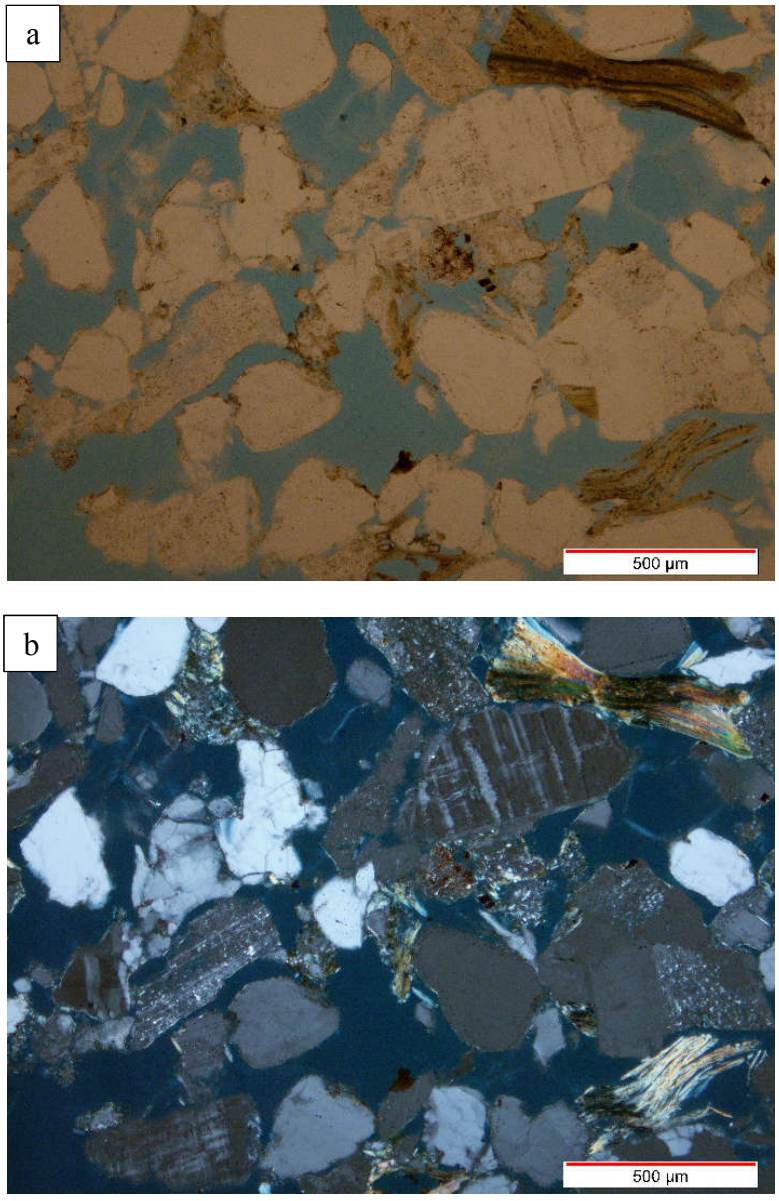

Figure 3.45: a) PPL-view (10X): Optical micrograph showing very high primary porosity and little bending in detrital biotite grains indicating towards low to moderate compaction. (b) XPL-view (10X): Optical micrograph showing perthitic texture associated with microcline grain. The surface of the plagioclase feldspar is showing flakes of sericite mica in response to hydrothermal alteration. No major cement is present except minor patches of early diagenetic pyrite cement.

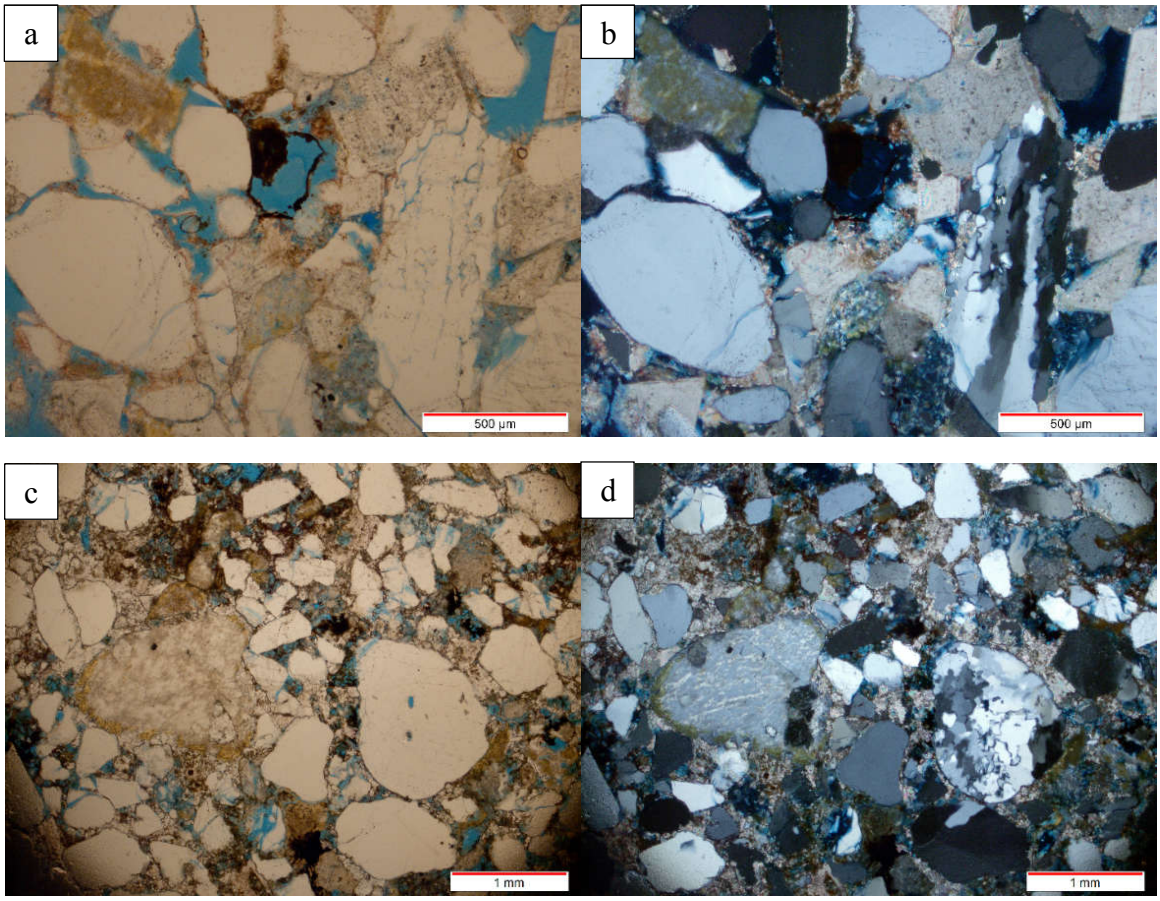

Figure 3.46: (a) PPL-view (10X): Photomicrograph showing the remnant outline of completely dissolved grain, later replaced by hematite cement in the center of the micrograph. (b) XPL-view (10X): A metamorphic rock fragment. Coarse-crystalline and euhedral rhombic crystals of dolomite cement is filling the intergranular pores and reducing the primary porosty. (c) PPL-view (4X): Photo micrograph showing different phases of cementation. Calcite cement (Phase-1) filled the pores and hematite cement came later (Phase-2) and filling the space created due to the dissolution of calcite cement. Secondary dissolution porosity is visible. (d) PPL-view (4X): Photomicrograph showing a polycrystalline quartz of metamorphic origin. Perthitic texture on nearby large orthoclase crystal is also visible.

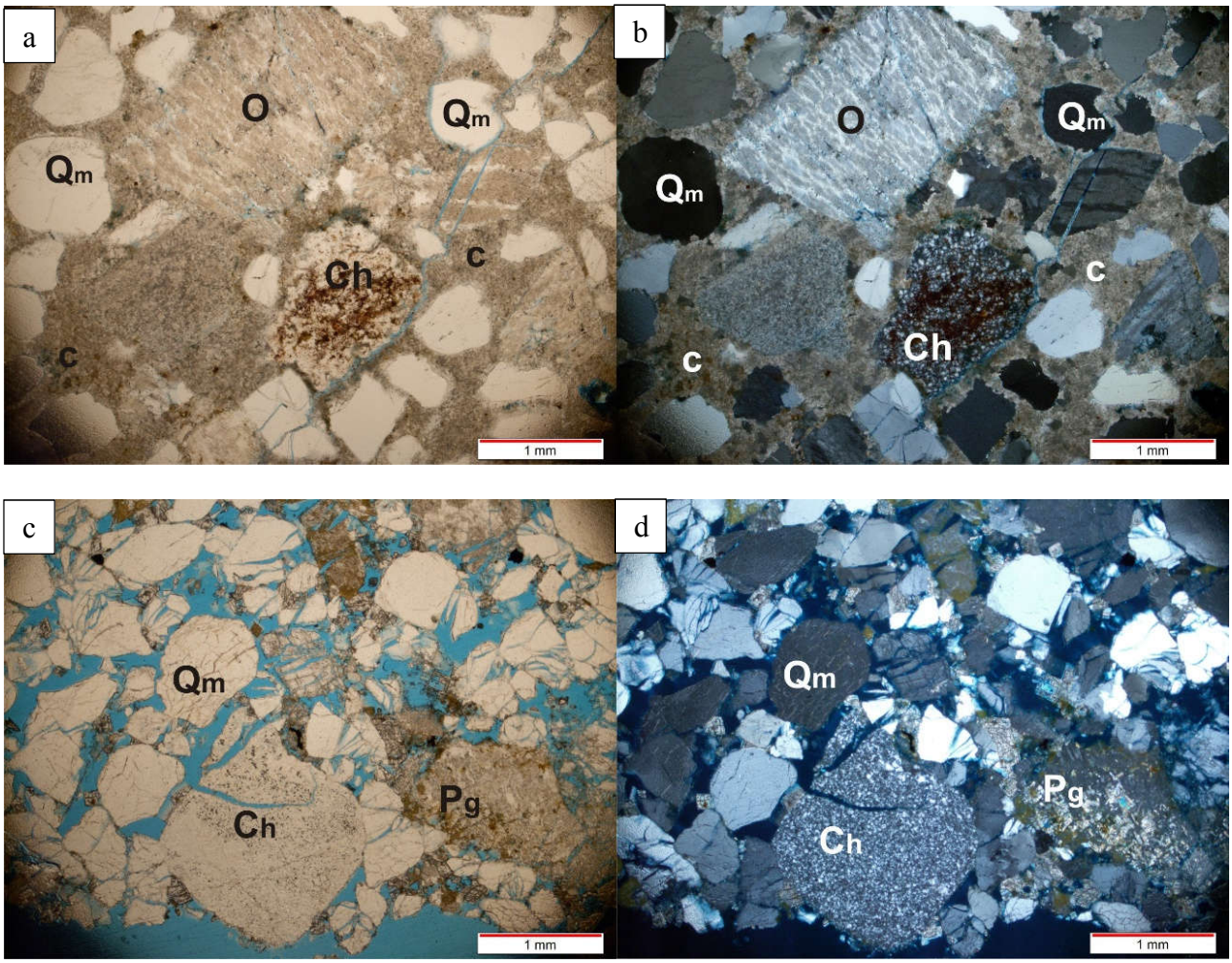

Figure 3.47: a) PPL-view (4X): Photomicrograph showing fracture porosity and hematite cement as coating within the chert (Ch) fragment. (b) XPL-view (4X): Photomicrograph contains perthitic texture within orthoclase (O), monocrystalline quartz (Q_m), calcite cement (C) and microcrystalline quartz/Chert (Ch) fragment. (c) PPL-view (4X): A quartz rich sandstone sample with very high primary and secondary porosity. (d) XPL-view (4X): Photomicrograph showing monocrystalline quartz (Q_m), sericitized plagioclase feldspar (P_g) and chert fragment (C_h).

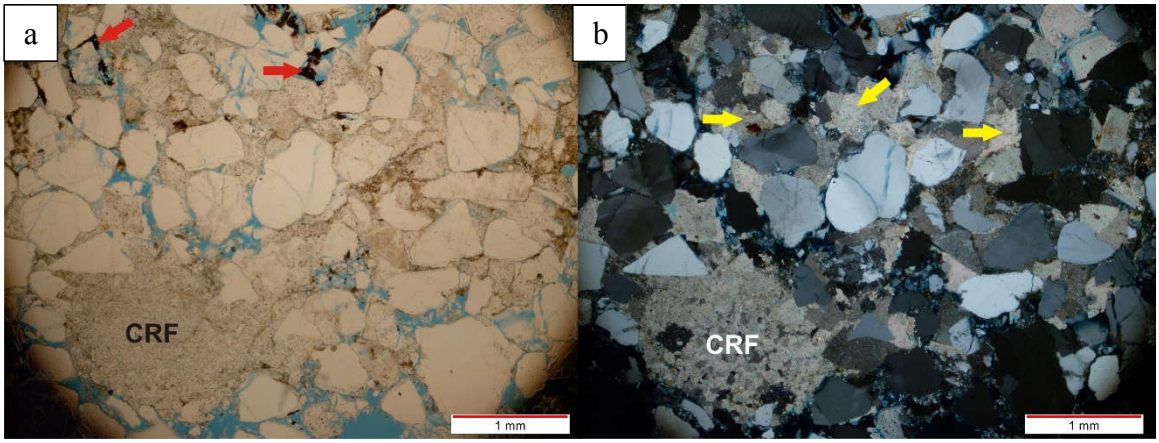

Figure 3.48: (a) PPL-view (4X): The primary porosity has been lost due to syndepositional euhedral to subhedral dolomite cement. A Carbonate rock fragment (CRF) is also present. Red arrows show the replacement of partially dissolved grains with hematite cement. (b) XPL-view (4X): Yellow arrows show that Coarse-mosaic dolomite cement is killing the primary porosity.

3.3 Diagenesis

Studying diagenetic features of the Burqan Formation reveals that the outcrops of the Burqan Formation have been subjected to physical compaction whereas the characteristic signatures of chemical compaction have not been observed. The studied samples show that the carbonate cements are the major binding cements between the grains along with pyrite and hematite as minor cements. The percentage of diagenetic clays is very low .Overall high porosities have been calculated via modal analysis and can be observed in the thin sections of low to moderately cemented samples.

3.3.1 Mechanical Compaction

Mechanical compaction is manifested in sandstone by the bending in ductile grains such as mud intraclasts and micas when squeezed between brittle framework grains like quartz, feldspars and rock fragments. The majority of the studied sandstone samples shows low to moderate compaction (Figure 3.41). Chemical compaction such as stylolite/pressure solution and penetration of muscovite in quartz grains has not been observed in any sandstone thin section.

3.3.2 Carbonate Cementation

Almost every examined sample has diagenetic cements but the degree of cementation is different in all samples. Based on the visual estimation, the total percentage of authigenic carbonate cement against the total volume in any cemented sample varies between 5-20%. Major type of authigenic cements are calcite, dolomite and Fe-dolomite. Carbonate cements occur as syn-depositional coarse- to finely crystalline in shape. The XRD analysis

and electron microprobe analysis data also supports the petrographic results by identifying that the major types of carbonate cement are calcite, dolomite and Fe-dolomite. (Table-7, Table-8). The petrographic analysis shows that the carbonate cement occurs either as pore-filling or grain replacing material (Figures 3.46, 3.49, 3.50). Calcite cement shows characteristics calcite twinning while filling a continuous fracture in a thin section (Figure 3.55)

Fe-dolomite and dolomite cements both occur as euhedral to anhedral rhomb-shaped crystals of various sizes ranges from fine to coarse crystalline among the framework grains (Figure 3.49). The coarse- to fine, clear or cloudy crystalline dolomite cement also found as pre-compactional cement killing the primary porosity of the sandstone.

3.3.3 Pyrite, Iron Oxide and Quartz Cementation

Pyrite and hematite cements are the least abundant authigenic cements found in the sandstone samples as revealed by XRD analysis. These cements occur as scattered patches. The amount of these opaque cements calculated from point counting method ranges from 0.1 to 3%, whereas XRD analysis shows that their amount is less than 1% in representative sandstone samples (Figures 3.39, 3.46, 3.50). Quartz cement is absent in all the thin section. The overgrowth around quartz grains has been observed in few thin sections but the morphology of the grain boundaries shows the sign of reworking due to the presence of small pits and undulations.

3.3.4 Clay Minerals

The percentage of diagenetic clays observed in thin sections ranges from 1-8% but the actual amount is low about < 1% average revealed by XRD analysis of clay separated from sandstone samples. Booklet shaped *Kaolinite* clay was found in few thin sections at very high magnification (20X) as patches of 50-200 μm in size. This fan shaped or accordion-like kaolinite has expanded and filled the surrounding pores (Figure 3.52 a & b). The detrital or grain coating smectite clay has not been observed under the petrographic microscope probably due to the ultra-thin layers around the framework grains but SEM photomicrographs and XRD data has revealed their presence as grain coatings (SEM micrograph Figure 3.52 c & d). Minor quantity of chlorite and illite clay has also been found in XRD analysis but these clays has not been observed under optical microscope of SEM photomicrographs (Table 7). The alteration product on the surface of albite feldspars are sericite micas (white micas flakes) (Figure 3.45). In case of alkali feldspars, microcline and orthoclase shows perthitic texture.

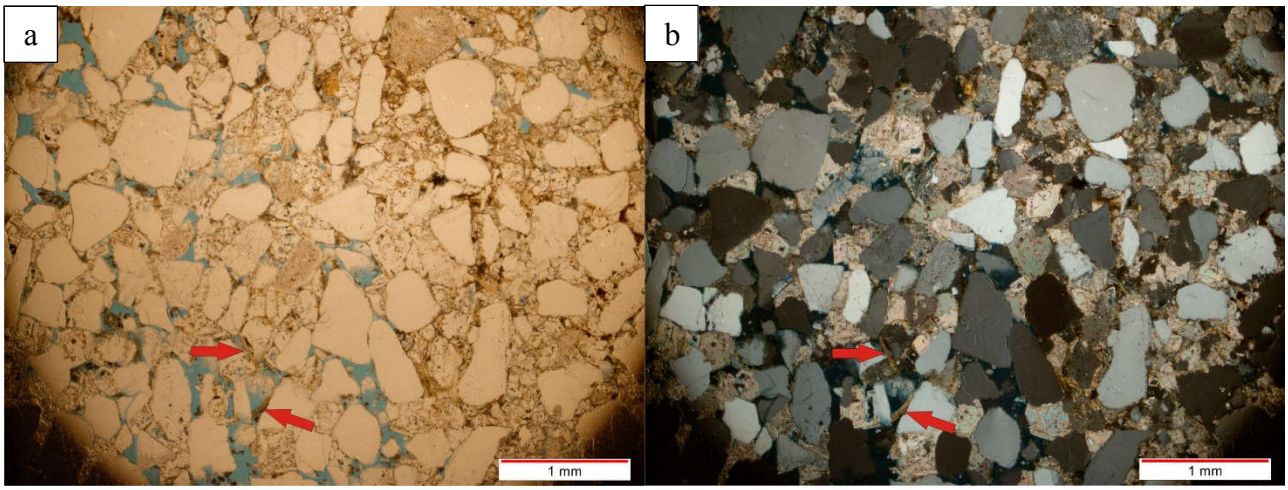

Figure 3.49: a) PPL-view (4X): Optical micrograph showing very low primary porosity (Blue color). Red arrows indicate towards biotite grains showing no effect of mechanical compaction as bending is absent. b) XPL-view (4X): Pre-compactional Fe-dolomite is filling primary pores and reducing the overall porosity.

Sample ID	Sample Composition and Pickering Facies	Quartz	K-Feldspar	Plagioclase	Calcite	Fe Dolomite	Dolomite	Pyrite	Gypsum	Total Phyllosilicates	Total
BQ-2-1-2	Ss B2.1	61.1	5	10.2	1.1	0	17.1	0.5	0	5	100
BQ-2-1-5	Ss B2.1	75	3.1	5.3	1.9	11.2	0	0.2	0	3.3	100
BQ-4-3	Ss C2.1	50.5	7	9.1	0	0	30.2	0.2	0	3	100
BQ-4-4	Ss C2.1	68.5	6.4	8.1	0	0	15	0.3	0	1.7	100
BQ-4-11	Ss B2.1	62.8	5.2	6.9	0.5	0	19.9	0	0	4.7	100
BQ-4-18	Ss C2.1	43.9	5.7	7.6	0	0	36	0.4	0	6.4	100
BQ-4-20	Ss C2.1	32.6	8	13.6	0	0	40.2	0.3	0	5.3	100
BQ-5-11	Ss C2.1	60.6	6.3	16.1	1.8	0	8	0.4	0	6.8	100
BQ-5-14	Ss A2.2	53.6	5.8	12.1	1.6	0	21.8	0.5	0	4.6	100
BQ-5-23	Ss C2.1	64.6	6.7	17.3	0.6	0	0	0.7	0	10.1	100
BQ-5-27	Ss C2.1	67.6	6.1	20	0.8	0	0.6	0.4	0	4.5	100
BQ-5-28	Ss C2.1	51.6	8.2	18.1	0.5	0	15.4	0.2	0	6	100
BQ-9-1	Ss A2.7	23.1	14.7	22.6	29.3	2.8	0	0.7	1.1	5.7	100

Table 8: Summarized XRD analysis results of representative sandstone samples from Burqan Formation.

Sample ID (Cement Type)	Ca (moles)	Mg (moles)	Fe (moles)	Total Moles in Carbonate	Mole fraction Ca	Mole fraction Mg	Mole fraction Fe	Charge to Balance (CO_3) or (CO_3)$_2$	Ca Atom Units	Mg Atom Units	Fe Atom Units	Mineral Formula
BQ-8-7-2a (Dolomite)	0.53	0.50	0.04	1.07	0.50	0.46	0.04	4.00	1.00	0.93	0.07	$CaMg_{0.93}Fe_{0.07}(CO_3)_2$
BQ-8-7-3a (Dolomite)	0.54	0.49	0.04	1.07	0.50	0.46	0.03	4.00	1.01	0.92	0.07	$Ca_{1.01}Mg_{0.92}Fe_{0.07}(CO_3)_2$
BQ-8-7-4a (Dolomite)	0.54	0.49	0.04	1.07	0.50	0.46	0.04	4.00	1.01	0.92	0.07	$Ca_{1.01}Mg_{0.92}Fe_{0.07}(CO_3)_2$
BQ-8-7-5a (Calcite)	0.99	0.03	0.00	1.02	0.97	0.02	0.00	2.00	0.97	0.02	0.00	$Ca_{0.97}Mg_{0.02}(CO_3)$
BQ-8-7-6a (Calcite)	0.98	0.03	0.01	1.02	0.96	0.03	0.01	2.00	0.96	0.03	0.01	$Ca_{0.96}Mg_{0.03}Fe_{0.01}(CO_3)$
BQ-8-9-1a (Dolomite)	0.53	0.49	0.04	1.07	0.50	0.46	0.04	4.00	1.00	0.92	0.08	$Ca_{1.00}Mg_{0.92}Fe_{0.08}(CO_3)_2$
BQ-8-9-2a (Dolomite)	0.54	0.48	0.05	1.07	0.51	0.45	0.04	4.00	1.02	0.90	0.09	$Ca_{1.02}Mg_{0.90}Fe_{0.09}(CO_3)_2$
BQ-8-9-3a (Dolomite)	0.54	0.48	0.05	1.07	0.50	0.45	0.04	4.00	1.01	0.90	0.09	$Ca_{1.01}Mg_{0.90}Fe_{0.09}(CO_3)_2$
BQ-8-9-4a (Dolomite)	0.54	0.49	0.04	1.07	0.50	0.46	0.04	4.00	1.00	0.92	0.08	$CaMg_{0.92}Fe_{0.08}(CO_3)_2$
BQ-8-12-1a (Calcite)	0.97	0.04	0.01	1.03	0.94	0.04	0.01	2.00	0.94	0.04	0.01	$Ca_{0.95}Mg_{0.04}Fe_{0.01}(CO_3)$
BQ-8-12-2a (Calcite)	0.99	0.03	0.00	1.02	0.97	0.02	0.00	2.00	0.97	0.02	0.00	$Ca_{0.97}Mg_{0.03}(CO_3)$
BQ-8-12-4a (Calcite)	0.99	0.02	0.00	1.01	0.97	0.02	0.00	2.00	0.97	0.02	0.00	$Ca_{0.97}Mg_{0.03}(CO_3)$
BQ-8-12-5a (Calcite)	0.99	0.03	0.00	1.02	0.97	0.03	0.00	2.00	0.97	0.03	0.00	$Ca_{0.97}Mg_{0.03}(CO_3)$

BQ-2-1-5-1a (Calcite)	0.99	0.02	0.00	1.01	0.97	0.02	0.00	2.00	0.97	0.02	0.00	$Ca_{0.97}Mg_{0.03}(CO_3)$
BQ-2-1-5-2a (Calcite)	0.99	0.01	0.00	1.01	0.99	0.01	0.00	2.00	0.99	0.01	0.00	$Ca_{0.99}Mg_{0.01}(CO_3)$
BQ-2-1-5-2a (Dolomite)	0.59	0.47	0.01	1.07	0.55	0.43	0.01	4.00	1.10	0.87	0.03	$Ca_{1.10}Mg_{0.87}Fe_{0.03}(CO_3)_2$
BQ-2-1-5-3a (Calcite)	0.99	0.02	0.00	1.01	0.98	0.02	0.00	2.00	0.98	0.02	0.00	$Ca_{0.98}Mg_{0.02}(CO_3)$
BQ-2-1-5-4a (Calcite)	0.99	0.03	0.00	1.02	0.97	0.03	0.00	2.00	0.97	0.03	0.00	$Ca_{0.97}Mg_{0.03}(CO_3)$
BQ-2-1-5-4a (Dolomite)	0.60	0.45	0.02	1.07	0.57	0.42	0.02	4.00	1.13	0.84	0.03	$Ca_{1.13}Mg_{0.84}Fe_{0.03}(CO_3)_2$
BQ-2-1-5-5a (Dolomite)	0.59	0.45	0.02	1.07	0.56	0.42	0.02	4.00	1.11	0.85	0.03	$Ca_{1.11}Mg_{0.85}Fe_{0.03}(CO_3)_2$
BQ-2-1-5-6a (Dolomite)	0.57	0.48	0.02	1.07	0.53	0.45	0.02	4.00	1.07	0.90	0.03	$Ca_{1.07}Mg_{0.90}Fe_{0.03}(CO_3)_2$
BQ-2-1-5-7a (Dolomite)	0.57	0.48	0.02	1.07	0.53	0.45	0.02	4.00	1.06	0.90	0.04	$Ca_{1.06}Mg_{0.90}Fe_{0.04}(CO_3)_2$
BQ-2-1-5-8a (Dolomite)	0.61	0.44	0.02	1.07	0.57	0.42	0.02	4.00	1.14	0.83	0.03	$Ca_{1.14}Mg_{0.83}Fe_{0.03}(CO_3)_2$
BQ-2-1-5-9a (Calcite)	0.99	0.03	0.00	1.02	0.97	0.03	0.00	2.00	0.97	0.03	0.00	$Ca_{0.97}Mg_{0.03}(CO_3)$
BQ-5-11-1a (Calcite)	0.96	0.10	0.00	1.06	0.90	0.09	0.00	2.00	0.90	0.09	0.00	$Ca_{0.91}Mg_{0.09}(CO_3)$
BQ-5-11-2a (Calcite)	0.98	0.05	0.00	1.03	0.95	0.05	0.00	2.00	0.95	0.05	0.00	$Ca_{0.95}Mg_{0.05}(CO_3)$
BQ-5-11-3a (Calcite)	0.98	0.05	0.00	1.03	0.95	0.05	0.00	2.00	0.95	0.05	0.00	$Ca_{0.95}Mg_{0.05}(CO_3)$
BQ-5-11-4a (Calcite)	0.53	0.50	0.04	5.23	0.50	0.46	0.04	2.00	1.00	0.93	0.07	$Ca_{0.93}Mg_{0.07}(CO_3)$
BQ-5-20-1a (Dolomite)	0.55	0.49	0.03	1.07	0.51	0.45	0.03	4.00	1.03	0.91	0.06	$Ca_{1.03}Mg_{0.91}Fe_{0.06}(CO_3)_2$
BQ-5-20-3a (Dolomite)	0.55	0.49	0.03	1.07	0.51	0.46	0.03	4.00	1.02	0.91	0.06	$Ca_{1.03}Mg_{0.91}Fe_{0.06}(CO_3)_2$

BQ-4-4-1a (Calcite)	0.99	0.01	0.00	1.01	0.99	0.01	0.00	2.00	0.99	0.01	0.00	$Ca_{0.99}Mg_{0.01}(CO_3)$
BQ-4-4-2a (Calcite)	0.99	0.01	0.00	1.01	0.99	0.01	0.00	2.00	0.99	0.01	0.00	$Ca_{0.99}Mg_{0.01}(CO_3)$
BQ-4-4-3a (Calcite)	0.99	0.01	0.00	1.01	0.99	0.01	0.00	2.00	0.99	0.01	0.00	$Ca_{0.99}Mg_{0.01}(CO_3)$
BQ-4-4-4a (Calcite)	1.00	0.01	0.00	1.00	0.99	0.01	0.00	2.00	0.99	0.01	0.00	$Ca_{0.99}Mg_{0.01}(CO_3)$
BQ-4-15-1a (Calcite)	0.99	0.03	0.00	1.02	0.97	0.03	0.00	2.00	0.97	0.03	0.00	$Ca_{0.97}Mg_{0.03}(CO_3)$
BQ-4-15-2a (Dolomite)	0.56	0.49	0.02	1.07	0.52	0.46	0.02	4.00	1.04	0.92	0.04	$Ca_{1.04}Mg_{0.92}Fe_{0.04}(CO_3)_2$
BQ-4-15-3a (Dolomite)	0.56	0.49	0.02	1.07	0.52	0.46	0.02	4.00	1.04	0.91	0.05	$Ca_{1.04}Mg_{0.91}Fe_{0.05}(CO_3)_2$
BQ-4-15-4a (Dolomite)	0.56	0.49	0.03	1.07	0.52	0.45	0.03	4.00	1.04	0.91	0.05	$Ca_{1.04}Mg_{0.91}Fe_{0.05}(CO_3)_2$
BQ-2-1-2-1a (Dolomite)	0.55	0.49	0.03	1.07	0.51	0.46	0.03	4.00	1.03	0.92	0.05	$Ca_{1.03}Mg_{0.92}Fe_{0.05}(CO_3)_2$
BQ-2-1-2-2a (Dolomite)	0.55	0.50	0.03	1.07	0.51	0.46	0.02	4.00	1.03	0.93	0.05	$Ca_{1.03}Mg_{0.92}Fe_{0.05}(CO_3)_2$
BQ-2-1-2-3a (Dolomite)	0.55	0.50	0.02	1.07	0.51	0.46	0.02	4.00	1.02	0.93	0.05	$Ca_{1.02}Mg_{0.93}Fe_{0.05}(CO_3)_2$
BQ-2-1-2-4a (Dolomite)	0.56	0.49	0.03	1.07	0.52	0.46	0.02	4.00	1.04	0.91	0.05	$Ca_{1.04}Mg_{0.91}Fe_{0.05}(CO_3)_2$
BQ-2-1-2-5a (Dolomite)	0.56	0.49	0.02	1.07	0.52	0.46	0.02	4.00	1.04	0.92	0.04	$Ca_{1.04}Mg_{0.92}Fe_{0.04}(CO_3)_2$
BQ-2-1-2-6a (Dolomite)	0.57	0.47	0.02	1.07	0.54	0.44	0.02	4.00	1.07	0.88	0.05	$Ca_{1.07}Mg_{0.88}Fe_{0.05}(CO_3)_2$
BQ-2-3-3-1a (Dolomite)	0.55	0.49	0.03	1.07	0.51	0.46	0.03	4.00	1.02	0.92	0.05	$Ca_{1.03}Mg_{0.92}Fe_{0.05}(CO_3)_2$
BQ-2-3-3-2a (Dolomite)	0.69	0.21	0.12	1.02	0.67	0.21	0.12	4.00	1.35	0.41	0.24	$Ca_{1.35}Mg_{0.41}Fe_{0.24}(CO_3)_2$
BQ-2-3-3-3a (Dolomite)	0.55	0.50	0.03	1.07	0.51	0.47	0.02	4.00	1.02	0.94	0.05	$Ca_{1.02}Mg_{0.94}Fe_{0.04}(CO_3)_2$

BQ-2-3-3-4a (Dolomite)	0.55	0.50	0.03	1.07	0.51	0.46	0.03	4.00	1.02	0.93	0.05	$Ca_{1.02}Mg_{0.93}Fe_{0.05}(CO_3)_2$
BQ-2-5-3-1a (Dolomite)	0.54	0.51	0.03	1.08	0.50	0.47	0.02	4.00	1.00	0.95	0.05	$Ca_{1.00}Mg_{0.95}Fe_{0.05}(CO_3)_2$
BQ-2-5-3-2a (Dolomite)	0.54	0.51	0.02	1.08	0.50	0.47	0.02	4.00	1.01	0.94	0.05	$Ca_{1.01}Mg_{0.94}Fe_{0.05}(CO_3)_2$
BQ-2-5-3-3a (Dolomite)	0.54	0.50	0.02	1.08	0.51	0.47	0.02	4.00	1.01	0.94	0.05	$Ca_{1.01}Mg_{0.94}Fe_{0.05}(CO_3)_2$
BQ-2-5-3-4a (Dolomite)	0.54	0.50	0.03	1.08	0.50	0.47	0.02	4.00	1.01	0.94	0.05	$Ca_{1.01}Mg_{0.94}Fe_{0.05}(CO_3)_2$
BQ-4-3-1a (Dolomite)	0.54	0.51	0.03	1.08	0.50	0.48	0.02	4.00	1.00	0.95	0.05	$CaMg_{0.95}Fe_{0.05}(CO_3)_2$
BQ-4-3-2a (Dolomite)	0.54	0.51	0.03	1.08	0.50	0.47	0.02	4.00	1.00	0.95	0.05	$CaMg_{0.95}Fe_{0.05}(CO_3)_2$
BQ-4-3-3a (Dolomite)	0.53	0.52	0.03	1.08	0.50	0.48	0.02	4.00	0.99	0.96	0.05	$Ca_{0.99}Mg_{0.96}Fe_{0.05}(CO_3)_2$
BQ-4-3-4a (Dolomite)	0.55	0.50	0.02	1.08	0.51	0.47	0.02	4.00	1.02	0.94	0.05	$Ca_{1.02}Mg_{0.93}Fe_{0.05}(CO_3)_2$
BQ-4-9-1a (Dolomite)	0.54	0.51	0.03	1.08	0.50	0.48	0.02	4.00	1.00	0.95	0.05	$CaMg_{0.95}Fe_{0.05}(CO_3)_2$
BQ-4-9-2a (Dolomite)	0.55	0.49	0.03	1.07	0.51	0.46	0.03	4.00	1.03	0.92	0.05	$Ca_{1.03}Mg_{0.92}Fe_{0.05}(CO_3)_2$
BQ-4-9-3a (Dolomite)	0.53	0.52	0.03	1.08	0.49	0.48	0.03	4.00	0.98	0.96	0.05	$Ca_{0.98}Mg_{0.96}Fe_{0.05}Mn_{0.01}(CO_3)_2$
BQ-4-9-4a (Dolomite)	0.53	0.52	0.02	1.08	0.49	0.48	0.02	4.00	0.99	0.96	0.04	$Ca_{0.99}Mg_{0.96}Fe_{0.04}Mn_{0.01}(CO_3)_2$
BQ-4-10-1a (Dolomite)	0.54	0.51	0.03	1.07	0.50	0.47	0.03	4.00	1.00	0.95	0.05	$CaMg_{0.95}Fe_{0.05}(CO_3)_2$
BQ-4-10-2a (Dolomite)	0.54	0.51	0.03	1.08	0.50	0.48	0.03	4.00	1.00	0.95	0.05	$CaMg_{0.95}Fe_{0.05}(CO_3)_2$
BQ-4-10-3a (Dolomite)	0.54	0.51	0.03	1.07	0.50	0.47	0.03	4.00	1.00	0.94	0.06	$CaMg_{0.94}Fe_{0.06}(CO_3)_2$
BQ-4-10-4a (Dolomite)	0.54	0.51	0.03	1.07	0.50	0.47	0.03	4.00	1.00	0.95	0.06	$CaMg_{0.94}Fe_{0.06}(CO_3)_2$

BQ-4-18-1a (Dolomite)	0.54	0.50	0.03	1.07	0.51	0.47	0.03	4.00	1.01	0.93	0.05	$Ca_{1.01}Mg_{0.93}Fe_{0.05}(CO_3)_2$
BQ-4-18-2a (Dolomite)	0.55	0.50	0.03	1.07	0.51	0.47	0.03	4.00	1.01	0.93	0.05	$Ca_{1.01}Mg_{0.93}Fe_{0.05}(CO_3)_2$
BQ-4-18-3a (Dolomite)	0.54	0.51	0.03	1.08	0.50	0.47	0.03	4.00	1.00	0.95	0.05	$CaMg_{0.95}Fe_{0.05}(CO_3)_2$
BQ-4-18-4a (Dolomite)	0.56	0.49	0.03	1.07	0.52	0.46	0.02	4.00	1.04	0.91	0.05	$Ca_{1.04}Mg_{0.91}Fe_{0.05}(CO_3)_2$
BQ-4-18-5a (Dolomite)	0.54	0.51	0.02	1.08	0.50	0.47	0.02	4.00	1.01	0.95	0.05	$Ca_{1.01}Mg_{0.95}Fe_{0.04}(CO_3)_2$
BQ-4-20-1a (Dolomite)	0.54	0.50	0.03	1.07	0.50	0.47	0.03	4.00	1.01	0.93	0.06	$Ca_{1.01}Mg_{0.93}Fe_{0.06}(CO_3)_2$
BQ-4-20-2a (Dolomite)	0.54	0.51	0.03	1.07	0.50	0.47	0.03	4.00	1.00	0.95	0.06	$CaMg_{0.95}Fe_{0.05}(CO_3)_2$
BQ-4-20-3a (Dolomite)	0.54	0.51	0.02	1.08	0.51	0.47	0.02	4.00	1.01	0.95	0.04	$Ca_{1.01}Mg_{0.95}Fe_{0.04}(CO_3)_2$
BQ-4-20-4a (Dolomite)	0.55	0.50	0.03	1.07	0.51	0.46	0.02	4.00	1.02	0.93	0.05	$Ca_{1.02}Mg_{0.93}Fe_{0.05}(CO_3)_2$
BQ-4-20-6a (Dolomite)	0.54	0.50	0.03	1.07	0.51	0.46	0.03	4.00	1.01	0.93	0.06	$Ca_{1.01}Mg_{0.93}Fe_{0.06}(CO_3)_2$
BQ-5-2-1a (Dolomite)	0.55	0.47	0.04	1.07	0.52	0.44	0.04	4.00	1.04	0.88	0.08	$Ca_{1.04}Mg_{0.88}Fe_{0.08}(CO_3)_2$
BQ-5-2-2a (Dolomite)	0.54	0.48	0.04	1.07	0.51	0.45	0.04	4.00	1.02	0.90	0.08	$Ca_{1.02}Mg_{0.90}Fe_{0.08}(CO_3)_2$
BQ-5-2-3a (Dolomite)	0.54	0.48	0.04	1.07	0.51	0.45	0.04	4.00	1.02	0.90	0.08	$Ca_{1.02}Mg_{0.90}Fe_{0.08}(CO_3)_2$
BQ-5-2-4a (Dolomite)	0.55	0.47	0.04	1.07	0.51	0.44	0.04	4.00	1.03	0.89	0.08	$Ca_{1.03}Mg_{0.89}Fe_{0.08}(CO_3)_2$

Table 9: Summarized quantitative results obtained from electron microprobe analysis (EMP) for various type of carbonate cements in sandstone samples of Burqan Formation.

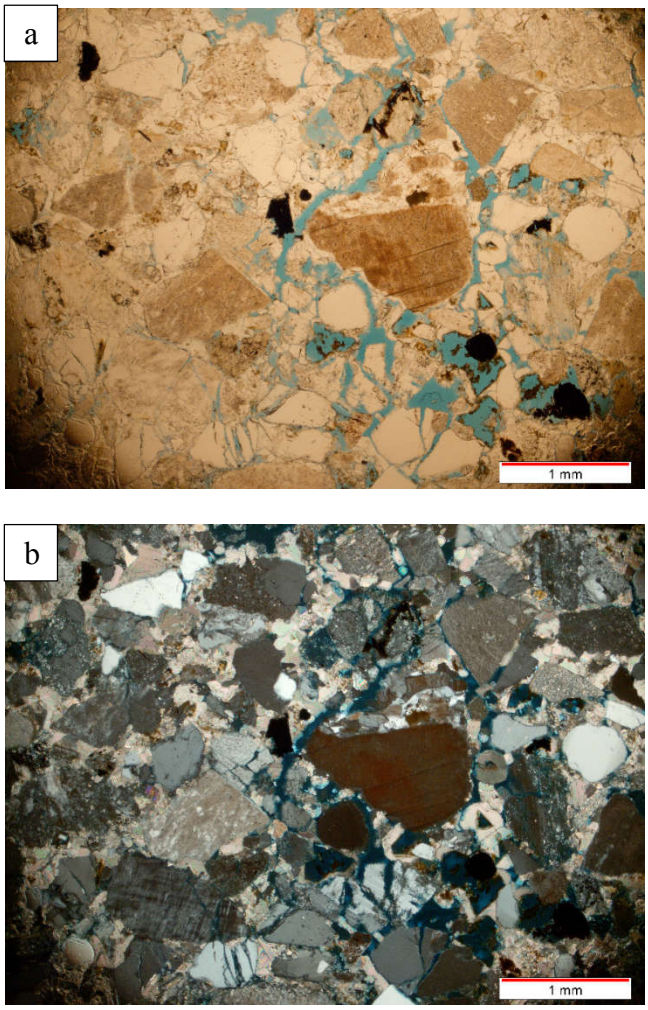

Figure 3.50: a) PPL-view (4X): Optical micrograph showing abundant pre-compaction calcite cement filling the primary pores among framework grains. The secondary porosity has been created due to the grain and cement dissolution (blue color). Pyrite cement is engulfed by the calcite cement shows it's predate precipitation than post-date calcite cementation. (b) XPL-view (4X): cross nicols view of the same photomicrograph.

3.3.5 Porosity

Total visible porosity of Burqan outcrop sandstones averages 15% (±7.0) and ranges from 3%-35%. Porosity is about equally distributed between intergranular primary porosity and secondary porosity formed by dissolution of feldspar and/or rock fragments. Secondary porosity includes fracture porosity and partial to complete dissolution of framework grains as well as intergranular cements. Very low point-counted porosity (≤10%) is due to depositional matrix or high-volume carbonate cement (calcite or dolomite), mostly the latter. The high percentage of primary porosity up to 33% in few samples is caused by the low to moderate compaction and lack of diagenetic cements. These samples are friable (Figures 3.45, 3.51).

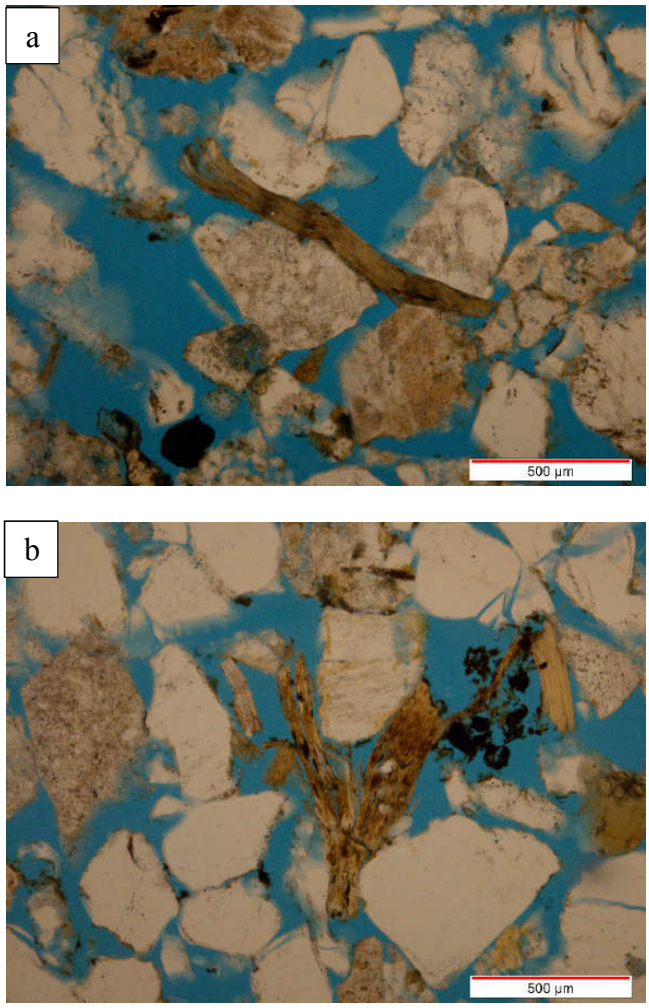

Figure 3.51: PPL-view (10X): Optical micrographs showing low to moderate compaction indicated by slight bending in biotite micas due to relatively low overburden pressure. Splitting of biotite grain is shown in photomicrograph (b) due to the invasion of feldspar grain. Very high primary porosity is visible between framework grains. Grain dissolution and fracture porosities are also present. Sporadic early stage pyrite cement is also visible.

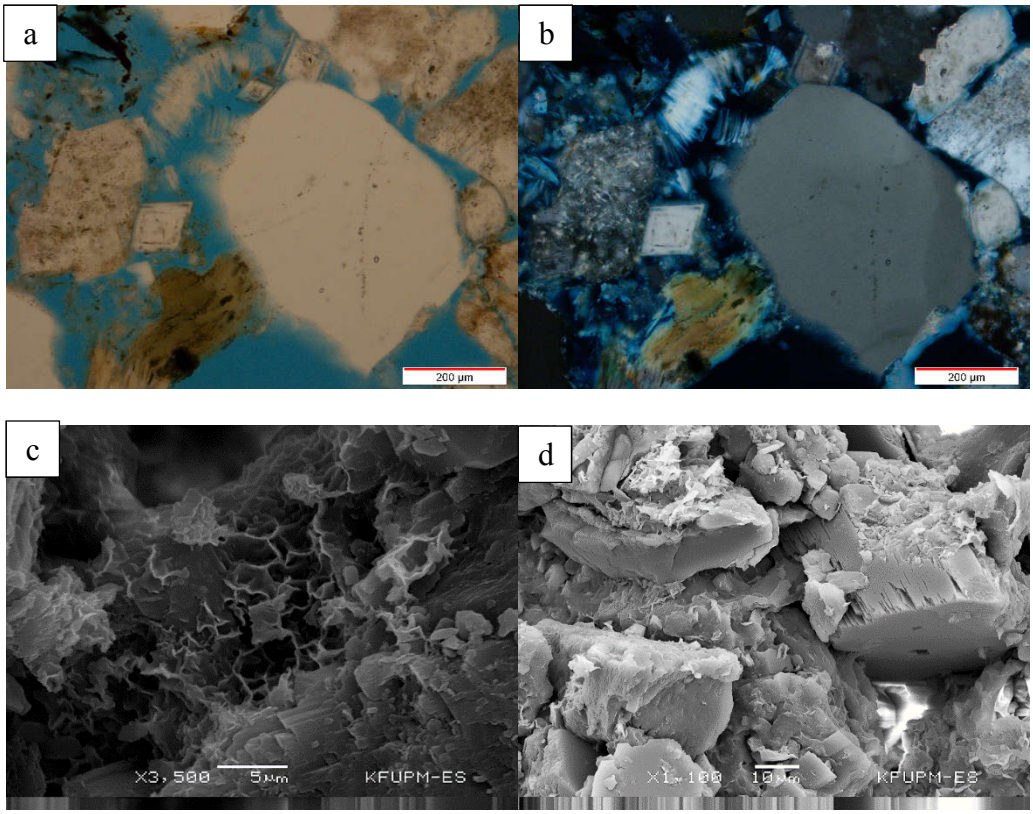

Figure 3.52: a) PPL-view (20X): Optical micrograph is showing two booklet-like patches of kaolinite clay near the upper left part of large quartz grain. b) XPL-view (20X): Kaolinite clay patch of 50-200 micron in size. Euhedral dolomite cement is present as pore filling cement c) SEM micrograph showing the presence of honeycomb-like smectite clay as grain coating. d) SEM micrograph showing high primary porosity, secondary porosity and large crystal of altered grain near the upper right and left corner with smectite clay as an alteration product on the corroded grain surface.

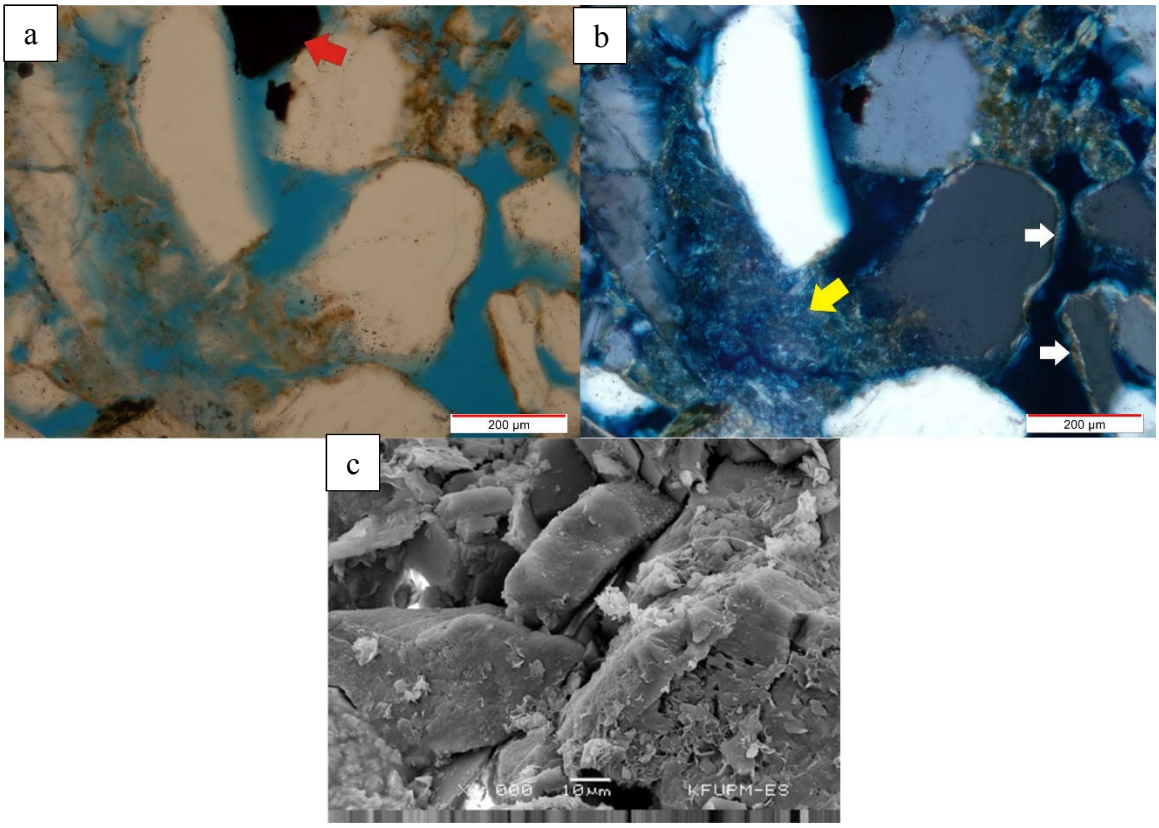

Figure 3.53: (a) PPL-view (20X): High primary porosity is visible. Red arrow indicates hematite cement. (b) XPL-view (20X): Yellow arrow shows partially altered and dissolved feldspar grain. Small white arrows are indicating towards probably smectite clay coating around quartz grains to inhibit quartz overgrowth. (c) SEM micrograph showing secondary porosity in feldspar grain and semctite clay as alteration product on its surface.

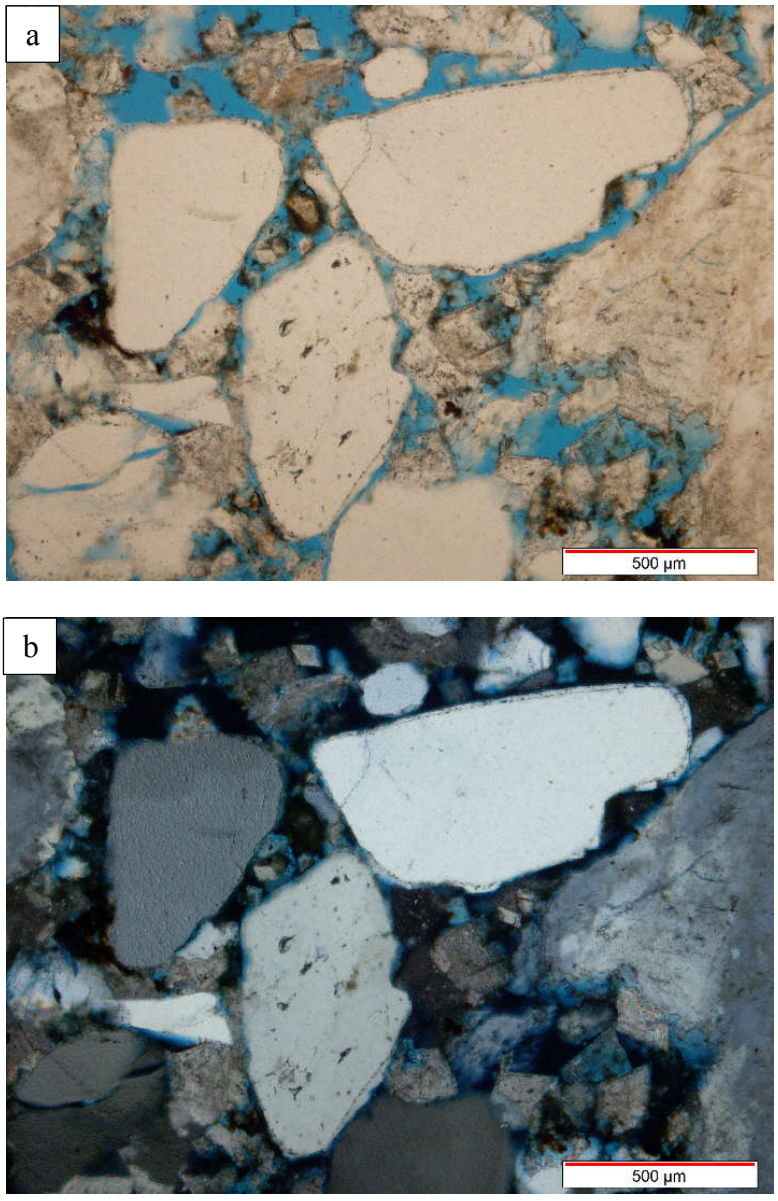

Figure 3.54: Photomicrographs showing abraded morphology of quartz overgrowth with uneven thickness around the dust line. Magnification-10X.

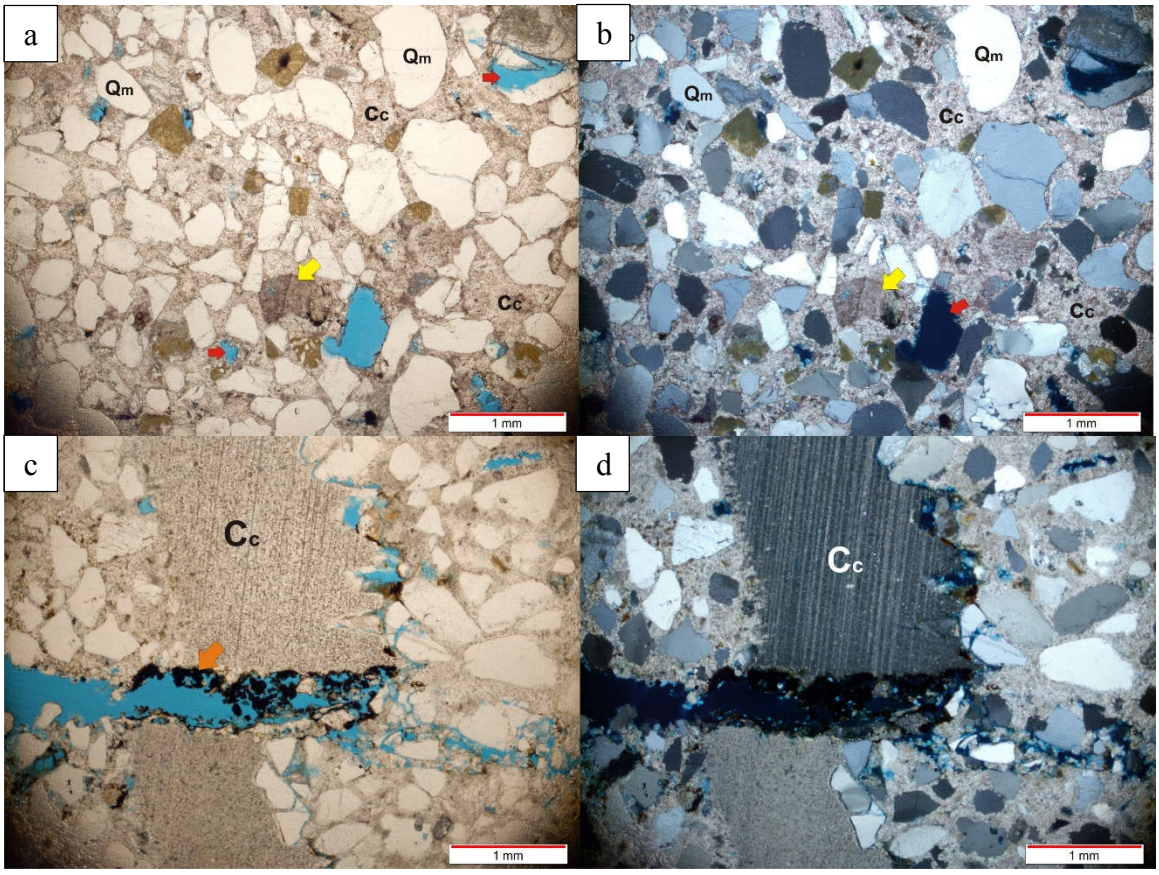

Figure 3.55: a) PPL-view (4X): Quartz rich sandstone cemented with finely crystalline precompactional authigenic calcite (Cc) present as pore-filling cement and filling almost all the pores. Yellow arrows indicate the cast of unknown framework grain dissolved and later replaced by calcite cement. Red arrows are indicating the secondary porosity. b) XPL-view (4X) of the same thin section. c) PPL-view (4X): Micritic calcite cement is present as fracture filling. Twinning planes are also visible. Hematite cement (phase-2) postdate the calcite cement. d) XPL-view (4X): Lamellar twinning is visible in fracture-filling calcite cement.

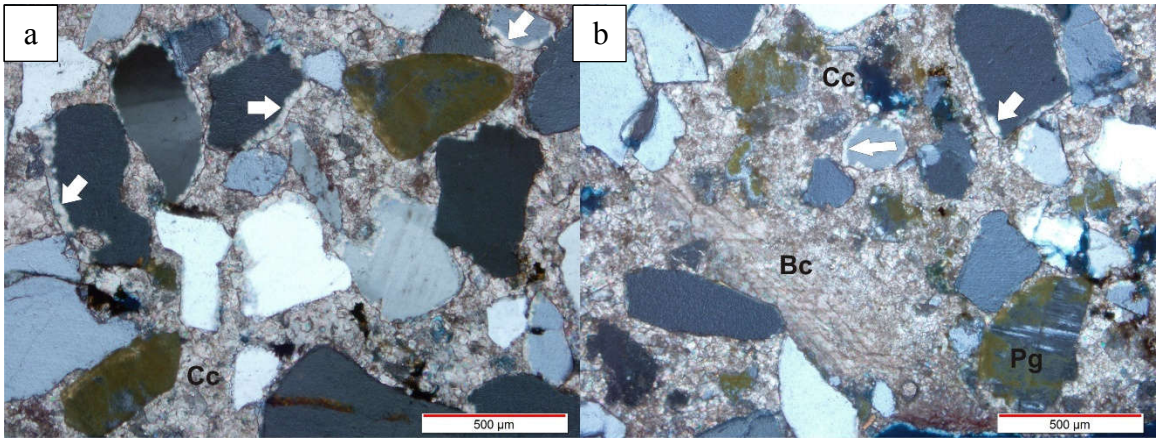

Figure 3.56: (a & b) XPL-view (10X): White arrows in optical micrographs are indicating towards rims of authigenic carbonate cement precipitated within pits of corroded boundaries of quartz grains. Finely crystalline authigenic calcite cement (Cc) occur as pore-filling occluding almost all pore spaces. A Bioclast (Bc) and secondary porosity is visible in optical micrograph-b. The framework grains show "Floating Texture" due to the presence of precompactional calcite cement.

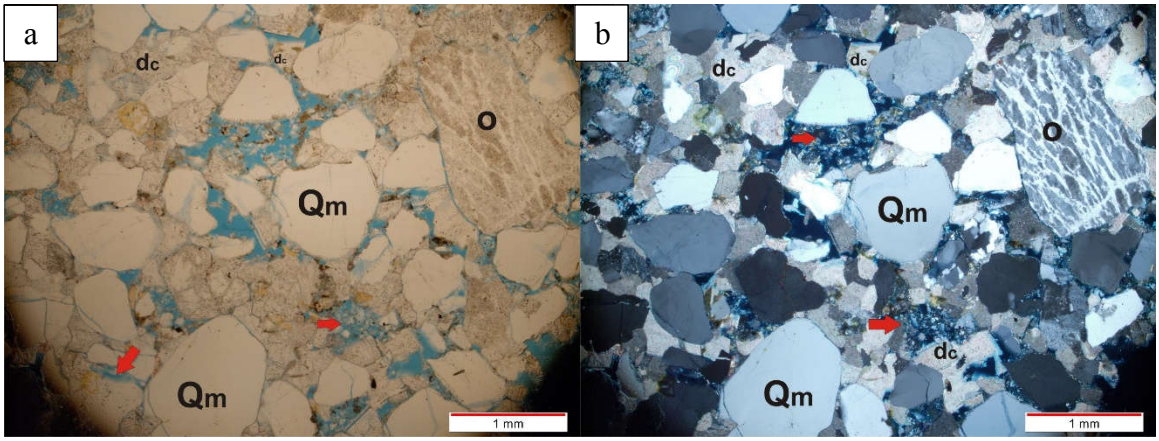

Figure 3.57: a) PPL-view (4X): Optical micrograph showing secondary porosity (red arrows) created due to partial dissolution of framework grains. Primary porosity is reduced due to cloudy dolomite cement (dc). b) XPL-view (4X): Photomicrograph showing coarse crystalline rhombs of dolomite cement (dc) present between the framework grains. Perthitic texture is present on the surface of orthoclase grain (O).

4 DISCUSSION

4.1 Facies Analysis

Lithological forecast of clastic deposits in submarine depositional environment requires comprehensive and proper interpretation of depositional processes within shelf-slope and basin floor system. A wide variety of gravity driven processes are responsible for deposition in submarine system. These processes include slide-slump flow, grain flow, debris flow and turbidity currents of different densities (Walker, 1978; Pickering *et al.*, 1986; Stow, 1986; Shanmugam and Moiola, 1988). A wide range of lithofacies has been identified as turbidity current deposits in the ancient rock record apart from only classical Bouma Sequence which shows basinward fining and thinning of grain size and resulting deposits (Lowe, 1982; Pickering and Hiscott, 1985).

The depositional processes of various lithofacies within Burqan Formation has been identified primarily by using lithofacies classification scheme of Pickering *et al.*, 1986. Pickering *et. al.,* 1986 has developed his facies scheme by extending the facies association scheme of Mutti and Ricci-Lucchi (1972). They have extended seven facies (A to G) of Mutti and Ricci-Lucchi (1972) into forty-one distinct sub lithofacies.

The gravity driven depositional processes for identified lithofacies in the Burqan Formation ranges from debris flow, high to low concentration turbidity currents, frictional freezing, grain traction and suspension processes. The depositional process for each lithofacies has been explained below in alphabetical order.

A1.1 Disorganized Gravels: The lack of organization of gravels and range of grain sizes observed in these facies has suggested that these sediments may have been transported by high-density turbidity currents or debris flows and rapidly deposited by frictional freezing (Table-1, Stratigraphic Section-3) (Marschalko, 1964; Hendry, 1973; Carter and Norris, 1977; Long, 1977; Stanley, Palmer and Dill, 1978; Johnson and Walker, 1979; Hein, 1982; Hein and Walker, 1982; Surlyk, 1984; Hiscott and James, 1985; Pickering *et al.*, 1986).

A1.2 Disorganized Muddy Gravels: The matrix supported, unorganized and crudely stratified gravely deposits in these facies may have been deposited by cohesive debris flow followed by freezing due to inter-granular friction (Table-1, Stratigraphic Section-3) (Hampton, 1972, 1975; Mutti and Ricci Lucchi, 1972; Donald R. Lowe, 1982; Pickering, 1984; Hiscott and James, 1985).

A1.4 Disorganized Pebbly Sands: The characteristics features of these facies include poor sorting and disorganization of constituent sediments such as cobbles and pebbles with sandy matrix among the grains. These features suggests that these facies may have been transported over long distance by high-density turbidity currents and rapidly deposited by inter-granular friction (Table-1, Stratigraphic Section-3) (Ricci Lucchi, 1969; Lowe, 1976; Surlyk, 1978; Walker, 1978).

A2.2 Inversely Graded Gravels: The presence of inverse grading and clast supported nature of these facies suggests that these may have been rapidly deposited by frictional freezing of high-density traction carpet or dispersion process below the high-density turbidity current flow (Table-2, Stratigraphic Section-4) (Surlyk, 1978, 1984; Johnson and Walker, 1979; Hein, 1982; Lash, 1984).

A2.4 Graded Stratified Gravels: The thick bedded, poorly sorted, stratified and normally graded sediments in this facies may have been deposited mainly by suspension and partly by traction from high-density turbidity currents (Table-1, Stratigraphic Section-3) (Hendry, 1972; Surlyk, 1978, 1984; Johnson and Walker, 1979; Hein, 1982; Hein and Walker, 1982).

A2.5 Stratified Pebbly Sands: The thin layers of pebbly sand showing clear stratification suggests that these facies may have been deposited by bed-load traction or traction carpet process from high concentration turbidity current (Table-1, Stratigraphic Section-3) (Hendry, 1973; Surlyk, 1978, 1984; Hein, 1982; Hein and Walker, 1982).

A2.7 Normally Graded Pebbly Sands: As these facies show characteristic poor sorting and normal grading within thickly bedded pebbly sands which their deposition due to rapid grain by grain deposition from high-concentration turbidity currents with rapid grain settling and burial without significant traction transport (Table-2, Stratigraphic Section-4) (Long, 1977; Walker, 1978; Hein, 1982).

B2.1 Parallel Stratified Sands: Nearly horizontal multiple layers of medium to very coarse grained sandy deposits of these facies suggest that they have been rapidly deposited from high-density turbidity currents followed by freezing of dense cohesion-less suspension. Sand creep or other grain flow process can produce similar kind of deposits on steep slopes (Table-1, Stratigraphic Section-3) (Hendry, 1972; Hiscott and Middleton, 1979, 1980).

C1.1 Poorly sorted muddy sand: These individual beds in these facies shows characteristics coarse grained sand with little mud matrix in the basal part which changes into silty mud near the top of the unit. It suggests that these facies may have been deposited

rapidly from high density turbidity currents or debris flow rich in sand, silt and mud (Table-4, Stratigraphic Section-6) (Mutti, Nilsen and Ricci Lucchi, 1978; Hiscott and Middleton, 1979; Pickering, 1981; Pickering and Hiscott, 1985).

C2.1 Very Thick to Thick Bedded Sand-Mud Couplet, C2.2 Medium Bedded Sand-Mud Couplet and C2.3 Thin Bedded Sand-Mud Couplet: Very coarse to pebble sized thickly bedded sandstone with intercalated mudstone layers are present in facies C2.1 which probably grades basinward into fine grained sandstone-mudstone couplet with little to no mud matrix in facies C2.3. It suggests that these facies might have been deposited during the evolution of flow from turbidity currents of high concentration (C2.1) to low concentration (C2.3) (Table-4, Stratigraphic Section-6) (Mutti, Nilsen and Ricci Lucchi, 1978; Piper, 1978; Siemers, Tillman and Williamson, 1981; Stow and Piper, 1984).

E1.1 Structureless Mud Depositional Process: These massive mudstone facies shows their deposition by quick settling from thick but dilute turbidity currents. These hemipelagic deposits may also be deposited by lateral transfer of deep ocean currents or through sliding process (Table-3 and 5, Stratigraphic Section-5 and Section-7) (Piper, 1978; Stanley and Maldonado, 1981; Pickering and Hiscott, 1985).

4.2 Petrography and Provenance

The quantitative results of modal analysis show that the average composition of the Burqan Formation is $Q_{71}F_{21}L_8$ (Table-7). The Burqan formation is chemically immature due to the high feldspar content. The poor sorting and sub-angular to sub-rounded shapes of the quartz grains also show the textural immature nature of the Burqan Formation. The dominance of plagioclase percentage over K-feldspar in thin sections of the Burqan Formation validates the interpretation that sediments result from rapid erosion and weathering in the source region (Al-Ramadan *et. al.,* 2013).

The mineralogy of the Burqan Formation is consistent with the mineralogy of the granitic, metamorphic and sedimentary rocks of the crystalline basement of the surrounding of Midyan Basin, which is mainly granitic in nature with abundant plagioclase and alkali feldspars. The geological map of the Al Bad' quadrangle (thesis area) (Fig 1.2) shows that these rocks consist of an igneous (intrusive and extrusive) basement of both felsic and intermediate composition due to the presence of abundant orthoclase and albite along with heavy minerals like zircon and rutile (Boggs, 2014). Different type of granitic intrusion including monzogranite, syenogranite and microgranite are cutting through alkali feldspar syenite and nepheline syenites. Rhyolite, andesite and volcaniclastics are present near the eastern margin of the Midyan Basin. Apart from the granitic basement, metamorphic and sedimentary rocks are also present along the faulted margin of the Midyan Basin. The metamorphic rocks include metamorphosed volcaniclastcs, mafic and felsic schists, amphibolite, marble amongst others are present in the north, northeast and along the eastern margin of the Midyan Basin. The metamorphic source for the Burqan Formation is most

likely low grade in nature. As the abundant undulatory quartz and deformed polycrystalline quartz grains composed of more than 3 quartz crystals per grain have been observed under the optical microscope during modal analysis of the samples of the Burqan Formation (Figure 3.46) (Basu *et al.*, 1975). Uplifted sandstones and limestones younger than the Burqan Formation were most likely the sedimentary source in this region.

The provenance region has not undergone multiple weathering cycles as shown by the presence of large chemically unstable feldspar grains. The feldspar rich granites in the source region might have been affected by hydrothermal solutions as the surface of several plagioclase feldspars shows sericite mica due to sericitization (Que and Allen, 1996). All major framework grains range from very fine grained to very coarse-grained in size and angular to sub-rounded grain shapes which indicates the shorter transportation distance between source and site of deposition.

4.3 Diagenesis and Diagenetic Evolution

Based upon the presence and absence of certain characteristic diagenetic features, two main stages of diagenesis being eodiagenesis (< 2 km depth) and telodiagenesis have been identified in the thin sections of the Burqan Formation (*sensu* Morad *et. al.* 2000) .The petrographic analysis is primarily used to define the relative timing of diagenetic events in the Burqan Formation. The paragenetic sequence chart is built upon the visual identification of textural relationship and superposition of different diagenetic alterations (Figure 4.1). The sequence of diagenetic events during early diagenetic alterations at shallow burial or eodiagenesis include mechanical infiltration of grain coating detrital clays (mainly smectite), kaolinitization of feldspars, mica and mud intraclasts, low to moderate

physical compaction, early pyrite cementation, syndepositional calcite precipitation, Fe-dolomite cementation, leaching of unstable framework grains and cement by marine water. The order of diagenetic episodes occurred during tectonic uplifting or telodiagenesis include late stage minor cementation by iron oxide cementation most likely happened due to the oxidation of early diagenetic pyrite and dissolution of grains and carbonate cements was probably done by meteoric water. The outcrops of the Burqan Formation have not been buried more than 2 km depth due to the absence of authigenic quartz overgrowths, features related to chemical compaction such as stylolites or pressure solution along grain contacts and high Illite/Smectite ratio which are the important indicators of deep burial.

4.3.1 Physical Compaction and Porosity Preservation.

The overall high primary porosity in poorly cemented samples is due to the low to moderate physical compaction as shown by the near complete absence of fractured quartz grains and little bending of ductile biotite mica grains and mud intraclasts (Figures 3.39, 3.41). Moreover, the absence of concavo-convex grain contacts, usually found at larger depths due to high overburden pressure and temperature, also confirms that the sand and conglomerates dominated Nutaysh member of the Burqan Formation has not been buried deep enough. Syndepositional carbonate cementation is also responsible in reducing the effect of mechanical compaction in sandstone samples of the Burqan Formation (Figures 3.46, 3.49, 3.50).

4.3.2 Corroded Quartz Periphery

Petrographic analysis reveals that the corroded outline of quartz grains are characterized by pits and embayments that are filled with authigenic calcite cement (Figure 3.56). This process of corrosion is usually associated with chemically alkaline conditions also suitable for the precipitation of calcite cement (Epstein and Friedman, 1982; Zaid and Al Gahtani, 2015). This feature suggests that the dissolution of silicate minerals and pure silica such as feldspars and quartz respectively is facilitated by biologic activity occurring at elevated pH of surrounding water, therefore, other factors such as free energy of quartz and crystallography could affect the degree of dissolution (Burley and Kantorowicz, 1986).

4.3.3 Carbonate cements

The petrographic analysis shows suggests that all type of carbonate cements including calcite, Fe-dolomite and dolomite are present as pre-compaction cements. It indicates the precipitation during eodiagenesis which is also evident from loose compaction of detrital grains showing "floating" texture (Figure 3.56) (Loucks, Bebout and Galloway, 1977; Hesse and Abid, 1998; Wanas, 2008; Liu *et al.*, 2014; Nyman *et al.*, 2014). The fractured quartz grains do not show filling of fractures by carbonate cements when observed under the optical microscope. It helps to rule out the post-compactional precipitation of authigenic carbonate cements.

4.3.4 Accessory Cements

Opaque cements including pyrite and thick hematite patches are present as accessory authigenic minerals in sandstone samples as shown by the XRD and petrographic analysis

on representative samples (Table-2) (Figure 3.39, 3.46, 3.50). Thin sections show the presence of patches of opaque pyrite that are engulfed by the calcite cement. This implies that the pyrite cement was precipitated earlier than the calcite cements. The presence of hematite most likely represents a late diagenetic stage during which iron oxide was formed close to the surface due to the oxidation of early pyrite cement.

Quartz cement is absent but clay cements including illite and chlorite, which are typical mesogenetic cements, are present in very low amount in the sandstone samples. It agrees with a shallow burial scenario for the Burqan Formation and shows that the formation has not experienced subsurface temperature exceeding 90°C (Morad, Ketzer and De Ros, 2000).

The clay separated from sandstone samples for XRD analysis reveals that the expansion in smectite is at least 90% pointing towards very low thermal maturity. This agrees with the low to moderate physical compaction and lack of thermal effect (e.g; absence of quartz cement or overgrowth). The SEM photographs shows the presence of smectite as grain coating in sandstone samples of Burqan Formation which could result in the preservation of reservoir quality at greater depth by prohibiting the quartz overgrowths (Moraes and De Ros, 1990; Al-ramadan *et al.*, 2006). Contrary to this, the alteration of smectite to illite (fibrous or flaky) at temperature range from 50° to 95°C in the presence of K^+ ions derived by the leaching of K-feldspars in the presence of acidic water could severely decrease the permeability of the reservoir even when overall porosity of the sandstone remains high. (Worden and Morad, 2009)

4.4 Reservoir Quality of Burqan Formation

This study shows that several key factors control the reservoir quality of the Burqan Formation, as discussed below.

1. The coarse grain size of the Burqan Formation deposits analyzed will have a positive impact on the porosity and permeability of the reservoir sand bodies as compared to the fine-grained units (Chilingar, 1964; Chuhan *et al.*, 2002; Hu and Huang, 2017).
2. The majority of the samples shows poor to moderate sorting during petrographic analysis which implies negative effect on reservoir quality of the Burqan Formation by filling the pores with fine grains in response to increased overburden pressure at greater burial depth (Chilingar, 1964; Chuhan *et al.*, 2002; Hu and Huang, 2017).
3. Relative percentage of framework grains also affect the reservoir quality. For instance, the average composition of the Burqan Formation is a lithic arkose with abundant feldspar and lithic fragments as compared to quartz rich sub arkose or arenite compositions. This can lead towards lowering the mechanical strength and high impact of mechanical compaction during deep burial. It will result in decreasing the porosity and permeability of the Burqan Formation. However, the abundance of rigid granitic lithic rock fragments as compared to fine grained sedimentary rock fragments or fine volcanics might preserve reservoir quality to some extent at substantial depth (Worden, Mayall and Evans, 1997). Contrary to this, the feldspars can play dual role to determine the reservoir quality of the Burqan Formation. Their presence could give moderate strength to the framework

composition to preserve reservoir quality or they can act as source for different authigenic cements that will occlude the pore space and reduce the porosity and permeability of the reservoir units. Calcic plagioclase can alter to Na-plagioclase (albite) by releasing Ca-ions for carbonate cements (Sadoon Morad, 1998). Although, higher granitic rock fragments suggest that the source area contains feldspars of intermediate composition rather than highly calcic plagioclase.

4. The grain coating by smectite and chlorite has been observed in SEM micrographs of the Burqan Formation. While smectite converts typically to flaky or fibrous illite during deep burial diagenesis it may significantly reduce the reservoir quality by filling of the pore spaces. But it can still inhibit quartz overgrowth and help in preserving the quality of the reservoir. Likewise, the presence of chlorite as grain coating has a positive effect in conserving the reservoir quality by blocking the quartz cementation.
5. Feldspars usually alter to kaolinite and hence might reduce the pore quality. However, the Burqan Formation shows a low percentage of kaolinite as pore filling cement as supported by petrographic and XRD analysis. As higher amount of kaolinite can lead towards illite formation in the presence of potassium ions derived from K-feldspars therefore it has a negative effect on reservoir quality (Hancock and Taylor, 1978; Sommer, 1978; Dutta and Suttner, 1986). However, lower content of kaolinite in our case may help in limiting the illitization and maintaining the higher reservoir quality.

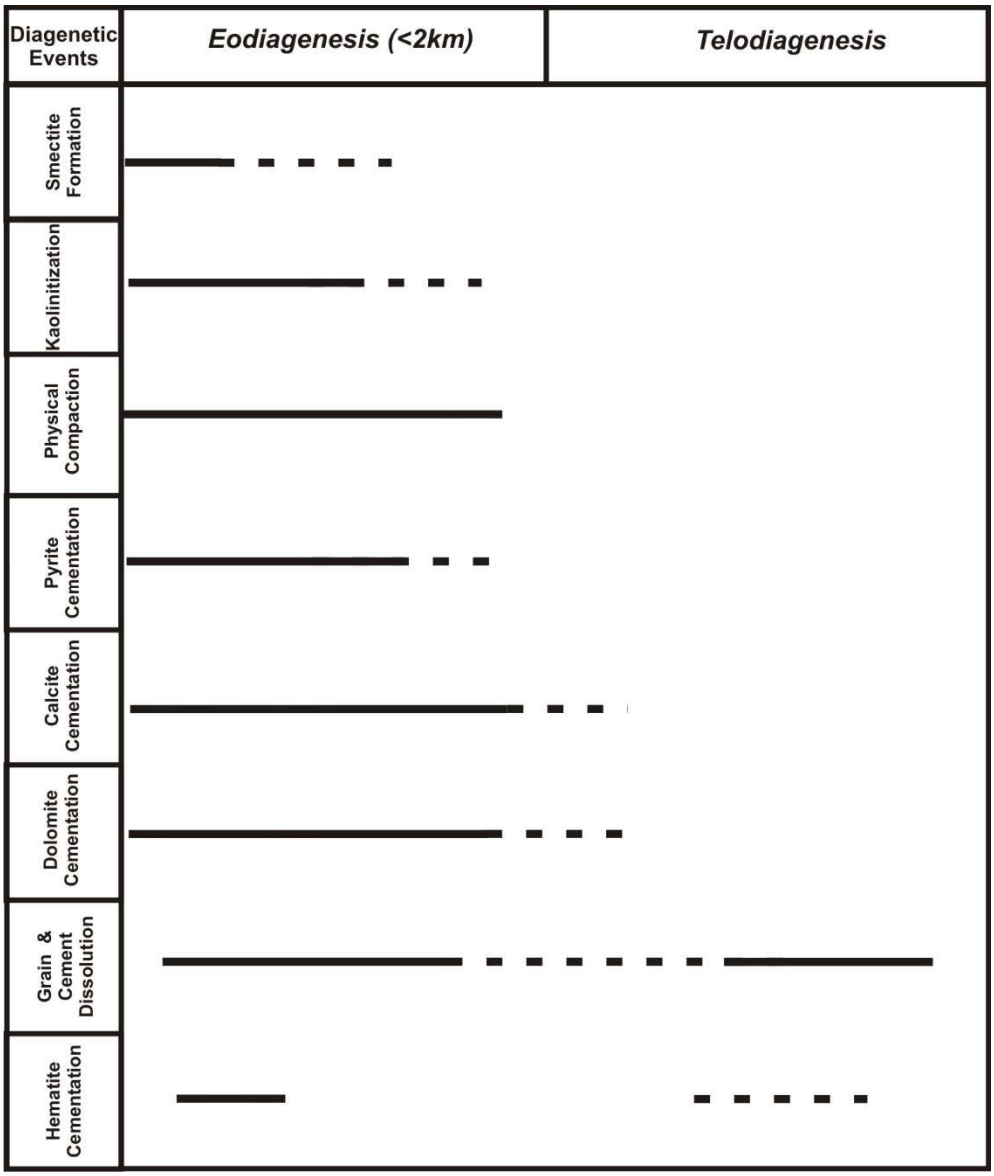

Figure 4.1: Paragenetic sequence summary chart showing the relative occurrence of diagenetic events in the Burqan Formation.

4.5 Conceptual Submarine Fan Model of the Burqan Formation

The submarine fan model for the Burqan Formation in the Midyan region of Saudi Arabia resembles to the classical submarine fan model proposed by Mutti and Ricci Lucchi, 1972 (Figure 4.2). This model consists of a feeder canyon in the proximal part of the submarine fan starting from the continental shelf region. The mid fan region of this submarine fan model consists of well-developed channel-levee complex system. The distal part of the fan is composed of attached lobes composed of small-sized, channel-levee deposits and sheet-like mudstone. Certain facies are associated with each sub-environment.

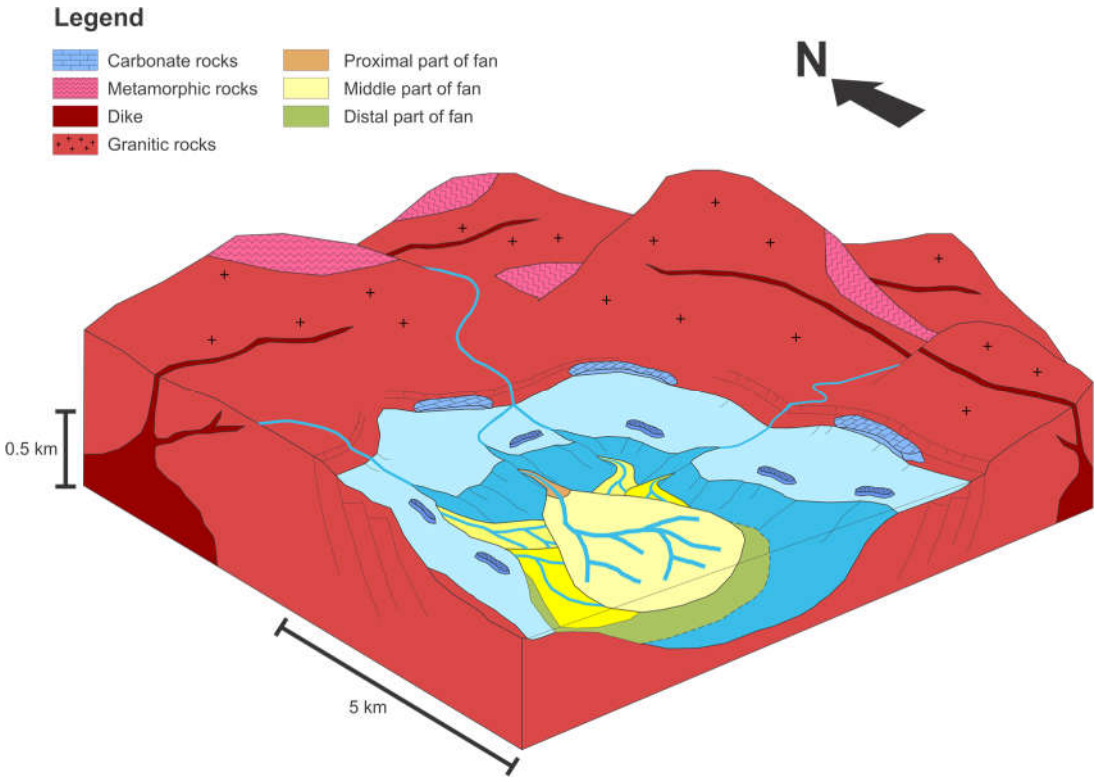

Figure 4.2: The submarine fan model of the Burqan Formation in the Midyan region, NW Saudi Arabia.

The facies associated with feeder canyon in the proximal fan region is shown by major Pickering Facies class A and class B. The observed sub-classes of Facies A and B include A1.1, A1.2, A1.4, A2.2, A2.4, A2.5, A2.7 and B2.1 respectively. The medial part of the fan is composed of Pickering Facies class B and class C. The sub-classes observed in the stratigraphic sections of the mid-fan region consists of B2.1, C1.1, C2.1, C2.2 and C2.3 respectively. The distal part of the fan is shown by the presence of channel-levee deposits (C2.2 and C2.3) along with thick sheet-like, structureless mud deposits of Pickering Facies E1.1.

Each stratigraphic section consists of submarine fan deposits of different sub-environment stacking above each other. It might indicate the coalescing of different submarine fan deposits originating from different source point. Due to the structural complexity of the Midyan basin, it is nearly impossible to trace all the architectural elements of the individual submarine fan.

5 CONCLUSION

The following conclusions could be drawn from the above discussion:

The primary focus of this study was to enhance the understanding of distribution of reservoir quality of the Burqan Formation in Midyan Basin. The target is achieved by selecting outcrops from different parts of the Midyan Peninsula and describing the lithology, lithofacies and their related depositional processes, interpreting the provenance and diagenetic processes operating within the Burqan Formation. The summary of this research is given below.

Lithologically, the Burqan Formation is composed primarily of conglomerate, sandstones, mudstones and, rarely carbonate. Four Pickering classes have been identified (A, B, C and E) based on grain size, as well as one carbonate lithofacies. Thirteen sub-classes (A1.1, A.1.2, A1.4, A2.2, A2.4, A2.5, A2.7, B2.1, C1.1, C2.1, C2.2, C2.3 and E1.1) based on thickness of individual units, sedimentary structures. Consideration of bed thickness, sedimentary structures, grain size and grading pattern indicate that Burqan Formation was deposited by several gravity driven processes which include debris flow, high and low density turbidity currents, traction carpet and suspension.

The composition of lithic fragments suggests the presence of several source points which could produce reservoirs of different quality. However, the effect of grain size is more important unless there are large differences in sandstone composition.

Quartz cementation is absent in the outcrop and will not be significant in the subsurface in Pickering facies classes which are predominantly medium to coarse grained sandstones

(Facies A and B) due to low detrital quartz content and grain size effects. The average porosity observed in these sandstones ranges from 15-20% with good permeability. Diagenetic illite will have minor effect on the reservoir quality of coarse- to very coarse sandstones (mainly in Pickering facies class A and B). In medium to very fine sandstones (mostly in Pickering facies classes B and C), illite poses no threat to the reservoir quality of outcrops but will be an issue in the subsurface for permeability even though porosity is expected to be on the order of 10-15% but permeability will be relatively less than the coarse-grained sandstones.

Early smectite grain coatings likely will convert to fibrous or flaky illite (possibly chlorite where more mafic rock fragments are present) at higher temperatures and greater depth; these coatings may preserve porosity but will adversely affect permeability by closing the pore spaces among framework grains. Chlorite grain coatings may be developed in more lithic rich (usually coarser) sandstones in the subsurface, but these were not extensively developed in outcropping sandstones with low thermal exposure.

Although Burqan sandstones are lithic rich, a large proportion of the lithics are granitic in composition. These are more mechanically stable than volcanic or fine-grained sedimentary rock fragments, therefore compaction may cause less problem for reservoir quality than in some lithic sandstones.

Carbonate cements are present in significant amounts (>15%) in nearly half of the analyzed samples of Burqan Formation. Source of the carbonate cement is largely a function of the presence of biogenic carbonate, especially foraminiferal tests. Additional sources of carbonate cements may be detrital carbonate derived from older carbonates (e.g. Musayr).

REFERENCES

Abdullatif, O. and Olagoke, S. (2010) 'The Early Miocene Deep Marine Turbidities of Burqan Formation : Facies Characteristics and Reservoir Quality , Midyan Region , Saudi Arabia', in *Geophysical Research Abstract, EGU*, p. 8093.

Al-Laboun, A. *et al.* (2014) 'Reservoir characterization of the Burqan Formation sandstone from Midyan Basin, northwestern Saudi Arabia', *Turkish Journal of Earth Sciences*, 23(2), pp. 204–214.

Al-ramadan, K. *et al.* (2006) 'Linking Diagenesis and Porosity Preservation to Sequence Stratigraphy of Reservoir Sandstones in the Jauf Formation (Lower Devonian), Eastern Saudi Arabia', in *7th Middle East Geosciences Conference and Exhibition (GEO2006)*.

Al-Ramadan, K., Dogan Ahmet, U. and Muhittin, S. (2013) 'Sedimentology and diagenesis of the Miocene Nutaysh member of the Burqan formation in the Midyan area (Northwestern Saudi Arabia)', *Geological Quarterly*, 57(1), pp. 165–174.

Alsharhan, A. S. (2003) 'Petroleum geology and potential hydrocarbon plays in the Gulf of Suez rift basin, Egypt', *AAPG Bulletin*, 87(1), pp. 143–180.

Anderson, J. E. *et al.* (2000) 'Controls on turbidite sand deposition during gravity-driven extension of a passive margin: Examples from Miocene sediments in Block 4, Angola', *Marine and Petroleum Geology*, 17(10), pp. 1165–1203.

Basu, A. *et al.* (1975) 'Re-evaluation of the Use of Undulatory Extinction and Polycrystallinity in Detrital Quartz for Provenance Interpretation', *Journal of*

Sedimentary Petrology, 45(4), pp. 873–882.

Bayer, H. J. *et al.* (1988) 'Sedimentary and structural evolution of the northwest Arabian Red Sea margin', *Tectonophysics*, 153(1–4), pp. 137–151.

Boggs, S. (2014) *Principles of Sedimentology and Stratigraphy*. 5th edn. Pearson Education Limited.

Bosworth, W. (1993) 'Nature of the Red Sea crust: A controversy revisited.', *Geology*, 21, pp. 574–575.

Bosworth, W., Huchon, P. and McClay, K. (2005) 'The Red Sea and Gulf of Aden Basins', *Journal of African Earth Sciences*, 43(1–3), pp. 334–378.

Burley, S. D. and Kantorowicz, J. D. (1986) 'Thin section and SEM textural criteria for the recognition of cement-dissolution porosity in sandstones.', *Sedimentology*, 33, pp. 587–604.

Carter, R. M. and Norris, R. J. (1977) 'Redeposited conglomerates in Miocene flysch sequence at Blackmount Western Southland, New Zealand.', *Journal of Sedimentary Geology*, 18, pp. 289–319.

Chilingar, G. V. (1964) 'Relationship Between Porosity, Permeability, and Grain-Size Distribution of Sands and Sandstones', *Developments in Sedimentology*, 1(C), pp. 71–75. doi: 10.1016/S0070-4571(08)70469-2.

Chuhan, F. A. *et al.* (2002) 'Porosity loss in sand by grain crushing - Experimental evidence and relevance to reservoir quality', *Marine and Petroleum Geology*, 19(1), pp. 39–53. doi: 10.1016/S0264-8172(01)00049-6.

Clark, M. D. (1986) 'Explanatory Notes to the Geologic Map of the Al Bad' Quadrangle, Sheet 28A, Kingdom of Saudi Arabia, Ministry of Petroleum and Mineral Resources, Jeddah, Saudi Arabia'.

Conolly, J. R. (1965) 'The Occurrence of Polycrystallinity and Undulatory Extinction in Quartz in Sandstones', *Journal of Sedimentary Petrology*, 35(1), pp. 116–135.

Dickinson, W. R. (1970) 'Interpreting Detrital Modes of Graywacke and Arkose.', *Journal of Sedimentary Petrology*, 40(2), pp. 695–707.

Dickinson, W. R. and Suczek, C. A. (1979) 'PlateTectonics and Sandstone Compositions', *The American Association of Petroleum Geologist Bulletin*, pp. 2164–2182.

Donald R. Lowe (1982) 'Sediment Gravity Flows: II Depositional Models with Special Reference to the Deposits of High-Density Turbidity Currents', *SEPM Journal of Sedimentary Research*, Vol. 52(1), pp. 279–297.

Dullo, W.-C., Hötzl, H. and Jado, A. R. (1983) 'New stratigraphical results from the Tertiary sequence of the Midyan area, NW Saudi Arabia; Contributions to the geology of the eastern margin of the Red Sea', *Newsletters on Stratigraphy*, 12(2), pp. 75–83.

Dutta, P. K. . and Suttner, L. J. (1986) 'Alluvial sandstone composition and paleoclimate, II. Authigenic Mineralogy 1', *Journal of Sedimentary Petrology*, 56(3), pp. 346–358.

Epstein, S. A. and Friedman, G. M. (1982) 'Processes controlling precipitation of carbonate cement and dissolution of silica in reef and near-reef settings', *Sedimentary*

Geology, 33(3), pp. 157–171.

Folk, R. L. (1980) *Petrologie of sedimentary rocks*, *Hemphll Publishing Company, Austin*. Texas.

Gardner, W. C., Khan, M. A. and Al-Hinai, K. G. (1996) 'Interpretation of Midyan and Sinai geology from a Landsat TM image.', *Arabian Journal for Science and Engineering*, 21, pp. 571–586.

Gazzi, P. (1966) 'Le Arenarie del Flysch Sopracretaceo dell'Appennino Modenese: Correlazioni con il Flysch di Monghidoro.', *Mineralogica e Petrografica*, 12, p. 69–97.

Hakami, A. M., Alramadan, K. A. and Senalp, M. (no date) 'Markov Chain Analysis of Turbiditic Facies – Nutaysh Member of the Burqan Formation , NW Saudi Arabia'.

Hampton, M. A. (1972) 'The role of subaqueous debris flow in generating turbidity currents.', *Journal of Sedimentary Petrology*, 42(4), pp. 775–793.

Hampton, M. A. (1975) 'Competence of fine-grained debris flows.', *Journal of Sedimentary Petrology*, 45(4), pp. 834–844. Available at: -.

Hancock, N. J. . and Taylor, A. M. (1978) 'Clay minerals diagenesis and oil migration in the Middle Jurassic Brent Sand Formation.', *Journal of the Geological Society of London*, 135, pp. 69–72.

Hein, F. J. (1982) 'Depositional mechanisms of deep-sea coarse clastic sediments, Cap Enrage Formation, Quebec.', *Canadian Journal of Earth Sciences*, 19, pp. 267–287.

Hein, F. J. . and Walker, R. G. (1982) 'The Cambro-Ordovician Cap Enrage Formation, Quebec, Canada: conglomeratic deposits of a braided submarine channel with terraces.', *Sedimentology*, 29, pp. 309–329.

Hendry, H. E. (1972) 'Breccias deposited by mass flow in the Breccia Nappe of the French pre-Alps.', *Sedimentology*, 8, pp. 277–292.

Hendry, H. E. (1973) 'Sedimentation of deep water conglomerates quebec--composite, lower Ordovician rocks of liquefaction, bedding produced by progressive sediment?', *Journal of Sedimentary Petrology*, 43(1), pp. 125–136.

Hesse, R. and Abid, L. A. (1998) 'Carbonate cementation-the key to reservoir properties of four sandstone levels (Cretaceous) in the Hibernia Oilfield, Jeanne d'Arc Basin, Newfoundland, Canada.', in *In: Morad, S. (Ed.), Carbonate Cementation in Sandstones: Distribution Patterns and Geochemical Evolution.* International Association of Sedimentologists Special Publication, 26., pp. 363–393.

Hiscott, R. N. . and Middleton, G. V. (1979) 'Depositional mechanics of thick-bedded sandstones at the base of a submarine slope, Tourelle Formation (Lower Ordovician), Quebec, Canada.', *The Society of Economic Paleontologists and Mineralogists (SEPM)*, Sp. Pub.27, pp. 307–326.

Hiscott, R. N. and James, N. P. (1985) 'Carbonate Debris Flows, Cow Head Group, Western Newfoundland', 55(5), pp. 735–745.

Hiscott, R. N. and Middleton, G. V (1980) 'Fabric of coarse deep-water sandstones, Tourelle Formation, Quebec, Canada', *Journal of Sedimentary Petrology*, 50(3), pp.

703–722.

Hu, X. and Huang, S. (2017) ‘Physical Properties of Reservoir Rocks’, in X., H. et al. (eds) *Physics of Petroleum Reservoirs.* Berlin, Heidelberg: Springer Mineralogy.

Hughes, G. W. (2014) ‘Micropalaeontology and palaeoenvironments of the Miocene Wadi Waqb carbonate of the northern Saudi Arabian Red Sea.’, *GeoArabia*, 19(4), pp. 59–108.

Hughes, G. W. A. and Johnson, R. S. (2005) ‘Lithostratigraphy of the Red Sea region’, *Geoarabia*, 10(3), pp. 49–126.

Hughes, G. W. and Filatoff, J. (1995) ‘Hughes & Filatoff_1995_New biostratigraphic constraints on Saudi Arabian Red Sea Pre-and Syn-rift sequences.pdf’, p. 12.

Hussain, M. and Al-ramadan, K. (2009) ‘Microfacies analysis of Wadi Waqb member (Miocene) in Wadi Aynunah , northwest of Saudi Arabia.’, *Carbonates and Evaporites*, (2), pp. 139–149.

Ikhane, P. R., Akintola, a I. and Bankole, S. I. (2014) ‘Provenance Studies of Sandstone Facies Exposed Near Igbile Southwestern Nigeria : Petrographic and Geochemical Approach’, *Journal of Geography and Geology*, 6(2), p. 47.

Johnson, B. A. . and Walker, R. G. (1979) ‘Paleocurrents and depositional environments of deep water conglomerates in the Cambro-Ordovician Cap Enrage Formation, Quebec Appalachians.’, *Canadian Journal of Earth Sciences*, 16, pp. 1375–1387.

Koeshidayatullah, A. *et al.* (2016) ‘Variations in architecture and cyclicity in fault-

bounded carbonate platforms: Early Miocene Red Sea Rift, NW Saudi Arabia', *Marine and Petroleum Geology*. Elsevier Ltd, 70, pp. 77–92.

Lash, G. G. (1984) 'Density-modified grain-flow deposits from an early Paleozoic passive margin', *Journal of Sedimentary Petrology*, 54(2), pp. 557–562.

Li, Q. *et al.* (2014) 'Factors controlling reservoir properties and hydrocarbon accumulation of lacustrine deep-water turbidites in the Huimin Depression, Bohai Bay Basin, East China', *Marine and Petroleum Geology*. Elsevier Ltd, 57, pp. 327–344.

Liu, S. B. *et al.* (2014) 'Diagenetic fluid evolution and water-rock interaction model of carbonate cements in sandstone: An example from the reservoir sandstone of the Fourth Member of the Xujiahe Formation of the Xiaoquan-Fenggu area, Sichuan Province, China', *Science China Earth Sciences*, 57(5), pp. 1077–1092.

Long, D. G. F. (1977) 'Resedimented conglomerates of Huronian (Lower Aphebian) age, from the north shore of Lake Huron, Ontario, Canada', *Canadian Journal of Earth Sciences*, 14, pp. 2495–2509.

Loucks, R. G., Bebout, D. G. and Galloway, W. E. (1977) 'Relationship of Porosity Formation and Preservation to Sandstone Consolidation History--Gulf Coast Lower Tertiary Frio Formation (1).', *Gulf Coast Association of Geological Societies Transactions*, 27, pp. 109–120.

Lowe, D. R. (1976) 'Grain flow and grain flow deposits', *Journal of Sedimentary Petrology*, Vol. 46(1), pp. 188–199.

Mansurbeg, H. *et al.* (2008) 'Diagenesis and reservoir quality evolution of palaeocene

deep-water, marine sandstones, the Shetland-Faroes Basin, British continental shelf', *Marine and Petroleum Geology*, 25(6), pp. 514–543.

Marschalko, R. (1964) 'Sedimentary structures and paleocurrents in the marginal lithofacies of the Central-Carpathian flysch.', in Bouma;, A. H. and Brouwer, A. (eds) *Turbidites. Developments in Sedimentology*. Amsterdam: Elsevier, p. pp;106-126.

McCaffrey, W. and Kneller, B. (2001) 'Process controls on the development of stratigraphic trap potential on the margins of confined turbidite systems and aids to reservoir evaluation.', 6(6), pp. 971–988.

McLennan, S. M. *et al.* (1993) 'Geochemical approaches to sedimentation, provenance, and tectonics.', in Johnson, M. J. and Basu, A. (eds) *Processes Controlling the Composition of Clastic Sediments.* Geological Society of America. Special Paper 284, pp. 21–40.

Meulenkamp, J. E. and Sissingh, W. (2003) 'Tertiary palaeogeography and tectonostratigraphic evolution of the Northern and Southern Peri-Tethys platforms and the intermediate domains of the African-Eurasian convergent plate boundary zone', *Palaeogeography, Palaeoclimatology, Palaeoecology*, 196(1–2), pp. 209–228.

Morad, S., Ketzer, J. M. and De Ros, L. R. (2000) 'Spatial and temporal distribution of diagenetic alterations in siliciclastic rocks: Implications for mass transfer in sedimentary basins', *Sedimentology*, 47(SUPPL. 1), pp. 95–120.

Moraes, M. A. S. . and De Ros, L. F. (1990) 'Infiltrated clays in fluvial Jurassic sandstones of Reconcavo Basin, Northern Brazil.', *Journal of Sedimentary Petrology*,

60, pp. 809–819.

Mutti, E. ., Nilsen, T. H. . and Ricci Lucchi, F. (1978) ‘Outer fan depositional lobes of the Laga Formation (Upper Miocene and Lower Pliocene), east-central Italy.’, in Stanley;, D. J. and Kelling, G. (eds) *Sedimentation in Submarine Canyons, Fans, and Trenches*. Pennsylvania: Dowden, Hutchinson and Ross, Stroudsburg, pp. 210–223.

Mutti, E. . and Ricci Lucchi, F. (1972) ‘Turbidites of the northern Apennines: introduction to facies analysis.’, *International Geology Review*, 20, pp. 25–166.

Nyman, S. L. *et al.* (2014) ‘Origin and distribution of calcite concretions in Cretaceous Wall Creek Member, Wyoming: Reservoir-quality implication for shallow-marine deltaic strata’, *Cretaceous Research*. Elsevier Ltd, 48, pp. 139–152.

Osae, S. *et al.* (2006) ‘Provenance and tectonic setting of Late Proterozoic Buem sandstones of southeastern Ghana: Evidence from geochemistry and detrital modes’, *Journal of African Earth Sciences*, 44(1), pp. 85–96.

Pettijohn, F. J., Potter, P. E. and Raymond Siever (1972) *Sand and Sandstone*. 2nd edn. New York NY: Springer Science and Business Media, LLC.

Pettingill, H. S. (1998) ‘Turbidite plays’ immaturity means big potential remains’, *Oil and Gas Journal*, 5, pp. 106–112.

Pickering, K. *et al.* (1986) ‘Deep-water facies, processes and models: A review and classification scheme for modern and ancient sediments’, *Earth Science Reviews*, 23, pp. 75–174.

Pickering, K. T. (1981) ‘Two types of outer fan lobe sequence, from the late

Precambrian Kongsfjord Formation submarine fan, Finnmark, North Norway', *Journal of Sedimentary Research*, 51(4), pp. 1277–1286.

Pickering, K. T. (1984) 'The Upper Jurassic "Boulder Beds" and related deposits: a fault-controlled submarine slope , NE Scotland.', *Journal of Geological Society of London*, 141, pp. 357–374.

Pickering, K. T. and Hiscott, R. N. (1985) 'Contained (reflected) turbidity currents from the Middle Ordovician Cloridorme Formation, Quebec, Canada: an alternative to the antidune hypothesis.', *Sedimentology*, 32, pp. 373–394.

Piper, D. J. W. (1978) 'Turbidite muds and silts on deep-sea fans and abyssal plains.', in Stanley, D. J. and Kelling, G. (eds) *Sedimentation in Submarine Canyons, Fans, and Trenches.* Dowden, Hutchinson and Ross, Stroudsburg, Pennsylvania, pp. 163–176.

Polis, S. R. *et al.* (2005) 'Preferential deposition and preservation of structurally-controlled synrift reservoirs: Northeast Red Sea and Gulf of Suez.', *GeoArabia*, 10, pp. 97–124.

Purser, B. H., Philobbos, E. R. and Soliman., M. (1990) 'Sedimentation and Rifting in the NW Parts of the Red Sea: a review', *Bulletin de la Societe Geologique de France*, 6(3), pp. 371–384.

Que, M. and Allen, A. (1996) 'Sericitization of Plagioclase in the Rosses Granite Complex, Co. Donegal, Ireland', *Mineralogical Magazine*, 60(December), pp. 927–936.

Ravnås, R. and Steel, R. J. (1998) 'Architecture of Marine Rift Basin Successions',

AAPG Bulletin, 82(1), pp. 110–146.

Ricci Lucchi, F. (1969) 'Channelized deposits in the Middle Miocene flysch of Romagna (Italy)', *Giornale di Geologia*, 36, pp. 203–282.

Sadoon Morad (1998) *Carbonate Cementation in Sandstones: Distribution Patterns and Geochemical Evolution*. 1st edn. Edited by Sadoon Morad. Blackwell Sciene Ltd.

Shanmugam, G. and Moiola, R. J. (1988) 'Submarine fans: Characteristics, models, classification, and reservoir potential', *Earth Science Reviews*, 24(6), pp. 383–428.

Sharland, P. R. *et al.* (2001) *Arabian Plate Sequence Stratigraphy – revisions3.pdf*. GeoArabia, Special Publication 2, Gulf Petrolink.

Siemers, C. T. ., Tillman, R. W. . and Williamson, C. R. (1981) 'Deep Water Clastic Sediments: A Core Workshop.', in Siemers, C. T. ., Tillman, R. W. ., and Williamson, C. R. (eds) *Society of Economic Paleontologists and Mineralogists (SEPM)*. Core Works, p. 416.

Sommer, F. (1978) 'Diagenesis of Jurassic sandstones in the Vicking Graben.', *Journal of the Geological Society of London*, 125, pp. 63–67.

Stampfli, G. M. *et al.* (2001) 'Permo-Mesozoic evolution of the western Tethys realm: The Neo-Tethys East-Mediterranean Basin Connection', in *PeriTethyan Rift/Wrench Basins and Passive Margins*, pp. 51–108.

Stanley, D. J. and Maldonado, A. (1981) 'Depositional models for fine-grained sediments in western Hellenic Trench, eastern Mediterranean.', *Sedimentology*, 28, pp. 273–290.

Stanley, D. J., Palmer, H. D. and Dill, R. F. (1978) 'Coarse sediment transport by mass flow and turbidity current processes and downslope transformation in Annot Sandstone canyon-fan valley systems.', in Stanley, D. J. . and Kelling, G. (eds) *Sedimentation in Submarine Canyons, Fans, and Trenches.* Dowden, Hutchinson and Ross, Stroudsburg, Pennsylvania, pp. 85–115.

Stow, D. A. V. . (1986) 'Deep Clastic Seas.', in H. G. Reading (ed.) *Sedimentary Environments and Facies*. Blackwell Scientific Publications, Oxford., pp. 398–444.

Stow, D. A. V. . and Piper, D. J. W. (1984) 'Deep-water fine-grained sediments: facies models.', in Stow, D. A. V. . and Piper, D. J. W. (eds) *Fine-Grained Sediments: Processes and Facies.* Geological Society of London. Special Publication, pp. 611–645.

Sultan, M. *et al.* (1993) 'Nature of the Red Sea crust: A controversy revisited: Reply.', *Geology*, 21, pp. 575–576.

Surlyk, F. (1978) 'Submarine fan sedimentation along fault scarps on tilted fault blocks173 (Jurassic-Cretaceous boundary, East Greenland)', *Grønlands Geologiske Undersøgelse. Bulletin*, 128, p. 108.

Surlyk, F. (1984) 'Fan-delta to submarine fan conglomerates of the Volgian-Valanginian Wollaston Foreland Group, East Greenland.', in Koster, E. H. . and Steel, R. J. (eds) *Sedimentology of Gravels and Conglomerates*. Memoir 10. Canadian Society of Petroleum Geologists., pp. 359–382.

Suttner, L. J. *et al.* (1985) 'The effect of grain size on detrital modes; a test of the Gazzi-

Dickinson point-counting method; discussion and reply', *Journal of Sedimentary Research*, pp. 616–618.

Tubbs, R. E. *et al.* (2014) 'Midyan Peninsula , northern Red Sea , Saudi Arabia : Seismic imaging and regional interpretation', (3), pp. 165–184.

Walker, R. G. (1978) 'Deep water sandstone facies and ancient submarine fans; models for exploration for stratigraphic traps.', *AAPG Bulletin*, 62, pp. 932–966.

Wanas, H. A. (2008) 'Calcite-cemented concretions in shallow marine and fluvial sandstones of the Birket Qarun Formation (Late Eocene), El-Faiyum depression, Egypt: Field, petrographic and geochemical studies: Implications for formation conditions', *Sedimentary Geology*. Elsevier B.V., 212(1–4), pp. 40–48.

Weimer, P. and Link, M. H. (1991) *Seismic Facies and Sedimentary Processes of Submarine Fans and Turbidite Systems*. 1st edn.

Worden, R. H., Mayall, M. J. and Evans, I. J. (1997) 'Predicting reservoir quality during exploration: lithic grains, porosity and permeability in Tertiary clastic rocks of the South China Sea basin', *Geological Society, London, Special Publications*, 126(1), pp. 107–115. doi: 10.1144/GSL.SP.1997.126.01.08.

Worden, R. H. and Morad, S. (2009) 'Clay minerals in sandstones: controls on formation distribution and evolution.', in *Clay Mineral Cements in Sandstones*, pp. 3–41.

Zaid, S. M. and Al Gahtani, F. (2015) 'Provenance, diagenesis, tectonic setting, and geochemistry of Hawkesbury Sandstone (Middle Triassic), southern Sydney Basin,

Australia', *Turkish Journal of Earth Sciences*, 24(1), pp. 72–98.

Ziegler, P. A. (1992) 'Geodynamics of rifting and implications for hydrocarbon habitat', *Tectonophysics*, 215(1–2), pp. 221–253.

Vitae

Name	MUHAMMAD NAVEED TAHIR BUTT
Nationality	PAKISTANI
Date of Birth	5/30/1984
Email	g201407400@kfupm.edu.sa
Address	House # 74, Street # 3, Khairdin Park Shad Bagh Lahore.
Academic Background	Master in Applied Geology (University of the Punjab, Lahore, Pakistan, 2010

Muhammad Naveed has joined KFUPM as a graduate student in Geosciences department in January, 2015. He has been working as a drilling supervisor in GEOPAK Services Company, where he was involved in handling the drilling problems, making ceaseless drilling operations and collecting the shallow soil cores for soil analysis. He was in-charge of one of the project-sites initiated by the Government of Punjab under the title of "Reserve Estimation of Coal in Eastern Salt Range, Pakistan". His main research interest is in sedimentology and diagenesis of siliciclastic hydrocarbon reservoirs. He has received his master degree in Applied Geology from University of the Punjab, Lahore, Pakistan in 2010. During his master at KFUPM, he has been the official part of several geological field trips as Teaching Assistant and Field Assistant in Al-Quwaiiyah, Ra'as Abu Qamys, Midyan, Shaibah (Rub Al Khali) and Tabuk cities. He has also participated in international

geological field trip to Spain to see the geology of Sorbas and Tabernas Basins in Almeria. He has participated in several workshops related to Petrography, Image analysis, presentation skill's improvement and how to write scientific articles during the course of master at KFUPM. He was acting as the secretary and member of the executive committee for student chapter activities of American Association of Petroleum Geologists (AAPG) at KFUPM. He is an active member of Dhahran Geosciences Society (DGS), American Association of Petroleum Geologists (AAPG), Pakistan Association of Petroleum Geoscientists (PAPG) and European Association of Geoscientist and Engineers (EAGE). Currently, his two manuscripts from his thesis research are ready for submission in ISI journals.